

**Amplification of Broad-Bandwidth Phase-Modulation
Laser Pulses and Applications**

by

Yung-Ho Chuang

September 1991

**Laboratory No. 229
Ph.D. Thesis**

ACKNOWLEDGEMENTS

It is a pleasure to acknowledge the expert advice and continued interest of my advisor, Professor David D. Meyerhofer, throughout the course of this research. I am most grateful to Dr. Martin C. Richardson for his advice and friendship in the early stages of my research.

This work encompasses several fields. Special thanks to Dr. Ansgar Schmid and Dr. Zheng-Wu Li for their help in developing the $\chi^{(3)}$ measurement. The work of Dr. R. Steve Craxton in calculations of the second harmonic conversion of ultrashort pulses is particularly noted. I would like to thank Yanjie Wang and B. Luther-Davies for their cooperation in SHG experiments; without their help this work certainly would not have been possible. I am also indebted to Dr. Jack Kelly for his advice regarding glass amplifiers, and to Dr. Stanley Skupsky and Dr. Robert Short for helpful discussions of SSD.

One thing that makes research so interesting is working with many people. I wish to thank all members of the TTT group, particularly, to Shigeaki Uchida, Steve Augst, and Justin Peatross for their help and humor. I am grateful to Li Zheng for doing computer work. I also wish to thank Dick Fellows, Carl Petras, G. Raffaele-Addamo, and Philip Torti for their expert technical support.

Many thanks to Dr. Oscar Lopez-Raffo and Dr. Paul Jaanimagi for many discussions and suggestions throughout my graduate studies.

Finally, my sincerest thanks go to Mr. David L. Brown. He has served as supervisor and friend, and provided the advice, encouragement and support necessary for the successful completion of this thesis.

This work was supported by the U.S. Department of Energy Office of Inertial Fusion under agreement No. DE-FC03-85DP40200 and by the Laser Fusion Feasibility Project at the Laboratory for Laser Energetics which is sponsored by the New York State Energy Research and Development Authority and the University of Rochester.

ABSTRACT

The amplification and propagation of broad-bandwidth, phase-modulated laser pulses was studied experimentally and theoretically. The near 1053 nm Chirped-Pulse-Amplification (CPA) laser system at the Laboratory for Laser Energetics (LLE) at the University of Rochester was used for these experiments.

In theoretical analysis the power gain of the amplifier is treated as a function of the laser's instantaneous frequency. With this approximation non-ideal amplification processes, such as gain narrowing, gain saturation, and self-phase modulation (SPM), can be clearly expressed and understood. Experimental results from the CPA laser system are in good agreement with the theory.

The sources of the pedestal (pre-pulse and post-pulse) associated with a CPA laser were identified, and carefully eliminated. This allows the CPA laser to generate ultrahigh-power Gaussian pulses of 0.9-ps duration with an intensity contrast exceeding $10^5:1$. This work makes possible the study of high density laser-plasma interactions with a fiber-grating CPA laser system.

Experiments on second harmonic conversion of 1.6-ps pulses at 1053 nm were performed with the CPA laser system using a KDP type II crystal. A pre-delay between the extra-ordinary and ordinary pulses was introduced at the input of the doubling crystal in order to compensate the group-velocity mismatch in the crystal. This brought the energy conversion efficiency up to $\sim 75\%$.

Spectral windowing in the expansion stage of a CPA laser system allows the generation of multiple pulses with different frequencies. These pulses are synchronized with identical spatial profile. They are frequency tunable and pulse-width controllable. One application of this technique is to measure the nonlinear

refractive index using nearly degenerate four-wave mixing. This method automatically provides the phase-matching condition and can mix ultrashort pulses without jittering. Experimental and theoretical results are presented.

The theory of amplification of broad-bandwidth phase-modulated laser pulses is extended from the linear frequency chirp for CPA laser systems to the sinusoidal phase modulation (spatial and temporal) for the beam smoothing in laser fusion. An analogy of the Hamilton-Jacobi equation in classic mechanics is used to explain the laser propagation. Amplitude and phase modulations of the laser pulse due to the evolution of the initial phase modulation are investigated. Local self-focusing of light, enhanced by the initial phase modulation, is also studied.

TABLE OF CONTENTS

CURRICULUM VITAE	ii
ACKNOWLEDGEMENTS	iii
ABSTRACT	v
TABLE OF CONTENTS	vii
LIST OF TABLES	x
LIST OF FIGURES	xi
CHAPTER	
I. INTRODUCTION	1
A. High-Power Lasers for Laser-Matter Interactions	1
B. Pulse Preparation and Modulations	3
C. Amplification of Phase-Modulated Laser Pulses	4
D. Frequency Up-Conversion of Broadband Pulses	5
E. Outline	6
References	8
II. PROPAGATION OF LIGHT PULSES IN A CPA LASER	17
A. Introduction	17
B. Basic Equations	22
C. Solutions	25
1. Frequency Domain	25
2. Time Domain	27
D. Analysis	30

1. Power Spectrum	31
2. Pulse Compression and Pedestal	32
3. Gain Narrowing	35
4. Self-Phase Modulation	38
5. Gain Saturation	40
6. Frequency Mismatch	44
E. Experiments on Self-Phase Modulation	45
F. Conclusion	51
References	53
III. GENERATION OF HIGH-CONTRAST ULTRASHORT PULSES	56
A. Introduction	56
B. Laser System and Experimental Setup	58
C. Experiments on pedestal suppression	63
1. Spectral Shaping	63
2. Temporal Filtering	68
D. Conclusion	73
References	75
IV. FREQUENCY DOUBLING OF PICOSECOND PULSES	78
A. Introduction	78
B. Methods	81
C. Results	87
D. Summary	91
References	92
V. NONRESONANT $\chi_{1111}^{(3)}$ MEASUREMENTS	96
A. Introduction	96

B. Experimental Setup	98
C. Experimental Results	102
D. Error Analysis	107
E. Discussion	111
References	113
VI. AMPLIFICATION OF PHASE-MODULATED LIGHT FOR SSD	115
A. Introduction	115
B. Basic Equations	118
C. Analysis	120
1. Amplitude Modulation	125
2. Phase Modulation	131
3. Local Self-focusing	134
D. Conclusion	138
References	155
VII. SUMMARY	141
APPENDIX	147

LIST OF TABLES

4-1	Measured Relative Third-Order Nonlinear Susceptibilities $\chi^{(3)}/n^2$	106
-----	---	-----

LIST OF FIGURES

- 2-1 Chirped pulse amplification technique. The optical fiber can be removed when the initial ultrashort pulse has enough bandwidth. 18
- 2-2 Gratings can be used to generate negative or positive chirp. In positive chirp scheme a telescope relays the image of the first grating, as shown by dashed lines, to form an equivalent negative chirp scheme with negative separation between two gratings. 19
- 2-3 A schematic of diffraction analogy shows spectral and temporal modulations in CPA lasers. The net power gain $RG(t)$ is similar to an amplitude modulator. Phase variations $\phi_{NL}(t) + \phi_{SPM}(t) + \phi_a(t)$ are similar to the phase modulators. (a) The power spectrum is analogous to the near-field beam profile. (b) The intensity profile of a compressed pulse is analogous to the beam profile of a focal spot (far-field). The background pedestal is a result of scattered light spreading over a wide range depending on the nature of amplitude and phase aberrations. 34
- 2-4 (a) Power spectra for different spectral gain-narrowing conditions, $t/\tau_{eff} = 0, 1, 2,$ and 3 . They approach Gaussian in large gain narrowing limit. (b) The intensity profiles of compressed pulses. Pedestal suppression by spectral gain narrowing is shown. 37

- 2-5 (a) Intensity profiles of ultrashort pulses compressed from chirped Gaussian pulses ($m = 1$, $\tau = 100$, $b = 200$) under a variety of SPM conditions, i.e., peak B-integral values $B = 0, 2, 4, 6$. The compressed pulses become wider and have bumpy structures as B increases. (b) Intensity profiles of ultrashort pulses compressed from chirped super-Gaussian pulses ($m = 5$, $\tau = 100$, $b = 200$). The compressed pulses have wider pedestal as B increases. 39
- 2-6 (a) Relative total population inversion in gain saturation regime with different gain narrowing conditions, $\Delta\omega_L/\Delta\omega_a = 0, 0.2, 0.5$. (b) Amplified chirped pulses under different gain narrowing conditions with an input super-Gaussian pulse, $m = 5$, $I_{in}\tau/U_{sat} = 0.002$, and a small-signal gain $G_0 = 200$. 43
- 2-7 Calculated and measured initial temporal pulse shape with a 290-ps pulse width and a 20-Å bandwidth. The peaked edges of the chirped pulse is a result of using expansion gratings [$\phi_e(w) = -3.8 \times 10^{-23} w^2 + 4 \times 10^{-37} w^3$]. 47
- 2-8 Calculated and measured amplified temporal pulse shape. The total power gain is $G_0=10^{45}$, and the amplifier bandwidth is 210 Å (FWHM). (a) The chirped pulse initially has a 445-ps pulse width and a 35-Å bandwidth. Gain narrowing shapes the pulse to Gaussian. (b) The chirped pulse initially has a 290-ps pulse width and a 20-Å bandwidth. It retains peaked edges because of less gain narrowing. (c) Same chirped pulse as in (b) except the gain center is offset 5 Å. 48

- 2-9 Calculated and measured power spectra of amplified chirped pulses with gain center offset. (a) The chirped pulse is switched out of the regenerative amplifier in an earlier time. (b) The chirped pulse is switched out of the regenerative amplifier 15 round trips later than (a). Spectral modulation due to SPM ($B=5$) is clearly shown in (b). 50
- 3-1 Schematic diagram of the current chirped-pulse-amplification laser system: (a) Pulse preparation stage. The regenerative amplifier serves to amplify and shape the laser pulse; (b) Amplifier chain and compression stage. 59
- 3-2 Autocorrelator. The wedged beam splitter and slits are used to eliminate all etalon reflections from reaching the photomultiplier. The PIN diode detects shot-to-shot laser energy fluctuations. This setup becomes a single-shot autocorrelator when the slits are removed and the photomultiplier is replaced by a linear array detector. 62
- 3-3 (a) Spectrum of the chirped pulse leaving the fiber, $\text{FWHM} = 37 \text{ \AA}$. (b) Autocorrelation trace of the compressed pulse before amplification, $\text{FWHM} = 1.6 \text{ ps}$, assuming a Gaussian profile. The pulse wings and the satellite pulses are the results of compressing a square-top chirped pulse with the nonlinear chirp locating at the leading and trailing edges. 64

- 3-4 Autocorrelation traces of the compressed pulse shows the pedestal enhanced by SPM and gain-center mismatch. (a) With SPM and gain-center mismatch. (b) Without SPM. The Gaussian curve-fits show the ideal pulses. Each data point represents the average of 10 shots. 66
- 3-5 Autocorrelation trace of the compressed pulse shows the etalon effects. 67
- 3-6 (a) Spectrum of the pulse leaving the regenerative amplifier, FWHM = 12 Å. The Gaussian profile is a result of spectral gain narrowing. The spectral line center is the same as in Fig. 3-3(a). (b) Autocorrelation trace of the compressed pulse, FWHM = 1.6 ps, assuming a Gaussian profile. 69
- 3-7 (a) Spectrum of the pulse with a saturable absorber in the system, FWHM = 36 Å; (b) Autocorrelation trace of the compressed pulse, FWHM = 0.9 ps assuming a Gaussian profile. The baseline represents the noise level of our detector and data-acquisition system. The intensity contrast is now greater than 10^5 , the limit of our autocorrelator dynamic range. 71
- 3-8 Rescaled view of Fig. 3-7(b). A detailed autocorrelation trace of a 0.9-ps pulse with a Gaussian fit is shown. 72
- 4-1 Frequency doubling scheme for picosecond pulses with the use of a pre-delay crystal. 82
- 4-2 Schematic layout of frequency doubling experiments. 82

- 4-3 The laser beam profile. (a) Intensity contours relative to the maximum intensity. (b) Line-out of the beam profiles in two perpendicular directions. The dashed line was used as an average in the calculations (which assumed cylindrical symmetry). 85
- 4-4 Second harmonic energy conversion efficiency. (a) Without pre-delay, ~40% conversion efficiency is obtained. (b) With pre-delay, the conversion efficiency increases to ~75%. (c) A lower conversion efficiency (with pre-delay) is obtained with a non-optimum polarization angle of 51° . (d) The conversion efficiency (of single KDP doubler) falls off with polarization angle as predicted. 89
- 5-1 Schematic representation of pulse expansion, spectral windowing, amplification and pulse compression used in nearly-degenerate four-wave mixing measurements. 99
- 5-2 Second-harmonic autocorrelation trace of compressed, spectrally-segmented pulse pair. Each data point is a 10-shot average. For comparison, first-order Gaussian (dotted line) is overlaid. The experimentally measured modulation frequency equals the beat-frequency between two, 17-Å separated waves. 101
- 5-3 Multichannel detector record from a single-shot, four-wave mixing event in CS₂. Shorter wavelengths are to the left. The central two peaks represent $I(\omega_1)/10$ (left) and $I(\omega_2)/10$ (right). Clearly resolved (in full scale) are the coherent Stokes (furthest right) and anti-Stokes (second from left) peaks. 103

- 5-4 (a) Nonresonant CARS signal magnitude plotted against the input wave intensity product $I^2(\omega_1) I(\omega_2)$. (b) Nonresonant CSRS signal magnitude plotted against the input wave intensity product $I^2(\omega_2) I(\omega_1)$. The data point in (a) and (b) map into each other, i.e., pairs of CARS and CSRS signals were taken simultaneously. 104
- 6-1 The energy relation between the position $z = 0$ and the current position z is shown. Two neighboring rays with their initial positions at y_0 and $y_0 + \Delta y_0$ are used to illustrate the energy flow. 124
- 6-2 Intensity modulation of initially phase-modulated light after free propagating a distance $z = 30$ m in air, with $\delta = 4$, $\beta = 148 \text{ m}^{-1}$, and $k_0 = 5.967 \times 10^6 \text{ m}^{-1}$. (a) Three dimensional plot of laser intensity. The peaks are at the positions where $\sin[\omega_m t - \beta y_0(y, z, t)] \approx -1$. (b) The intensity profile of a 750 ps pulse at center part of the beam, $y = 0$. 128
- 6-3 Spectral gain narrowing of phase-modulated light can cause intensity modulation. The solid line represents the frequency matched case. The dotted line represents the case with 5 Å linecenter mis-match. The intensity modulation is enhanced because of larger gain difference within the laser bandwidth. Parameters: $\ln(G_0) = 25$, $\delta = 4\pi$, $\omega_m/2\pi = 10$ GHz, at $y = 0$. 130
- 6-4 (a) Power spectrum of the amplified pulse at $y = 0$, with B-integral = 5, $\delta = 4\pi$, and $\omega_m/2\pi = 10$ GHz. (b) Detailed view of (a) shows that each frequency mode separates into two bumps due to SPM. 133

6-5 Local self-focusing of light induced by the initial phase modulation.

(a) The ray trajectories under different self-focusing conditions, $U = 0, 1, \text{ and } 10$, and $\delta = 4, \alpha_r = 0$. (b) The normalized local self-focusing length z_f/z_r as a function of U in different values of δ . (c) Asymptotic solution of z_f/z_r for large U .

CHAPTER I

INTRODUCTION

A. High Power Lasers for Laser-Matter Interactions

High power lasers are the basic tools used to study laser-matter interactions. The properties required of the high power laser usually depend on the specific physical problems encountered.

In laser fusion,¹ attention is currently being focussed on the techniques to smooth the laser beam in order to produce a uniform plasma. The use of broad-bandwidth and spatially incoherent light has been proposed to average the interference between beamlets in time and space to achieve beam uniformity. Two important schemes are being developed. One is called induced spatial incoherence (ISI),^{2,3} first proposed in 1983. A chaotic broad-bandwidth laser beam with short coherence time is divided into numerous independent beamlets by an orthogonal pair of reflecting, echelon-like mirrors. The beamlets are overlapped onto the target by a lens to form an instantaneous interference pattern which converges to a smooth intensity profile when averaged over time. The other method developed at LLE in 1989, combining phase-plate techniques^{4,5} and a broad-bandwidth laser with sinusoidal phase modulation is called smoothing by spectral dispersion (SSD).⁶ The phase-modulated laser beam is broken up into beamlets using a phase plate and then focussed onto the target to form the time-averaged beam smoothing.

In ultrafast laser-matter interactions, controlling the pre-pulse level is required for understanding the fundamental atomic physics⁷⁻¹² and plasma physics,¹³⁻¹⁶ for the generation and application of short bursts of x-ray,¹⁷⁻²¹ and

for the development of x-ray lasers.¹³⁻²¹ Compact solid-state laser systems utilizing the chirped-pulse-amplification (CPA) technique are commonly used to generate high-power laser pulses.²²⁻³³ The CPA technique was originally introduced to increase the available power in radar over 40 years ago and was applied to solid-state lasers in 1985 by Strickland and Mourou.²² Recent efforts by several groups are towards higher peak power and shorter pulse durations. Nd:glass amplifier chain is still the favorite choice for ultra-high power extraction,²³⁻²⁹ which has recently brought the peak power up to 30 TW.²⁹ Broadband amplifiers such as alexandrite³⁰ and Ti:sapphire^{31,32} are used to amplify pulses as short as 100 femtosecond. This technique, however, usually brings the unwanted prepulse and postpulse (called pedestal) beneath the compressed pulse.³³ Methods utilizing spectral windowing,³⁴ spectral gain narrowing,²⁵ saturable absorber,^{27,33} temporal windowing,²⁹ and second harmonic generation^{35,36} to suppress the pedestal are in use or under development.

In general, it is desirable to develop a high-power laser capable of generating the custom-made pulse shapes for different applications. One successful example, combining the spectral shaping³⁷⁻⁴⁰ and the CPA techniques for nonlinear refractive index measurement, was reported.⁴¹ Synchronized pulses with an identical beam profile but different frequencies served this purpose. The basic scheme consists of passing a broad-bandwidth laser pulse through a pair of gratings and a spectral window to obtain the desired group velocity delay and frequencies. This temporal and spectral tunable laser can be a powerful tool for plasma physics, nonlinear optics, ultrafast spectroscopy, and other fields. The new laser technique with the use of spectral shaping and CPA not only reduces the cost

associated with the current multiple-beam configuration used for wave-mixing⁴² and pump-probe experiments but also greatly simplifies the alignment and synchronization. Multiple-beam synchronization problems are more severe for ultrafast applications.

B. Pulse Preparation and Modulations

The high-power lasers discussed above usually include three stages: pulse preparation, amplification, and final manipulation. In the pulse preparation stage, optical devices such as fibers, crystals, and gratings are commonly used to modulate laser pulses. As a result, these pulses are not Fourier transform limited. The bandwidths are affected by chaotic phase modulation for ISI, sinusoidal phase variation for SSD, and parabolic phase modulation (linear chirp) for CPA. Through the use of these optical devices the laser becomes more versatile.

Optical fibers are not only used in communication but also have been widely used in the field of nonlinear optics over the last 15 years.⁴³ The production of linearly chirped pulses through the processes of self-phase modulation (SPM) and group-velocity dispersion (GVD) in the optical fiber has created a new method to generate ultra-short pulses.^{43, 44} The compression of the linearly chirped pulses has led to optical pulses as short as 6-fs.⁴⁵ For high-power Nd:glass CPA laser systems, optical fibers are still the standard device used to generate the desired bandwidth. The phenomenon of cross-phase modulation (XPM), occurring when two pulses propagate simultaneously inside the fiber, has recently been used to produce the chaotic phase modulation necessary for ISI.

Crystals are commonly used as birefringent devices (wave plates, polarizers, etc.), frequency convertors, and electro-optical modulators.⁴⁶ They

have been proposed to up-convert the compressed pulses in CPA lasers to reduce the pedestal.³⁵ In ultra-fast applications, crystals are widely used as autocorrelators for pulse-width measurement.^{47,48} In SSD, the laser bandwidth is obtained by passing the laser beam through an electro-optical crystal.⁶

Gratings provide angular dispersion for different frequencies. In SSD the gratings are used to disperse the frequencies across the beam so that each beamlet will have different instantaneous frequency.⁶ In pulse compression and expansion, a grating pair is used to produce different time delays for different frequencies in order to eliminate or provide the frequency chirp.⁴⁹⁻⁵¹ This technique is used in CPA laser system. Further application of gratings includes the spectral windowing for pulse-shaping³⁷⁻⁴⁰ and multiple pulse generation.⁴¹

C. Amplification of Phase-Modulated Laser Pulses

Classical laser pulse amplification theory has been focused on transform limit pulses so that the laser pulses are either a narrow-bandwidth long pulse or a broad-bandwidth ultrashort pulse.⁵²⁻⁵⁷ In the present case, however, the laser bandwidth comes from the phase modulation instead of the envelope. This type of broad-bandwidth long pulse not only has its own response to spectral gain narrowing and gain saturation during the amplification, but also is sensitive to any nonlinear process such as SPM, self-focusing. Initial computer work has done by D. W. Hall et al. using classical theory superposing different frequency modes in the amplifier.⁵⁷ However, it does not include all frequency modes. And more importantly, it does not involve the calculation on the angular dispersion due to phase modulation, diffraction effects, and nonlinear effects.

D. Frequency Up-Conversion of Broadband Pulses

Frequency up-conversion extends the capability of these high-power pulses. The advantage of the frequency up-conversion is two fold. First, frequency up-conversion may increase the intensity contrast of the ultrashort pulse due to its nonlinear effect.³⁵ Second, short-wavelength laser pulses offer better absorption conditions in laser-plasma interactions.^{1,59}

After the first frequency up-conversion experiment reported by Franken et al. in 1961,⁶⁰ and later the theoretical analysis presented by Armstrong et al.,⁶¹ phase velocity matching became the primary requirement to bring up the conversion efficiency. However, phase velocity matching can only increase the conversion efficiency for long pump pulses with narrow bandwidth. For broadband pulses, the wavevector-frequency dependence is

$$k = k_0 + \frac{\partial k}{\partial \omega}(\omega - \omega_0) + \frac{1}{2} \frac{\partial^2 k}{\partial \omega^2}(\omega - \omega_0)^2 + \dots,$$

where k_0 is the wavevector at the carrier frequency ω_0 . The group velocity ($=\partial\omega/\partial k$) difference between mixed light waves and the group velocity dispersion ($=\partial^2\omega/\partial k^2$) for each wave in the dispersive conversion crystal should be considered.⁶²⁻⁶⁴ Recently there are two schemes being proposed to increase the up-conversion efficiency. One method introduces a spectral angular dispersion by using gratings (and lenses) to match wavevectors for all frequencies.⁶⁵⁻⁶⁹ The other method requires the introduction of a pre-delay between two pump waves at the entrance of the type II doubling crystal to compensate the group velocity delay.^{70,35} In this research we use the later scheme for second harmonic generation in a CPA laser system.

E. Outline

This work includes the theoretical development of the amplification of broad-bandwidth, phase-modulated laser pulses for CPA and SSD, and the experimental verification using a CPA laser system. Other experiments on high-contrast ultrashort pulse generation, second harmonic conversion of picosecond pulses, and multiple wave generation for the measurement of the nonlinear refractive index are presented.

In Chapter II the propagation and compression of a broadband laser pulse in a chirped-pulse-amplification (CPA) laser is studied. Spectral gain narrowing and self-phase-modulation (SPM) are the main mechanisms that modulate the final compressed pulse temporally and spectrally. The effect of gain saturation is also investigated. Due to the large chirp of this type of laser pulse, the power gain of the amplifier can be treated as a function of instantaneous frequency to simplify the analysis. Experimental results from an Nd:glass CPA laser system are in good agreement with the theory. Both experimental and theoretical results show that SPM can play an important role determining the final shape of the compressed pulse, even at relatively low values of the cumulative B-integral, $B \lesssim 2$.

In Chapter III the pedestal associated with a chirped pulse amplification (CPA) laser is studied. Four components have been identified which contribute to the pedestal. Pulses are spectrally shaped by gain-narrowing in a frequency-matched, regenerative amplifier while avoiding self-phase modulation. The intensity contrast is further improved through the use of a saturable absorber resulting in Gaussian pulses of ~ 0.9 -ps duration with an intensity contrast exceeding $10^5:1$.

In Chapter IV experiments on the second harmonic conversion of picosecond pulses are presented. A type-II KDP crystal is used for frequency doubling of 1053 nm, 1.6-ps pulses. When a 1.46-ps delay between the extraordinary and ordinary pulses is introduced at the input of the doubling crystal, the conversion efficiency increases from near 40 to 75%. Both pedestal suppression and second harmonic generation make possible the study of high-intensity ultrashort laser plasma interactions with a fiber-grating CPA system.

In Chapter V picosecond, chirped-pulse technology is used to generate two spectrally separate, time-synchronized pulses for $\chi^{(3)}$ measurements by nearly-degenerate four-wave mixing. Near 1053 nm, nonresonant, relative measurements of $\chi_{1111}^{(3)}$ are carried out on three model substances: nitrobenzene, α -chloronaphthalene, and 4'-decyloxynaphthyl-1'-(4 decyloxy benzoate). Their $\chi^{(3)}$ values are normalized to CS₂. Theoretical analyses of Stokes and anti-Stokes generation including two-beam coupling and self-phase modulation are presented.

The amplification of SSD laser pulses is modeled in Chapter VI. Distortion of this phase-modulated pulse due to propagation and spectral gain narrowing is presented. Phase variations due to propagation and self-phase-modulation (SPM) are investigated to ensure the preservation of the initial phase modulation of the pulse. Local self-focusing of light, enhanced by the initial phase modulation, is shown to be critical for pulse amplification. For a pulse with a 3 Å bandwidth and an angular dispersion $\Delta\theta/\Delta\lambda = 500 \mu\text{rad}/\text{Å}$, the local self-focusing length can be shorter than one meter at an intensity $I = 5 \text{ GW}/\text{cm}^2$.

The main results of this work are summarized in Chapter VII. The validity of the use of the instantaneous-frequency approximation for amplification in CPA and SSD is shown in the appendix.

References

1. R. S. Craxton, R. L. McCrory, and J. M. Soures, "Progress in laser fusion," *Scientific American*, August 1986, pp 68-79; C. E. Max, "Physics of the Coronal Plasma in Laser Fusion Targets," *Physics of laser fusion Vol. I*, LLNL Report No. UCRL-53107 (1982); H. G. Ahlstrom, "Diagnostics of experiments on laser fusion targets at LLNL," *Physics of laser fusion Vol. II*, LLNL Report No. UCRL-53106 (1982).
2. R. H. Lehmberg and S. P. Obenschain, "Use of induced spatial incoherence for uniform illumination of laser fusion targets," *Opt. Comm.* **46**, 27 (1983).
3. S. P. Obenschain, J. Grun, M. J. Herbst, K. J. Kearney, C. K. Manka, E. A. McLean, A. N. Mostovych, J. A. Stamper, R. R. Whitlock, S. E. Bodner, and R. H. Lehmberg, "Laser-target interaction with induced spatial incoherence," *Phys. Rev. Lett.* **56**, 2807 (1986).
4. Y. Kato, K. Mima, N. Miyanaga, S. Arinaga, Y. Kitagawa, M. Nakatsuka, and C. Yamanaka, "Random phase of high-power lasers for uniform target acceleration and plasma-instability suppression," *Phys. Rev. Lett.* **53**, 1057 (1984).
5. T. Kessler et al., "OMEGA Phase Conversion with Distributed Phase Plate," *LLE Rev.* **33**, 1 (1987).
6. S. Skupsky, R. W. Short, T. Kessler, R. S. Craxton, S. Letzring, and J. M. Soures, "Improved Laser-Beam Uniformity Using the Angular Dispersion of Frequency-Modulated Light," *J. Appl. Phys.* **66**, 3456, (1989).

7. T. S. Luk, U. Johann, H. Egger, H. Pummer, and C. K. Rhodes, *Phys. Rev. A* **32**, 214 (1985); C. K. Rhodes, *Phys. Scr.* **T17**, 193 (1987); G. Gibson, T. S. Luk, and C. K. Rhodes, *Phys. Rev. A* **41**, 5049 (1990).
8. S. L. Chin, C. Rolland, P. B. Corkum, and P. Kelly, "Multiphoton ionization of Xe and Kr with intense 0.62- μm femtosecond pulses," *Phys. Rev. Lett.* **61**, 153 (1988).
9. M. D. Perry, A. Szöke, O. L. Landen, and E. M. Campbell, *Phys. Rev. Lett.* **60**, 1270 (1988); M. D. Perry, O. L. Landen, A. Szöke, and E. M. Campbell, *Phys. Rev. A* **37**, 747 (1988).
10. F. Yergeau, S. L. Chin, and P. Lavigne, *J. Phys. B* **20**, 723 (1987); S. L. Chin, W. Xiong, and P. Lavigne, *J. Opt. Soc. Am. B* **4**, 853 (1987); S. L. Chin and W. Xiong, in *Fundamentals of Laser Interactions II*, F. Ehlotzky, ed. (Springer-Verlag, Berlin, 1989), p.80.
11. A. L'Huillier, L. A. Lompré, G. Mainfray, and C. Manus, *J. Phys. B* **16**, 1363 (1983).
12. S. Augst, D. Strickland, D. D. Meyerhofer, S. L. Chin, and J. H. Eberly, "Tunneling ionization of noble gases in a high-intensity laser field," *Phys. Rev. Lett.* **63**, 2212, (1989); S. Augst, D. D. Meyerhofer, D. Strickland, and S. L. Chin, "Laser ionization of noble gases by Coulomb-barrier suppression," *J. Opt. Soc. Am. B* **8**, 858 (1991).
13. H. M. Milchberg, R. R. Freeman, S. C. Davey, and R. M. More, "Resistivity of a Simple Metal from Room Temperature to 10^6 K," *Phy. Rev. Lett.* **61**, 2364, (1988); H. M. Milchberg and R. R. Freeman, "Light absorption in ultrashort scale length plasmas," *J. Opt. Soc. Am. B* **6**, 1351 (1989).

14. M. M. Murnane, H. C. Kapteyn, and R. W. Falcone, "High-Density Plasmas Produced by Ultrafast Laser Pulses," *Phys. Rev. Lett.* **62**, 155 (1989).
15. J. C. Kieffer, P. Audebert, M. Chaker, J. P. Matte, H. Pepin, T. W. Johnston, P. Maine, D. D. Meyerhofer, J. Delettrez, D. Strickland, P. Bado, and G. Mourou, "Short-pulse laser absorption in very steep plasma density gradients," *Phys. Rev. Lett.* **62**, 760, (1989).
16. R. Fedosejevs, R. Ottmann, R. Sigel, G. Kühnle, S. Szatmari, and F. P. Schafer, "Absorption of femtosecond laser pulses in high-density plasma," *Phys. Rev. Lett.* **64**, 1250, (1990).
17. O. L. Landen, E. M. Campbell, and M. D. Perry, "X-ray characterization of picosecond laser plasmas," *Opt. Commun.* **63**, 253 (1987).
18. D. Kühlke, U. Herpers, and D. von der Linde, "Soft x-ray emission from subpicosecond laser-produced plasmas," *Appl. Phys. Lett.* **50** 1785 (1987).
19. C. H. Nam, W. Tighe, S. Suckewer, J. F. Seely, U. Feldman, and L. A. Woltz, "Observation of asymmetric Stark profiles from plasmas created by a picosecond KrF laser," *Phys. Rev. Lett.* **59**, 2427 (1987).
20. D.G. Stearns, O.L. Landen, E.M. Campbell, and I.H. Scofield, "Generation of Ultrashort X-Ray Pulses," *Phys. Rev. A* **37**, 1684 (1988).
21. J. A. Cobble, G. A. Kyrala, A. A. Hauer, A. J. Taylor, C. C. Gomez, N. D. Delamater, and G. T. Schappert, "Kilovolt x-ray spectroscopy of a subpicosecond-laser-excited source," *Phys. Rev. A* **39**, 454 (1989).
22. D. Strickland and G. Mourou, "Compression of amplified chirped optical pulses," *Opt. Commun.* **56**, 219 (1985).

23. P. Maine, D. Strickland, P. Bado, M. Pessot, and G. Mourou, "Generation of ultrahigh peak power pulses by chirped pulse amplification," *IEEE J. Quantum Electron.* **QE-24**, 398 (1988).
24. M. Ferray, L. A. Lompré, O. Gobert, A. L'Huillier, G. Mainfray, C. Manus, A. Sanchez, and A. S. Gomes, "Multiterawatt picosecond Nd-Glass laser system at 1053 nm," *Opt. Commun.* **75**, 278 (1990).
25. M. D. Perry, F. G. Patterson, and J. Weston, "Spectral shaping in chirped-pulse amplification," *Opt. Lett.* **15**, 381 (1990).
26. F. G. Patterson, R. Gonzales, and M. D. Perry, "Compact 10-TW, 800-fs Nd:glass laser," *Opt. Lett.* **16**, 1107 (1991).
27. K. Yamakawa, C. P. J. Barty, H. Shiraga, and Y. Kato, "Generation of a high-energy picosecond laser pulse with a high-contrast ratio by chirped-pulse amplification," *IEEE J. Quantum Electron.* **QE-27**, 288 (1991).
28. C. Sauteret, D. Husson, G. Thiell, S. Seznec, S. Gary, A. Migus, and G. Mourou, "Generation of 20-TW pulses of picosecond duration using chirped-pulse amplification in a Nd:glass power chain," *Opt. Lett.* **16**, 238 (1991).
29. K. Yamakawa, H. Shiraga, Y. Kato, and C. P. J. Barty, "Prepulse-Free 30-TW, 1-ps Nd:Glass Laser," *Opt. Lett.*, to be published.
30. M. Pessot, J. Squier, G. Mourou, and D. J. Harter, "Chirped-pulse amplification of 100-fsec pulses," *Opt. Lett.* **14**, 797 (1989).
31. J. Squier, F. Salin, and G. Mourou, "100-fs pulse generation and amplification in Ti:Al₂O₃," *Opt. Lett.* **16**, 324 (1991).
32. J. D. Kmetec, J. J. Macklin, and J. F. Young, "0.5-TW, 125-fs Ti:sapphire laser," *Opt. Lett.* **16**, 1001 (1991).

33. Y.-H. Chuang, D. D. Meyerhofer, S. Augst, H. Chen, J. Peatross, and S. Uchida, "Suppression of the pedestal in a chirped-pulse-amplification laser," *J. Opt. Soc. Am. B* **8**, 1226 (1991).
34. J. P. Heritage, R. N. Thurston, W. J. Tomlinson, A. M. Weiner, and R. H. Stolen, "Spectral windowing of frequency-modulated optical pulses in a grating compressor," *Appl. Phys. Lett.* **47**, 87 (1985).
35. Yanjie Wang and R. Dragila, "Efficient conversion of picosecond laser pulses into second-harmonic frequency using group-velocity dispersion," *Phys. Rev. A* **41**, 5645 (1990).
36. Y. Wang, B. Luther-Davies, Y.-H. Chuang, R. S. Craxton, and D. D. Meyerhofer, "Highly efficient conversion of picosecond Nd laser pulses with the use of group-velocity-mismatched frequency doubling in KDP," *Opt. Lett.* **16**, 1862 (1991).
37. J. Desbois, F. Gires, and P. Tournois, "A new approach to picosecond laser pulse analysis shaping and coding," *IEEE J. Quantum Electron.* **QE-9**, 213 (1973).
38. J. P. Heritage, A. M. Weiner, and R. N. Thurston, "Picosecond pulse shaping by spectral phase and amplitude manipulation," *Opt. Lett.* **10**, 609 (1985).
39. A. M. Weiner, J. P. Heritage, and R. N. Thurston, "Synthesis of phase-coherent, picosecond optical square pulses," *Opt. Lett.* **11**, 153 (1986).
40. R. N. Thurston, J. P. Heritage, A. M. Weiner, and W. J. Tomlinson, "Analysis of picosecond pulse shape synthesis by spectral masking in a grating pulse compressor," *IEEE J. Quantum Electron.* **QE-22**, 682 (1986).

41. Y.-H. Chuang, Z.-W. Li, D. D. Meyerhofer, and A. Schmid, "Nonresonant $\chi_{1111}^{(3)}$ obtained by nearly degenerate four-wave mixing using chirped-pulse technology," *Opt. Lett.* **16**, 7, (1991).
42. R. Adair, L. L. Chase, and S. Payne, "Nonlinear refractive-index measurements of glass using three-wave frequency mixing," *J. Opt. Soc. Am. B* **4**, 875 (1987); R. Adair, L. L. Chase, and S. Payne, "Nonlinear refractive index of optical crystals," *Phys. Rev. B* **5**, 3337 (1989).
43. G. P. Agrawal, in Nonlinear Fiber Optics, Boston: Academic Press, 1989, Ch. 4, 6, and 7.
44. H. Nakatsuka, D. Grischkowsky, and A. C. Balant, *Phys. Rev. Lett.* **47**, 910 (1981); D. Grischkowsky and A. C. Balant, *Appl. Phys. Lett.* **41**, 1 (1982).
45. R. L. Fork, C. H. Brito Cruz, P. C. Becker, and C. V. Shank, *Opt. Lett.* **12**, 483 (1987).
46. A. Yariv and P. Yeh, Optical Waves in Crystals, NY: Wiley, 1984.
47. J. Janszky, G. Corradi, and R. N. Gyuzalian, "On a possibility of analysing the temporal characteristics of short light pulses," *Opt. Commun.* **23**, 293 (1977).
48. G. Albrecht, A. Antonetti, and G. Mourou, "Temporal Shape Analysis of Nd³⁺:YAG Active Passive Mode-locked Pulses," *Opt. Commun.* **40**, 59 (1981).
49. E. B. Treacy, "Optical pulse compression with diffraction gratings," *IEEE J. Quantum Electron.* **QE-5**, 454 (1969).
50. J. D. McMullen, "Analysis of compression of frequency chirped optical pulses by a strongly dispersive grating pair," *Appl. Opt.* **18**, 737 (1979).

51. O. E. Martinez, "3000 times grating compressor with positive group velocity dispersion: Application to fiber compensation in 1.3–1.6 μm regime," *IEEE J. Quantum Electron.* **QE-23**, 59 (1987).
52. L. M. Frantz and J. S. Nodvik, "Theory of pulse propagation in a laser amplifier," *J. Appl. Phys.* **34**, 2346 (1963).
53. R. Bellman, G. Birnbaum, and W. G. Wagner, "Transmission of monochromatic radiation in a two-level material," *J. Appl. Phys.* **34**, 780 (1963).
54. J. Wittke and P. J. Warter, "Pulse propagation in a laser amplifier," *J. Appl. Phys.* **35**, 1668 (1964).
55. P. G. Kryukov and V. S. Letokhov, "Propagation of a light pulse in a resonantly amplifying (absorbing) medium," *Sov. Phys. Usp.* **12**, 641 (1970).
56. A. Içsevçi and W. E. Lamb, Jr., "Propagation of light pulses in a laser amplifier," *Phys. Rev.* **185**, 517 (1969).
57. D. W. Hall, R. A. Haas, W. F. Krupke, and M. J. Weber, "Spectral and polarization hole burning in neodymium glass lasers," *IEEE J. Quantum Electron.* **QE-19**, 1704 (1983).
58. D. W. Hall, W. F. Hagen, and M. J. Weber, "Modeling broad-band and multiple-frequency energy extraction from glass laser amplifiers," *IEEE J. Quantum Electron.* **QE-22**, 793 (1986).
59. W. Kruer, *The Physics of Laser Plasma Interactions*, Addison-Wesley, NY, Chap. 5 (1987).
60. P. A. Franken, A. E. Hill, C. W. Peters, and G. Weinreich, "Generation of optical harmonics," *Phys. Rev. Lett.* **7**, 118 (1961).

61. J. A. Armstrong, N. Bloembergen, J. Ducuing, and P. S. Pershan, "Interactions between light waves in a nonlinear dielectric," *Phys. Rev.* **127**, 1918 (1962).
62. J. A. Armstrong, S. S. Jha, and N. S. Shiren, "Some effects of group-velocity dispersion on parametric interactions," *IEEE J. Quantum Electron.* **QE-6**, 123 (1970).
63. I. V. Tomov, R. Fedosejevs, and A. A. Offenberger, "Up-conversion of subpicosecond light pulses," *IEEE J. Quantum Electron.* **QE-18**, 2048 (1982).
64. R. C. Eckardt and J. Reintjes, "Phase matching limitations of high efficiency second harmonic generation," *IEEE J. Quantum Electron.* **QE-20**, 1178 (1984).
65. V. D. Volosov, S. G. Karpenko, N. E. Kornienko, and V. L. Strizhevskii, "Method for compensating the phase-matching dispersion in nonlinear optics," *Sov. J. Quantum Electron* **4**, 1090, (1975).
66. O. E. Martinez, "Achromatic phase matching for second harmonic generation of femtosecond pulses," *IEEE J. Quantum Electron.* **25**, 2464 (1989).
67. G. Szabo and Z. Bor, "Broadband frequency doubler for femtosecond pulses," *Appl. Phys. B* **50**, 51 (1990).
68. R. W. Short and S. Skupsky, "Frequency conversion of broad-bandwidth laser light," *IEEE J. Quantum Electron.* **26**, 580 (1990).
69. M. D. Skeldon, R. S. Craxton, T. Kessler, W. Seka, R. Short, S. Skupsky, and J. M. Soures, "Efficient harmonic generation with a broadband laser," submitted to *IEEE J. Quantum Electron.*

70. M. S. Pronko, R. H. Lehmberg, S. Obenschain, C. J. Pawley, C. K. Manka, and R. Eckardt, "Efficient second harmonic conversion of broad-band high-peak-power Nd:glass laser radiation using large-aperture KDP crystals in quadrature," *IEEE J. Quantum Electron.* **26**, 337 (1990).

CHAPTER II

PROPAGATION OF LIGHT PULSES IN A CPA LASER

The propagation, amplification, and compression of a broad-bandwidth laser pulse in a chirped-pulse-amplification (CPA) laser is studied. Spectral gain narrowing and self-phase-modulation (SPM) are the main mechanisms that modulate the final compressed pulse temporally and spectrally. The effect of gain saturation is also investigated. Due to the large chirp of this type of laser pulse, the power gain of the amplifier can be treated as a function of instantaneous frequency to simplify the analysis. Experimental results from an Nd:glass CPA laser system are in good agreement with the theory. Both experimental and theoretical results show that SPM can play an important role determining the final shape of the compressed pulse, even at relatively low values of the cumulative B-integral, $B \lesssim 2$.

A. INTRODUCTION

Chirped-pulse amplification (CPA) laser systems allow the production of high-power, ultrashort pulses in solid-state lasing media.^{1,2} The technique of CPA is shown in Fig. 2-1 schematically. A laser pulse is first generated in an optical resonator. Before amplification, it is frequency chirped and temporally expanded using a fiber,³ and/or an expansion grating pair.^{4,5} The longer pulse allows more energy to be extracted from the subsequent amplifier system than would be by a short pulse. After amplification, the pulse is compressed by a compression grating pair^{6,7} to picosecond or subpicosecond duration. There is a

resulting increase in power equal to the chirped-pulse duration divided by the compressed-pulse duration.^{1,8}

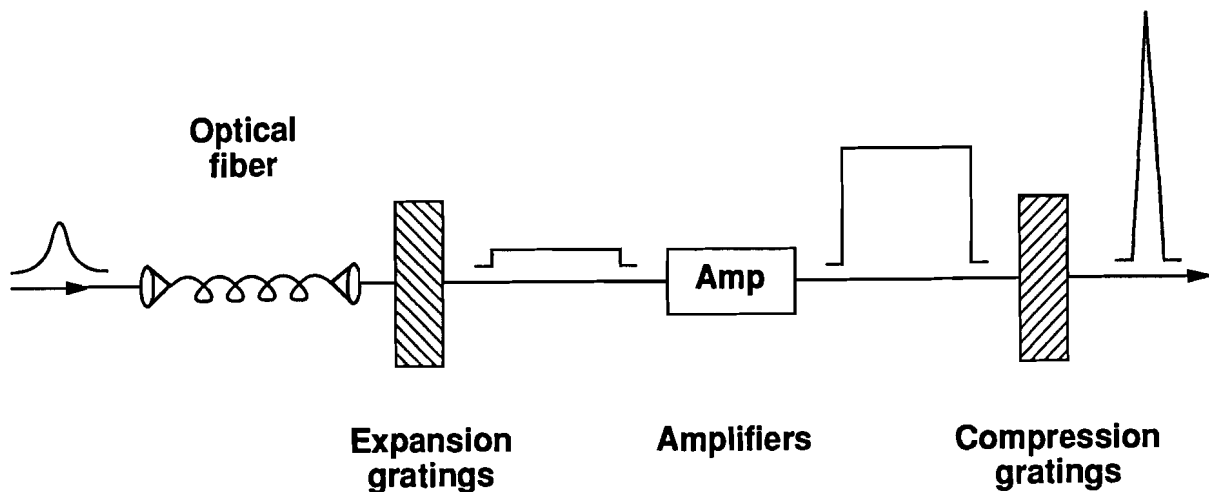


Fig. 2-1 Chirped pulse amplification technique. The optical fiber can be removed when the initial ultrashort pulse has enough bandwidth.

Gratings can be used to generate negative or positive frequency chirp as shown in Fig. 2-2. In the negative chirp scheme⁶ the ray with the longer wavelength λ_1 goes a longer distance inside a pair of parallel gratings than the ray with the shorter wavelength λ_2 . This results in an output pulse with a negative frequency chirp, that is, the frequency decreases with time. If the light goes backward, this scheme can be used as a pulse compressor for an input pulse with positive chirp. In the positive chirp scheme⁴ a telescope is placed inside an anti-parallel grating pair. This telescope relays the image of the first grating, as shown by dashed lines, to form an equivalent negative chirp scheme with negative

separation between two gratings. Therefore it gives the output pulse a positive chirp. A CPA laser system uses the latter (positive chirp) scheme for pulse expansion and the former (negative chirp) scheme, with the light going backwards, for pulse compression.

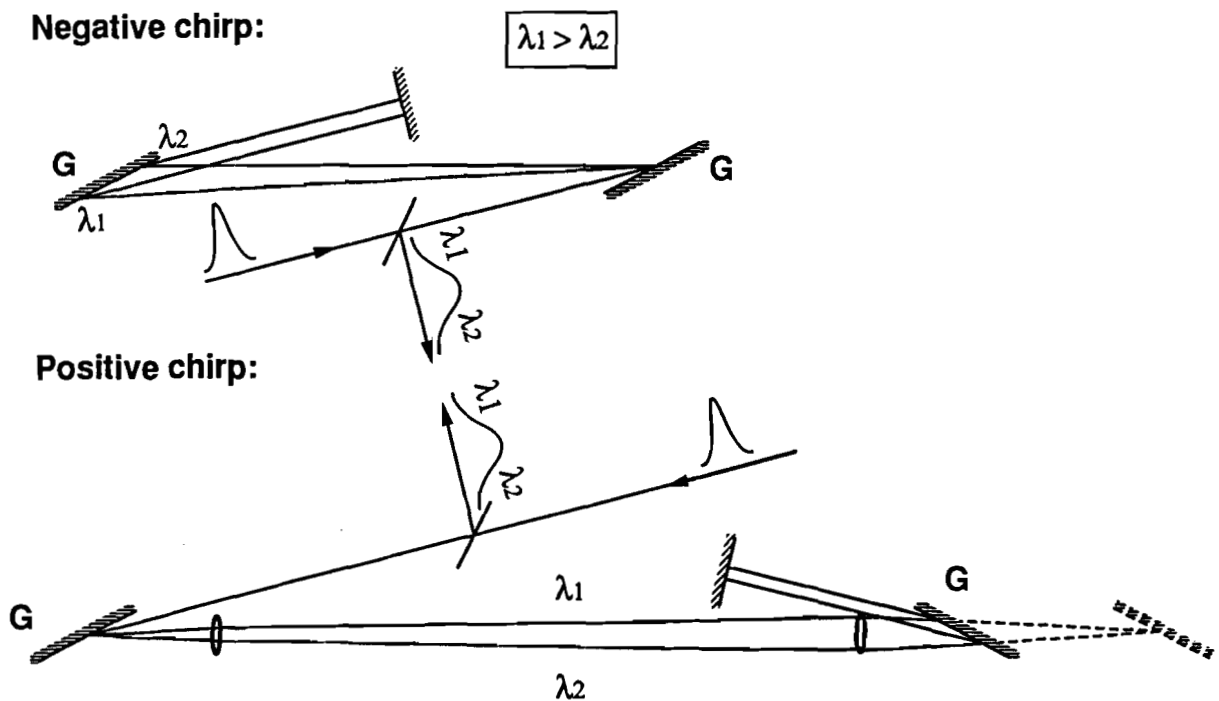


Fig. 2-2 Gratings can be used to generate negative or positive chirp. In positive chirp scheme a telescope relays the image of the first grating, as shown by dashed lines, to form an equivalent negative chirp scheme with negative separation between two gratings.

Experiments using this type of laser in high-density plasma physics,⁹ high-field atomic physics¹⁰ and nonlinear optics¹¹ have been reported. These fields are of great current interest. Detailed knowledge of the temporal shape of the ultrashort pulse is important for the analysis of experimental data. High-density plasma physics experiments, for example, require a laser pulse with high-intensity contrast. Also, short pulse x-ray conversion efficiency may be improved with an appropriate prepulse. A fully controllable pulse shape is desirable for the studies of these fields.

In this type of laser, the compressed pulse may carry a significant amount of energy which remains uncompressed. This uncompressed portion is commonly referred to as the pedestal.¹²⁻¹⁴ The sources of the pedestal will be investigated in next chapter. They are found to be the nonlinear chirp, the non-Gaussian pulse shape and the nonlinearities in the amplification process. Distortion of the frequency chirp due to self-phase-modulation (SPM) was shown to result in a large pedestal beneath the final compressed pulse¹⁴, even though the intensity profile of the chirped pulse was amplified without significant distortion. The pedestal is generated during the final pulse compression because the gratings only compress the original frequency chirp, and the new frequency chirp from SPM spreads out as low intensity pedestal due to a different group velocity dispersion. Envelope distortion of the chirped pulse due to spectral gain narrowing in the regenerative amplifier of the CPA laser system also affects the final pulse compression.¹⁵ However, one can shape the chirped pulse using spectral gain narrowing so that it compresses to a near Gaussian.^{13,16} Additional envelope distortion can occur due to frequency mismatch between the injected laser pulse and the gain center of the regenerative amplifier.^{13,14,17}

Theoretical work on chirped-pulse amplification has been mostly limited to the small signal gain (linear) regime.^{8,13,15} While the energy extraction is the main issue in a CPA laser system, nonlinearities due to high laser intensity such as gain saturation and SPM are important. For narrow-band optical pulses, gain saturation leads to pulse distortion,^{18,19} because the leading edge of the pulse undergoes higher gain than the trailing edge due to the depletion of the population inversion. In a CPA laser system the chirped pulse is a broadband long pulse, so that gain saturation and gain narrowing affecting the chirped-pulse envelope should be considered together. Furthermore, SPM should be considered as well, because it is necessary to preserve the original frequency chirp in order to produce a high-quality-compressed pulse.

The purpose of this chapter is to investigate how the amplitude and phase modulations of the chirped pulse in amplification affect the final pulse compression. In Sec. B we provide a set of basic equations that govern the chirped-pulse amplification, including gain, dispersion, and nonlinear polarization. In Sec. C, approximate solutions are obtained to give an intuitive way of understanding the amplitude and phase modulations during amplification process. A detailed analysis is given in Sec. D. The following topics are studied: (1) the power spectrum of a linearly chirped pulse, (2) pulse compression and the resulting pedestal, (3) spectral gain-narrowing in amplification process, (4) SPM induced from the amplifier, (5) the gain saturation, and (6) the results of the frequency mismatch between the center frequency of the chirped pulse and the linecenter of the amplifier, including the phase shift due to atomic response. In Sec. E we compare the theoretical results to experimental measurements using a Nd:glass regenerative amplifier. The main results of this chapter are summarized in Sec. F.

B. BASIC EQUATIONS

Since the transverse mode in the optical resonator (regenerative amplifier) is kept to 00 mode,²⁰ and the amplifiers are placed within the Rayleigh range, we can concentrate on pulse propagation in the longitudinal direction. Pulse propagation in amplifiers is governed by Maxwell's equation, which can be written in the following form

$$\frac{\partial^2 \mathbf{E}}{\partial z^2} - \frac{1}{c_0^2} \frac{\partial^2 \mathbf{E}}{\partial \hat{t}^2} = \mu_0 \frac{\partial^2}{\partial \hat{t}^2} (\mathbf{P}_L + \mathbf{P}_{NL} + \mathbf{P}), \quad (2.2.1)$$

where \hat{t} is the ordinary laboratory time frame; c_0 is the velocity of light in vacuum; \mathbf{P}_L , \mathbf{P}_{NL} , and \mathbf{P} are the linear, nonlinear polarization of the host material, and resonant polarization of the gain atoms, respectively; and \mathbf{E} is the electric field. The constitutive relations for \mathbf{P}_L and \mathbf{P}_{NL} are³

$$\mathbf{P}_L(z, \omega) + \epsilon_0 \mathbf{E}(z, \omega) = n_L^2(\omega) \epsilon_0 \mathbf{E}(z, \omega) \quad (2.2.2)$$

and

$$\mathbf{P}_{NL}(z, \hat{t}) = 2n_0 n_{2E} \langle E^2(z, \hat{t}) \rangle \epsilon_0 \mathbf{E}(z, \hat{t}), \quad (2.2.3)$$

where $\mathbf{P}_L(z, \omega)$ and $\mathbf{E}(z, \omega)$ are the Fourier transforms of $\mathbf{P}_L(z, \hat{t})$ and $\mathbf{E}(z, \hat{t})$, respectively, $n_L(\omega)$ is the linear index of refraction, $n_0 = n_L(\omega_0)$ is the linear index of refraction at the carrier frequency ω_0 , n_{2E} is the optical Kerr coefficient governing the nonlinear response, and $\langle E^2(z, \hat{t}) \rangle$ represents the time-averaged value of the field squared. In Eq. (2.2.3) the nonlinear response is assumed to be instantaneous. The resonant polarization \mathbf{P} for a homogeneously broadened two-

level gain medium is given by the following two equations, the resonant-dipole equation⁸

$$\frac{\partial^2 \mathbf{P}}{\partial \hat{t}^2} + \Delta\omega_a \frac{\partial \mathbf{P}}{\partial \hat{t}} + \omega_a^2 \mathbf{P} = -K\mathbf{N}\mathbf{E}, \quad (2.2.4)$$

and the population inversion equation⁸

$$\frac{\partial N}{\partial \hat{t}} + \frac{N - N_0}{T_1} = \left(\frac{2^*}{\hbar\omega_a} \right) \mathbf{E} \cdot \frac{\partial \mathbf{P}}{\partial \hat{t}}, \quad (2.2.5)$$

with

$$K \equiv \frac{3^* \omega_a \epsilon \lambda^3 \gamma_{\text{rad}}}{4\pi^2},$$

where $\Delta\omega_a$ is the full atomic linewidth, ω_a is the linecenter frequency, N is the population inversion, N_0 is the initial population inversion with no applied signal, T_1 is the decay time of the upper energy level, 2^* is a dimensionless population saturation factor with values between 1 and 2, depending on the gain medium,⁸ ϵ is the dielectric constant, λ is the laser wavelength in the amplifier, γ_{rad} is the purely radiative delay rate,⁸ and 3^* is the dimensionless population overlap factor for atomic interactions,⁸ with numerical value between 0 and 3. For inhomogeneously broadened gain media, the resonant polarization \mathbf{P} should be a summation of all resonant dipoles described by Eqs. (2.2.4) and (2.2.5) over all sites of population inversion N .

Equations (2.2.1) to (2.2.5) provide the general framework for light pulse propagation in homogeneously broadened two-level gain media. Since \mathbf{P}_L , \mathbf{P}_{NL} , \mathbf{P} , and \mathbf{E} are polarized in the same direction, we can drop the vector notation. Further

simplification of these equations typically includes the following steps.³ The fields can be written as

$$\begin{aligned} E(z, \hat{t}) &= \text{Re } E_0(z, \hat{t}) \exp[i(\omega_0 \hat{t} - k_0 z)] \\ P(z, \hat{t}) &= \text{Re } P_0(z, \hat{t}) \exp[i(\omega_0 \hat{t} - k_0 z)], \end{aligned} \quad (2.2.6)$$

where Re means the real part, and $k_0 \equiv n_0 \omega_0 / c_0$ is the propagation constant at carrier frequency ω_0 . The frequency-dependent wavevector $k(\omega)$ can be expanded in a Taylor series about ω_0

$$k(\omega) = \frac{\omega n_L(\omega)}{c_0} \approx k_0 + k'(\omega - \omega_0) + \frac{1}{2} k''(\omega - \omega_0)^2, \quad (2.2.7)$$

where k' and k'' are the first order and second order derivatives evaluated at ω_0 , and we have neglected losses in the gain medium. Substituting Eqs. (2.2.6), (2.2.2), and (2.2.3) into the wave Eq. (2.2.1), applying slowly varying envelope approximation (SVEA),⁸ making use of the dispersion relation (2.2.7) in frequency domain, transforming back to time domain, and introducing the moving pulse time frame

$$t = \hat{t} - k'z, \quad (2.2.8)$$

we obtain the following equation for pulse propagation in the amplifier

$$\frac{\partial E_0(z, t)}{\partial z} = -i \frac{\omega_0}{2\epsilon c} P_0(z, t) + i \frac{k''}{2} \frac{\partial^2 E_0(z, t)}{\partial t^2} - i \frac{\beta_2}{2} |E_0(z, t)|^2 E_0(z, t), \quad (2.2.9)$$

where $c = 1/k'$ is the speed of light in the amplifier, $\beta_2 \equiv 2\pi n_{2E} / \lambda_0$, and λ_0 is the laser wavelength in vacuum. Similarly, applying SVEA to Eqs. (2.2.4) and (2.2.5), we obtain

$$\frac{\partial P_0(z, t)}{\partial t} + \frac{\Delta\omega_a}{2} \left[1 + i \frac{2(\omega_0 - \omega_a)}{\Delta\omega_a} \right] P_0(z, t) = i \frac{K}{2\omega_0} N(z, t) E_0(z, t), \quad (2.2.10)$$

$$\frac{\partial N(z, t)}{\partial t} = i \frac{2^*}{4\hbar} \left[E_0^*(z, t) P_0(z, t) - E_0(z, t) P_0^*(z, t) \right], \quad (2.2.11)$$

where we have neglected the second term in Eq. (2.2.5), because the pulse width of the chirped pulse is much shorter than the decay time T_1 .

C. SOLUTIONS

In the small-signal-gain regime it is convenient to describe the pulse propagation in the Fourier domain. However, in the gain-saturation regime, time domain analysis becomes necessary. We describe both analyses below.

C.1 Frequency Domain

In the small-signal-gain regime, the population inversion N is treated as a constant, and SPM is negligible. Fourier transforming Eqs. (2.2.9) and (2.2.10), canceling $P_0(z, \omega - \omega_0)$, and integrating over amplifier length L , one can obtain the amplified chirped pulse. An advantage of the frequency domain analysis is that pulse compression (or expansion) using a pair of gratings can be described by a multiplicative phase term, $\exp[i\phi_c(\omega)]$ (or $\exp[i\phi_e(\omega)]$),^{4,6,7} with

$$\omega \equiv \omega - \omega_0.$$

By denoting the source pulse before expansion gratings as $E_0(0, \omega) = A(\omega) \exp[i\phi_s(\omega)]$, the power gain coefficient as $\alpha_r(\omega)$, the total power gain as $G(\omega) \equiv \exp[\alpha_r(\omega)L]$, and the total power loss as $1-R(\omega)$ for the CPA laser system, the final compressed pulse can be expressed as $E_0(t) = F^{-1}[E_0(\omega)]$, where F^{-1} denotes the inverse Fourier transform, and

$$E_0(\omega) = A(\omega)[R(\omega)G(\omega)]^{1/2} \exp\{i[\phi_s(\omega) + \phi_e(\omega) + \phi_a(\omega) + \phi_d(\omega) + \phi_c(\omega)]\}. \quad (2.3.1)$$

Here the phase shift due to atomic response, $\phi_a(\omega)$, and the phase shift due to the dispersion of the host material, $\phi_d(\omega)$, are defined as⁸

$$\phi_a(\omega) \equiv - \left\{ \frac{\frac{\omega - \omega_a}{\Delta\omega_a}}{1 + \left[\frac{2(\omega - \omega_a)}{\Delta\omega_a} \right]^2} \right\} \sigma_0 NL = - \frac{\omega - \omega_a}{\Delta\omega_a} \alpha(\omega) L, \quad (2.3.2)$$

$$\phi_d(\omega) \equiv - \frac{1}{2} k'' L \omega^2, \quad (2.3.3)$$

with

$$\sigma_0 \equiv K/(\epsilon c \Delta\omega_a)$$

and $\omega_a \equiv \omega_a - \omega_0$.

Equation (2.3.1) can be generalized for a laser system with multipass and multistage amplifiers by summing $\alpha_r(\omega)L$ and $\phi_a(\omega)$ over all the gain media and $\phi_d(\omega)$ over the entire laser system. In inhomogeneously broadened gain media, the power gain coefficient should be $\alpha_r = \int \sigma(\xi)N(\xi) d\xi \equiv \sigma'N$, with site parameter ξ describing spectral and polarization inhomogeneities,^{21,22} where $\sigma(\xi)$ is the atomic transition cross section of each site of atom, σ' is the effective cross section measured from experiment, and $N \equiv \int N(\xi) d\xi$.

For a CPA laser system using both expansion and compression grating pairs, one can adjust the separation and angle of the compression gratings to eliminate the quadratic and third order terms of the total phase described in Eq. (2.3.1) independently. Therefore, in the small-signal-gain regime, lower order phase variations such as dispersion $\phi_d(\omega)$ and atomic response $\phi_a(\omega)$ are not important. Furthermore if the initial power spectrum $A^2(\omega)$ is a flat top and

matches the linecenter of the amplifiers, the final power spectrum will be dominated by the line shape $G(\omega)$ due to spectral gain narrowing, and the compressed pulse will approach a Gaussian.^{13,14} However, if the spectrum has high-frequency amplitude or phase aberrations, either adjustment of gratings or spectral gain narrowing in amplification process can no longer eliminate these structures. We will discuss this later in Sub-Section D.2.

The dispersive phase $\phi_d(\omega)$ can be eliminated by adjusting $\phi_c(\omega)$, and its magnitude is usually much smaller than $\phi_c(\omega)$. This can be shown in the following numerical example in an Nd:glass CPA system: for the group velocity dispersion $k'' = 1.54 \times 10^{-26} \text{ sec}^2/\text{m}$ (Kigre, Q-98 laser glass), and a total amplification length $L = 10 \text{ m}$, $\phi_d(\omega) = -7.7 \times 10^{-26} \omega^2$. For a double-pass compression-grating pair with 1700 lines/mm, and a separation 1.5 m, $\phi_c(\omega) \approx 4.4 \times 10^{-23} \omega^2$. Therefore, for simplicity we drop this small dispersion effect in the following analysis.

C.2 Time Domain

In the time domain, we first simplify the resonant-dipole equation (2.2.10). The procedure includes solving $P_0(z, \omega)$ in the Fourier domain and transforming back to the time domain by asymptotic expansion of the integrals. The basic assumption is that the chirped-pulse duration is much longer than the dephasing time of the gain medium. This is generally true for an optical pulse with large frequency chirp because $\tau \gg (\Delta\omega_L/2)^{-1} > (\Delta\omega_a/2)^{-1} = T_2$, where τ is the half pulse width, $\Delta\omega_L$ is the laser bandwidth, and T_2 is the dephasing time. Detailed assumptions and calculations are shown in the appendix. The resulting resonant polarization is

$$P_0(z, t) = i \frac{K}{\omega_0 \Delta \omega_a} \frac{1 - i \frac{2[\omega_i(t) - \omega_a]}{\Delta \omega_a}}{1 + \left\{ \frac{2[\omega_i(t) - \omega_a]}{\Delta \omega_a} \right\}^2} N(z, t) E_0(z, t), \quad (2.3.4)$$

where $\omega_i(t)$ is the instantaneous frequency defined as the time derivative of the total light-field phase, $\omega_i(t) \equiv \partial \phi_{\text{tot}}(t) / \partial t$.

For homogeneously broadened gain media, substituting Eq. (2.3.4) into Eq. (2.2.9), one obtains

$$\frac{\partial E_0(z, t)}{\partial z} = \frac{1}{2} \{ \alpha_r[z, t, \omega_i(t)] + i \alpha_i[z, t, \omega_i(t)] \} E_0(z, t) - i \frac{\beta_2}{2} |E_0(z, t)|^2 E_0(z, t), \quad (2.3.5)$$

where the dispersion term has been dropped. The power-gain coefficient $\alpha_r[z, t, \omega_i(t)]$ is defined as

$$\alpha_r[z, t, \omega_i(t)] \equiv \frac{\sigma_0 N(z, t)}{1 + \left\{ \frac{2[\omega_i(t) - \omega_a]}{\Delta \omega_a} \right\}^2} \equiv \sigma[\omega_i(t)] N(z, t), \quad (2.3.6)$$

where $\sigma[\omega_i(t)]$ is the transition cross section as a function of the instantaneous frequency $\omega_i(t)$. The imaginary part of the power gain coefficient is defined as

$$\alpha_i[z, t, \omega_i(t)] \equiv - \frac{2[\omega_i(t) - \omega_a]}{\Delta \omega_a} \alpha_r[z, t, \omega_i(t)]. \quad (2.3.7)$$

Substituting Eq. (2.3.4) into Eq. (2.2.11) gives

$$\frac{\partial N(z, t)}{\partial t} = - \frac{2^*}{\hbar \omega_0} \sigma[\omega_i(t)] N(z, t) I(z, t), \quad (2.3.8)$$

where $I(z, t) = \epsilon c |E_0(z, t)|^2 / 2$, is the laser intensity.

For inhomogeneously broadened gain media, the pulse propagation is still described by Eq. (2.3.5), with the power-gain coefficient α_r summing over all class parameters of inhomogeneities,^{21,22}

$$\alpha_r[z, t, \omega_i(t)] = \int \sigma[\omega_i(t), \xi] N(z, t, \xi) d\xi \quad (2.3.9)$$

$$\alpha_i[z, t, \omega_i(t)] = \int \alpha_i[z, t, \omega_i(t), \xi] d\xi \quad (2.3.10)$$

The population inversion of each class $N(z,t,\xi)$ is then given by the following rate equation

$$\frac{\partial N(z, t, \xi)}{\partial t} = -\frac{2^*}{\hbar\omega_0} \sigma[\omega_i(t), \xi] N(z, t, \xi) I(z, t). \quad (2.3.11)$$

The distribution of the initial population inversion on the class parameter ξ must be known.

With the chirped pulse $E_0(0, t) = A(t) \exp[i\phi_m(t)]$ input to the amplifier, Eq. (2.3.5) is readily solved to obtain the amplified pulse in the form

$$E_0(t) = A(t)[RG(t)]^{1/2} \exp\{i[\phi_m(t) + \phi_{SPM}(t) + \phi_a(t)]\}, \quad (2.3.12)$$

where the power loss $1-R$ is added, and definitions

$$G(t) \equiv \exp\left\{ \int \alpha_r[z, t, \omega_i(z, t)] dz \right\} \quad (2.3.13)$$

$$\phi_{SPM}(t) \equiv -\left(\frac{2\pi}{\lambda_0}\right) n_2 \int I(z, t) dz \equiv -B \quad (2.3.14)$$

$$\phi_a(t) \equiv \frac{1}{2} \int \alpha_i[z, t, \omega_i(z, t)] dz \quad (2.3.15)$$

represent the power gain, the phase variation due to SPM, and the phase variation due to atomic response, respectively. In Eq. (2.3.14) we have used the identity,

$n_{2E}\langle E^2 \rangle = n_{2E} |E_0|^2/2 = n_2 I$, and we also related the phase variation ϕ_{SPM} to the so-called B-integral for a multipass laser system as a cumulative measure of the nonlinear interaction.

Equation (2.3.12) can be used to describe the final chirped pulse leaving multipass and multistage amplifiers by extending the integrals in Eqs. (2.3.13)–(2.3.15) over all amplifiers. Numerical methods are generally needed to solve these integrals because the instantaneous frequency $\omega_i(t) = \omega_0 + \partial/\partial t [\phi_m(t) + \phi_{\text{SPM}}(t) + \phi_a(t)]$ is also a function of pulse propagation. Since we are not interested in large phase variations occurring in the CPA process, we can make the reasonable assumption, $\omega_i(t) \approx \omega_0 + \partial\phi_m(t)/\partial t$ in the pulse propagation to see the influence of small phase variations on CPA lasers. With this assumption, and in the small-signal-gain regime, Eqs. (2.3.13)–(2.3.15) become

$$G(t) = \exp\{\alpha_r[\omega_i(t)]L\} \quad (2.3.16)$$

$$\phi_{\text{SPM}}(t) \equiv -\left(\frac{2\pi}{\lambda_0}\right) n_2 \frac{G(t) - 1}{\alpha_r[\omega_i(t)]} I_{\text{in}}(t) \quad (2.3.17)$$

$$\phi_a(t) = \frac{1}{2} \alpha_i[\omega_i(t)]L, \quad (2.3.18)$$

where $I_{\text{in}}(t)$ is the intensity of the input pulse.

D. ANALYSIS

Detailed analyses and numerical examples of CPA will be presented in this section. The initial chirped pulse is chosen in the form

$$E_0(t) = A \exp\left[-\frac{1}{2}\left(\frac{t}{\tau}\right)^{2m}\right] \exp\left\{i\left[\frac{1}{2}b\left(\frac{t}{\tau}\right)^2 + \phi_{\text{NL}}(t)\right]\right\}, \quad (2.4.1)$$

where τ is the half pulse width at e^{-1} intensity point, $b \approx \Delta\omega_L\tau/2$ defines the amount of linear chirp, and $\phi_{NL}(t) = O[(t/\tau)^3]$ represents the possible nonlinear frequency chirp generated from the optical fiber or expansion gratings. The envelope of the chirped pulse

$$A(t) = A \exp[-(t/\tau)^{2m}/2]$$

can be either Gaussian ($m = 1$), or super-Gaussian ($m > 1$). The former may be obtained by using a pair of expansion gratings to stretch an ultrashort pulse that is directly produced from an optical oscillator. The latter may be obtained from a pulse coupled into an optical fiber and chirped into a broadband long pulse due to both SPM and group-velocity-dispersion. The time derivative of the initial phase variation, $\partial\phi_m(t)/\partial t = bt/\tau^2 + \partial\phi_{NL}(t)/\partial t$, describes the frequency chirp of the input pulse.

D.1 Power Spectrum

Applying the Fourier transform to a linearly chirped pulse, $E_0(t) = A(t)\exp[i\pi b(t/\tau)^2/2]$, and performing simple algebra we can obtain the spectrum in the form

$$E_0(\omega) = \exp\left[-i\frac{\omega^2\tau^2}{2b}\right] \int A(t) \exp\left[i\frac{b}{2}\left(\frac{t}{\tau} - \frac{\omega\tau}{b}\right)^2\right] dt. \quad (2.4.2)$$

The integral in the right hand side of Eq. (2.4.2) has a similar form to Huygens' integral in the Fresnel approximation. This approximation is commonly used in diffraction theory. For light with wavelength λ , the diffracted field located at a distance z away from the source is given by⁸

$$E(x) = \frac{1}{\sqrt{\lambda z}} \exp\left[i\left(\frac{2\pi z}{\lambda} - \frac{\pi}{4}\right)\right] \int E(x') \exp\left[i\frac{\pi a^2}{\lambda z}\left(\frac{x'}{a} - \frac{x}{a}\right)^2\right] dx', \quad (2.4.3)$$

where a , the half-aperture width, is added here for comparison. Aside from the multiplicative factors preceding both integrals, the two expressions in Eqs. (2.4.2) and (2.4.3) are similar with the chirp parameter b equal to 2π times the Fresnel number $N_f \equiv a^2/\lambda z$ in the diffraction analogy. Just as the power spectrum of a Fourier-transform-limited optical pulse can be compared to Fraunhofer diffraction, the power spectrum of a linearly chirped pulse can be compared to Fresnel diffraction.

Following Eq. (2.4.2), the power spectrum of the amplified chirped pulse from Eq. (2.3.12), is proportional to

$$\left| \int A(t) [RG(t)]^{1/2} \exp\{i[\phi_{NL}(t) + \phi_{SPM}(t) + \phi_a(t)]\} \exp\left[i\frac{b}{2}\left(\frac{t}{\tau} - \frac{w\tau}{b}\right)^2\right] dt \right|^2. \quad (2.4.4)$$

The transformation from the time domain to frequency domain is similar to Fresnel diffraction, as shown in Fig. 2-3(a). The initial pulse envelope is similar to the light source. The net power gain $RG(t)$ which shapes the source pulse is similar to an amplitude modulator. Phase variations $\phi_{NL}(t)$, $\phi_{SPM}(t)$, and $\phi_a(t)$ which affect the power spectrum are similar to phase modulators. The chirp parameter, b , which behaves like the Fresnel number, is quite large in CPA lasers (for example, $b = 300$), and thus the power spectrum is analogous to the near-field diffraction pattern of the pulse envelope.

D.2 Pulse Compression and Pedestal

For a pulse with large frequency chirp, pulse compression is performed by using a pair of gratings to eliminate the phase term, $\exp[-iw^2\tau^2/(2b)]$, in Eq. (2.4.2). Applying the inverse Fourier transform to this spectrum and using the

amplified chirped pulse described by Eq. (2.3.12), we can obtain the compressed pulse

$$E_0(t) = \left[i \frac{b}{2\pi\tau^2} \right]^{1/2} \exp \left[-i \frac{b}{2} \left(\frac{t}{\tau} \right)^2 \right] \cdot \int A(t') [RG(t')]^{1/2} \exp \{ i [\phi_{NL}(t') + \phi_{SPM}(t') + \phi_a(t')] \} \exp \left[i \frac{btt'}{\tau^2} \right] dt'. \quad (2.4.5)$$

From Eq. (2.4.5), one can see that aside from the multiplicative factors preceding the integral the compressed pulse is a Fourier transform of the chirped-pulse.⁶ As shown in Fig. 2-3(b), this is analogous to focusing a beam (one transverse dimension) so that the focal spot is the Fourier transform of the input beam spatial profile. Again, the net power gain $RG(t)$ plays the role as an amplitude modulator and the phase variations $\phi_{NL}(t) + \phi_{SPM}(t) + \phi_a(t)$ play as phase modulators. These amplitude and phase modulations either distort the compressed pulse (low-frequency perturbations) or scatter the light to form a background pedestal (high-frequency perturbations). Low-frequency perturbations can be compensated by adjustment of compression gratings. This is similar to a compensating lens used to correct the low-spatial-frequency beam perturbations. For high-frequency perturbations, a fast temporal filter during pulse compression is important. This is the same when focusing a beam, one can use an pinhole as a spatial filter to eliminate the high-spatial-frequency beam perturbations. A saturable absorber has recently been used as this type of temporal filter (see Chap III).

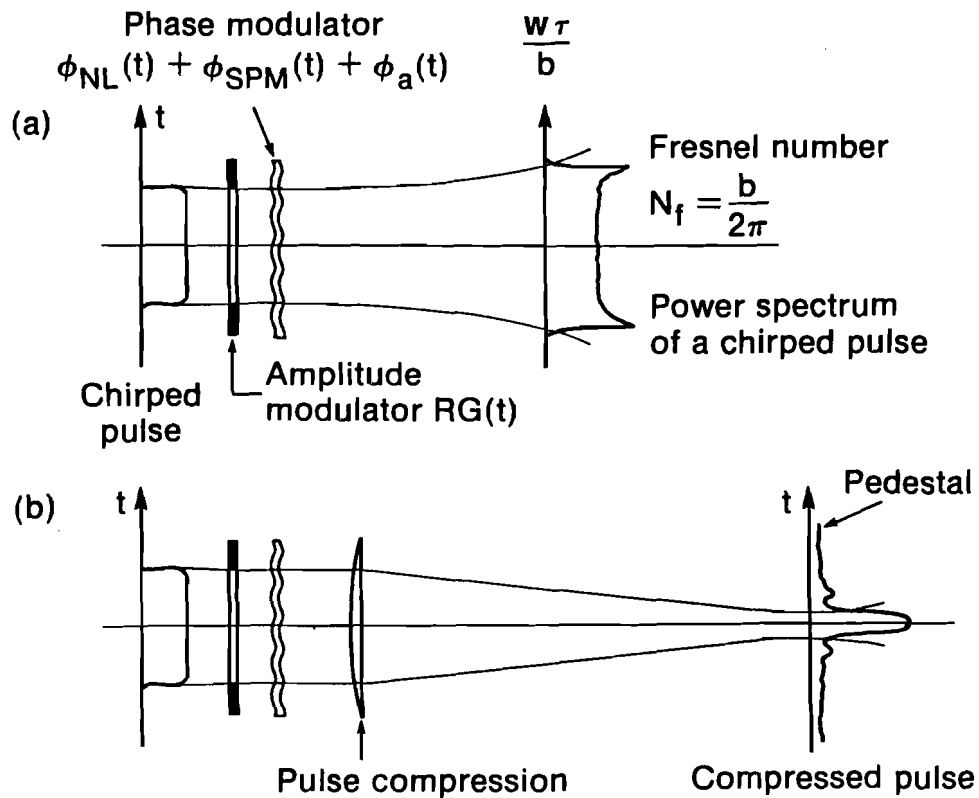


Fig. 2-3 A schematic of diffraction analogy shows spectral and temporal modulations in CPA lasers. The net power gain $RG(t)$ is similar to an amplitude modulator. Phase variations $\phi_{NL}(t) + \phi_{SPM}(t) + \phi_a(t)$ are similar to the phase modulators. (a) The power spectrum is analogous to the near-field beam profile. (b) The intensity profile of a compressed pulse is analogous to the beam profile of a focal spot (far-field). The background pedestal is a result of scattered light spreading over a wide range depending on the nature of amplitude and phase aberrations.

D.3 Gain Narrowing

To explain the amplitude modulation by spectral gain narrowing, we begin the amplified chirped pulse from Eq. (2.3.12), with an initial pulse described by Eq. (2.4.1). When the bandwidth of the applied signal $\Delta\omega_L$ is much smaller than the atomic linewidth of the gain medium $\Delta\omega_a$, the gain coefficient can be simplified to a quadratic form, $\alpha_r[\omega_i(t)] = \alpha_0 - (\alpha''/2)[\omega_i(t) - \omega_a]^2 \approx \alpha_0 - (\alpha''/2)(\omega_0 + bt/\tau^2 - \omega_a)^2$, where $\alpha'' = -d^2\alpha_r(\omega)/d\omega^2$ evaluated at midband frequency ω_a . In the frequency-matched case, $\omega_0 = \omega_a$, the total-power gain in the small-signal regime is

$$G(t) = G_0 \exp\left(-\frac{t^2}{\tau_{\text{eff}}^2}\right), \quad (2.4.6)$$

where $G_0 \equiv \exp(\alpha_0 L)$ is the small-signal power gain at midband, and $\tau_{\text{eff}} \equiv (2\tau^4/\alpha'' L b^2)^{1/2}$ represents the half-width of the gain curve.

A suitable pulse-shaping is accomplished when τ_{eff} is smaller than the half width (at e^{-1} intensity point) of the input chirped pulse τ , with gain-center match. In this case τ_{eff} represents the shortened half-width (at e^{-1} intensity point) of the amplified chirped pulse. With reasonable estimations $b \approx \tau\Delta\omega_L/2$ and $\alpha'' \approx 8\alpha_0/(\Delta\omega_a)^2$, which is exact for a Lorentzian gain profile, the inequality $\tau_{\text{eff}} < \tau$ becomes

$$\alpha_0 L > (\Delta\omega_a/\Delta\omega_L)^2, \quad (2.4.7)$$

where $\Delta\omega_L$ is the full bandwidth of the laser pulse, and $\Delta\omega_a$ is the atomic line width of the gain medium. If SPM is still negligible, the applied signal becomes a Gaussian pulse, which can then be compressed to a Fourier-transform-limited

pulse with half-width (at 1/e intensity point) approximately equal to $(\tau/\tau_{\text{eff}})(\tau/b)$ in the large-chirp limit $b/(\tau^2/\tau_{\text{eff}}^2) \gg 1$. The factor τ/τ_{eff} is the pulse broadening ratio for the compressed pulse, which is equal to the pulse shortening ratio of the chirped pulse in the amplifier due to the gain-narrowing effect. The power spectrum of this Gaussian pulse in the large-chirp assumption is proportional to $\exp[-(\tau^4 / b^2 \tau_{\text{eff}}^2)(\omega - \omega_0)^2] = \exp[-1/2 \alpha'' L(\omega - \omega_0)^2]$, which is exactly the line shape $G(\omega)^M$, as expected.^{13,14}

To illustrate the gain-narrowing, Fig. 2-4(a) shows the power spectra for different gain-narrowing conditions, $\tau/\tau_{\text{eff}} = 0, 1, 2,$ and 3 , with parameters $\lambda_0 = 1053$ nm, $\tau = 75$ ps, $m = 25$, $b = 236$, and a small amount of nonlinear phase variation $\phi_{\text{NL}}(t) = -(t/\tau)^3 - 4(t/\tau)^4$. The bandwidth for the initial pulse ($\tau/\tau_{\text{eff}} = 0$) is 37 \AA (FWHM), and this power spectrum looks like a diffraction pattern from a slit as explained in Fig. 2-3(a). The term $-(t/\tau)^3$ makes the spectrum asymmetric, and the term $-4(t/\tau)^4$ makes the spectrum more peaked near the two edges. Figure 2-4(b) shows the corresponding intensity profiles of the compressed pulses. For $\tau/\tau_{\text{eff}} = 0$ case, the compressed pulse width is 1.6 ps (FWHM) and the gross pedestal is the result of its original chirped pulse profile (nearly square top) and the nonlinear chirp. For other cases, the pedestal is significantly suppressed by spectral gain-narrowing.

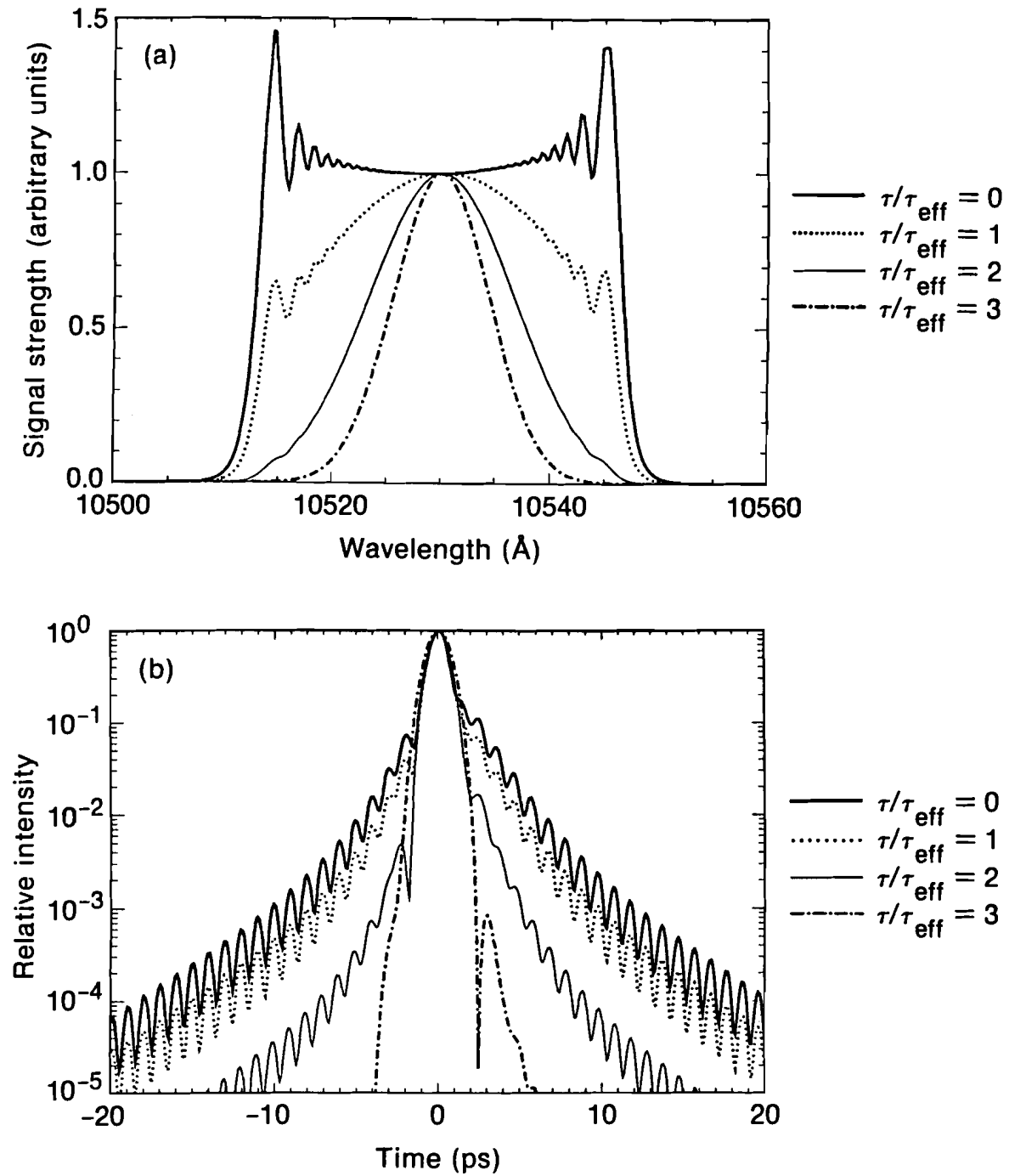


Fig. 2-4 (a) Power spectra for different spectral gain-narrowing conditions, $t/\tau_{\text{eff}} = 0, 1, 2,$ and 3 . They approach Gaussian in large gain narrowing limit. (b) The intensity profiles of compressed pulses. Pedestal suppression by spectral gain narrowing is shown.

D.4 Self-Phase Modulation

As depicted in Eq. (2.3.14), the laser pulse experiences a time-varying phase modulation, $\phi_{\text{SPM}}(t)$, produced by the intensity variation of the pulse itself. The new frequency chirp, $\Delta\omega_{\text{SPM}} = \partial\phi_{\text{SPM}}(t)/\partial t = -(2\pi/\lambda_0) \int n_2 \partial I/\partial t dz$, adds to the original linear frequency chirp of the laser pulse and changes the laser power spectrum. Since the additional frequency chirp has different group velocity delay than that of the linear chirp in the compression stage, it introduces a background pedestal to the compressed pulse. When a sharp change in the pulse envelope occurs, the induced phase variation $\phi_{\text{SPM}}(t)$ also change sharply. Thus, the background pedestal increases significantly even when the peak phase variation due to SPM is relatively small. This is similar to a phase plate, which diffracts light significantly at a sharp change in thickness, even for a small phase change. The maximum frequency shift occurs at the points of maximum slope of intensity $I(t)$ or maximum $dI(t)/dt$. Thus, the added frequency chirp for a super-Gaussian pulse is nearly m times higher than for a Gaussian pulse ($m = 1$). Gain-narrowing in the amplifier that reshapes the pulse to a near Gaussian can reduce $\Delta\omega_{\text{SPM}}$.

To illustrate the roles of SPM in a CPA laser, Fig. 2-5(a) shows the intensity profiles of ultrashort pulses compressed from chirped Gaussian pulses ($m = 1$, $\tau = 100$, $b = 200$) under a variety of SPM conditions, i.e., peak B-integral values $B = 0, 2, 4, 6$. Figure 2-5(b) shows the intensity profiles of ultrashort pulses compressed from chirped super-Gaussian pulses ($m = 5$, $\tau = 100$, $b = 200$) under the same SPM conditions as for Fig. 2-5(a). In both figures changes in the pulse shape are clearly shown. Note that because of the group velocity delay in grating pairs, the new frequency chirp $\Delta\omega_{\text{SPM}}$ determines the width of the pedestal. The energy associated with the pedestal is determined by the fraction of

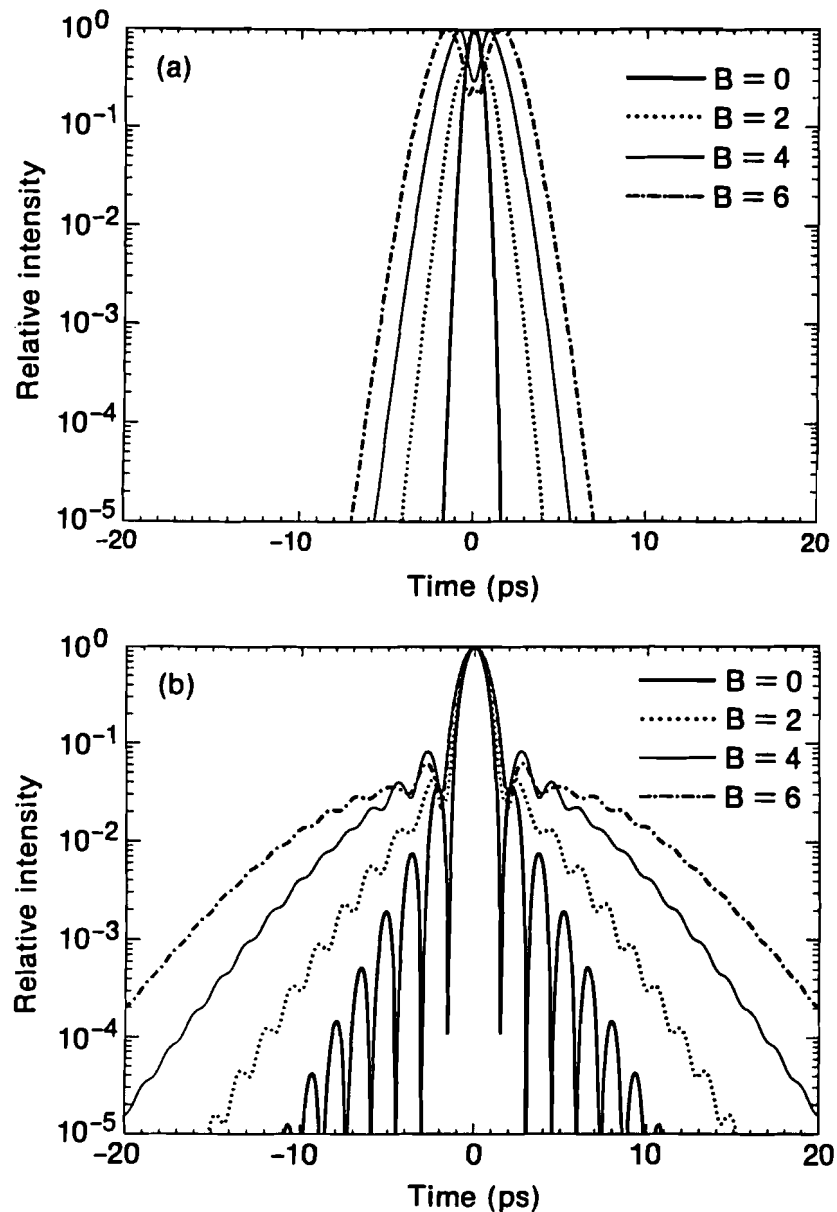


Fig. 2-5 (a) Intensity profiles of ultrashort pulses compressed from chirped Gaussian pulses ($m = 1$, $\tau = 100$, $b = 200$) under a variety of SPM conditions, i.e., peak B-integral values $B = 0, 2, 4, 6$. The compressed pulses become wider and have bumpy structures as B increases. (b) Intensity profiles of ultrashort pulses compressed from chirped super-Gaussian pulses ($m = 5$, $\tau = 100$, $b = 200$). The compressed pulses have wider pedestal as B increases.

the pulse energy near the maximum of $\partial I/\partial t$. In the case of a super-Gaussian pulse of high order, only a small fraction of the pulse energy is in the region of large $\partial I/\partial t$, whereas for a Gaussian pulse ($m = 1$), a much larger fraction of the pulse energy is contained within the region of large $\partial I/\partial t$. Thus, for a Gaussian pulse, while the added frequency chirp may be smaller than for a super-Gaussian pulse, the effect may be as important because of the larger amount of energy involved. These B-integral values can occur quite easily in a multiple-pass regenerative amplifier operating near gain saturation.²³ For example, a laser pulse at $\lambda_0 = 1053$ nm with peak intensity equal to 1 GW/cm^2 traveling through an amplifier with the nonlinear index of refraction $n_{2E} = 1.2 \times 10^{-13}$ esu (for Nd^{+3} -doped phosphate-glass Q98), and with the amplifier length $L = 115$ mm, the peak SPM is equal to 0.22. Thus, at this intensity level, a laser pulse can accumulate a significant amount of SPM in several passes through the amplifier, and the resulting new frequency chirp will increase the pedestal of the compressed pulse.

D.5 Gain Saturation

In gain saturation regime, both gain narrowing and gain saturation distort the chirped pulse. The former is a function of the atomic transition cross section $\sigma[\omega_i(t)]$. The latter is a function of the population inversion $N(z, t)$. For homogeneously broadened gain media, pulse propagation Eq. (2.3.5) can be written in the form

$$\frac{\partial I(z, t)}{\partial z} = \alpha_r[z, t, \omega_i(t)] I(z, t) = \sigma[\omega_i(t)] N(z, t) I(z, t). \quad (2.4.8)$$

This equation and the population inversion Eq. (2.3.8) govern the gain saturation. Combining both equations, one can obtain the energy conservation equation in the following form

$$\frac{\partial N(z, t)}{\partial t} = -\frac{2^*}{\hbar\omega_0} \frac{\partial I(z, t)}{\partial z}. \quad (2.4.9)$$

By integrating Eq. (2.4.9) over the amplifier length, and defining the total inverted population per amplifier area as

$$N_{\text{tot}}(t) \equiv \int_0^L N(z, t) dz, \quad (2.4.10)$$

Eq. (2.4.9) becomes

$$\frac{\partial N_{\text{tot}}(t)}{\partial t} = -\frac{1}{\sigma_0 U_{\text{sat}}} [I_{\text{out}}(t) - I_{\text{in}}(t)] = -\frac{I_{\text{in}}(t)}{\sigma_0 U_{\text{sat}}} \left(\exp\{ \sigma[\omega_i(t)] N_{\text{tot}}(t) \} - 1 \right), \quad (2.4.11)$$

where $U_{\text{sat}} \equiv \hbar\omega_0/(2^*\sigma_0)$ is the saturation fluence,⁸ and we have used the relation $I_{\text{out}}(t) = I_{\text{in}}(t)G(t) = I_{\text{in}}(t) \exp\{ \sigma[\omega_i(t)]N_{\text{tot}}(t) \}$. Equation (2.4.11) has to be solved numerically. However, for the special case that gain narrowing is not significant during gain saturation, by making the assumption $\sigma[\omega_i(t)] = \sigma(\omega_0)$, one can solve Eq. (2.4.11) analytically in the usual form¹⁵

$$\sigma N_{\text{tot}}(t) = -\ln \left\{ 1 - \left(1 - \frac{1}{G_0} \right) \exp \left[-\frac{U_{\text{in}}(t)}{U_{\text{sat}}} \right] \right\}. \quad (2.4.12)$$

Here G_0 is the small signal power gain at frequency ω_0 , and $U_{\text{in}}(t) \equiv \int_{-\infty}^t I_{\text{in}}(t') dt'$ is the input laser fluence.

For inhomogeneously broadened gain media, the pulse propagation Eq. (2.3.5) can be written as

$$\frac{\partial I(z, t)}{\partial z} = \alpha[z, t, \omega_i(t)] I(z, t) = \int \sigma[\omega_i(t), \xi] N(z, t, \xi) d\xi I(z, t). \quad (2.4.13)$$

To fully understand the gain saturation in the inhomogeneously broadened gain media, one needs to use numerical method to solve the pulse propagation Eq. (2.4.13) and the population inversion Eq. (2.3.9) simultaneously, with the distribution for inhomogeneities $N(z, t, \xi) = f(\xi)N(z, t)$.

For Nd:phosphate glasses, gain saturation can be approximately described by homogeneous theory.^{21,22} Figure 2-6 shows a linearly-chirped super-Gaussian pulse $I_{in}(t) = I_0 \exp[-(t/\tau)^{10}]$ undergoing both gain narrowing and gain saturation in an amplifier, with $\tau I_0/U_{sat} = 0.002$, $G_0 = 200$ and different bandwidth ratios $\Delta\omega_L/\Delta\omega_a = 0, 0.2, \text{ and } 0.5$. Figure 2-6(a) shows the calculation result of the depletion of the total population inversion from Eq. (2.4.11). Since CPA with larger bandwidth ratio causes higher degree of gain narrowing and chirped-pulse shortening, the depletion of the population inversion decreases as the bandwidth ratio increase. For $\Delta\omega_L/\Delta\omega_a = 0$ case, the calculation result can be obtained directly from Eq. (2.4.12). The amplified chirped pulses are shown in Fig. 2-6(b). A pulse under the small-signal-gain and without gain narrowing is shown as reference. Gain saturation tends to pull the chirped pulse toward its leading edge. Frequency-matched gain narrowing tends to shrink the chirped pulse toward the center. The balance of both mechanisms determines the final intensity profile of the chirped pulse.

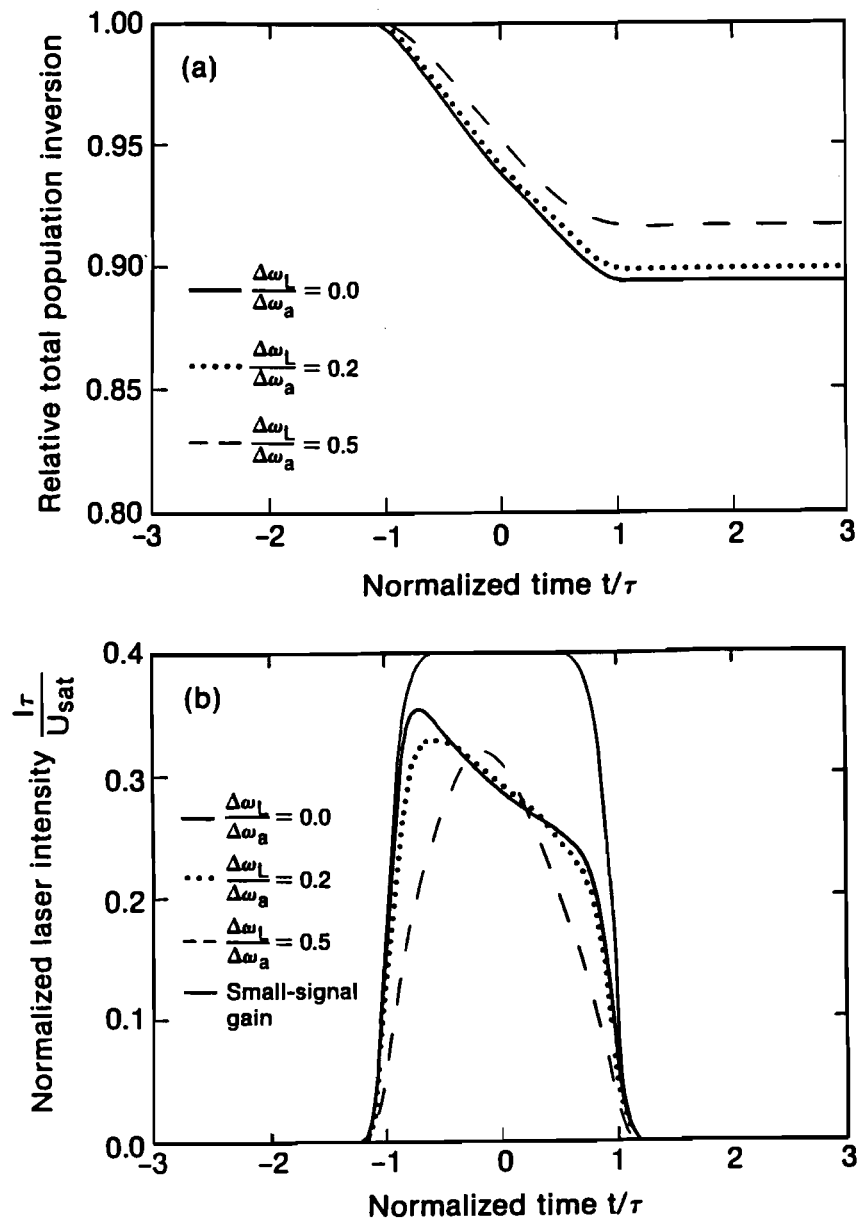


Fig. 2-6 (a) Relative total population inversion in gain saturation regime with different gain narrowing conditions, $\Delta\omega_L/\Delta\omega_a = 0, 0.2, 0.5$. (b) Amplified chirped pulses under different gain narrowing conditions with an input super-Gaussian pulse, $m = 5$, $I_{\text{in}}\tau/U_{\text{sat}} = 0.002$, and a small-signal gain $G_0 = 200$.

D.6 Frequency Mismatch

If a frequency mismatch exists between the carrier frequency of the seed pulse and the linecenter of the amplifier, i.e., $\omega_0 \neq \omega_a$, the small-signal power gain becomes

$$G(t) = G_0 \exp\left[-\frac{(t - t_0)^2}{\tau_{\text{eff}}^2}\right], \quad (2.4.14)$$

where $t_0 = \tau^2(\omega_a - \omega_0)/b \approx 2(\omega_a - \omega_0)\tau/\Delta\omega_L$. In the case of a chirped pulse generated from the optical fiber, one of the sharp edges of the super-Gaussian pulse (which also carries a higher order nonlinear chirp) cannot be suppressed sufficiently through gain narrowing. Thus, the pulse-shaping is poor and frequency distortion due to SPM remains strong at the sharp edge.

In Eq. (2.3.5) the imaginary part of the gain coefficient α_i occurring from frequency mismatch describes the phase shift (per distance) due to the resonant dipoles. In gain-saturation regime the reactive phase shift for a homogeneously broadened gain medium is

$$\phi_a(t) = -\frac{\phi'_m(t) + \omega_0 - \omega_a}{\Delta\omega_a} \sigma(t) N_{\text{tot}}(t), \quad (2.4.15)$$

where $\phi'_m(t) \equiv \partial\phi_m(t)/\partial t$, and Eqs. (2.3.15), (2.4.10) have been used. The total population inversion $N_{\text{tot}}(t)$ in Eq. (2.4.15) is obtained from solving Eq. (2.4.11). Therefore, $\phi_a(t)$ is a function of the applied laser intensity. This phase variation may become significant as to affect the pulse compression, if the frequency mismatch is large.

E. EXPERIMENTS ON SELF-PHASE MODULATION

In this section we present experimental data and calculated results using an Nd:glass regenerative amplifier as an example to explain the possible SPM encountered in CPA. The details of this CPA laser system will be described in the next chapter. Here we introduce the experimental setup related to SPM. The initial chirped pulse is prepared as follows. A train of 1053-nm, 50-ps pulses is generated from a cw-pumped mode-locked Nd:YLF oscillator. These pulses are coupled into a 800-m-long single-mode optical fiber to produce bandwidth and a frequency chirp due to the SPM and the group velocity dispersion. They are further stretched by expansion gratings (1700 lines/mm) with an effective separation of 1.4 meters. One of the pulses in the train is selected and seeded into the regenerative amplifier. The chirped pulse is amplified from approximately 1 nJ to 1 mJ. The power spectrum and the temporal shape of the chirped pulse are simultaneously measured by a spectrometer and a streak camera.

Experiments on SPM are quite well explained in Fig. 2-5: for Gaussian chirped pulses the compressed pulses broaden as SPM increases, and for chirped pulses with sharp changes in their envelopes such as super-Gaussian pulses the compressed pulses enhance their background pedestals as SPM increases. The distortion of the power spectrum due to SPM should not be significant because of the already existent large phase modulation in the chirped pulse. However, in some experimental cases strong distortion of the power spectra have been observed.

To explain the strong spectral distortion, there are two kinds of seeded chirped pulses were used in this experiment: (i) pulses with a 445-ps pulse width stretched by expansion gratings from pulses leaving the optical fiber which have a

pulse width of 147 ps and a bandwidth of 35 Å. (ii) Pulses with a 290-ps pulse width stretched from pulses leaving the optical fiber that have a pulse width of 110 ps and a bandwidth of 20 Å. The theoretical model begins from the super-Gaussian pulse (2.4.1) after the fiber with $m = 10$, $\tau = 74$ ps, $b = 219$, and $\phi_{NL}(t) = -(t/\tau)^3 - 3(t/\tau)^4$ for case (i), and with $m = 10$, $\tau = 55$ ps, $b = 93$, and same $\phi_{NL}(t)$ for case (ii). Then, in Fourier domain, both quadratic and third-order-phase variations are used to describe the expansion gratings,⁷ that is, $\phi_e(w) = -3.8 \times 10^{-23} w^2 + 4 \times 10^{-37} w^3$. A simple Gaussian net-power-gain $R(w)G(w)$ is used to describe the amplified chirped pulse in small-signal-gain regime. The total power gain is $G_0=10^{45}$, and the amplifier bandwidth is 210 Å (FWHM). The SPM calculation is performed in time domain using Eqs. (2.3.12) and (2.3.14).

Figure 2-7 shows the calculated and measured initial temporal pulse shape of case (ii). The peaked edges of the chirped pulse are a result of the stretching in the expansion gratings. These two peaked edges are the potential places for SPM to occur and generate a higher frequency chirp, and may form the pedestal of the compressed pulse. For case (i) the edges of stretched chirped pulses are less peaked. Generally speaking, the stretched pulse with large frequency chirp will have less sharply peaked edges.

Figure 2-8 shows the calculated and measured amplified temporal pulse shape in different experimental conditions. Figure 2-8(a) shows the amplified chirped pulse of case (i). The chirped pulse initially has a pulse energy of 1 nJ, and is amplified to 1 mJ. Spectral gain narrowing shapes the pulse to Gaussian. Figure 2-8(b) shows amplified chirped pulse of case (ii). It retains peaked edges because the spectral gain narrowing is less significant for the pulse with a smaller bandwidth ratio, $\Delta\omega_L/\Delta\omega_a$. Figure 2-8(c) shows the amplified temporal pulse

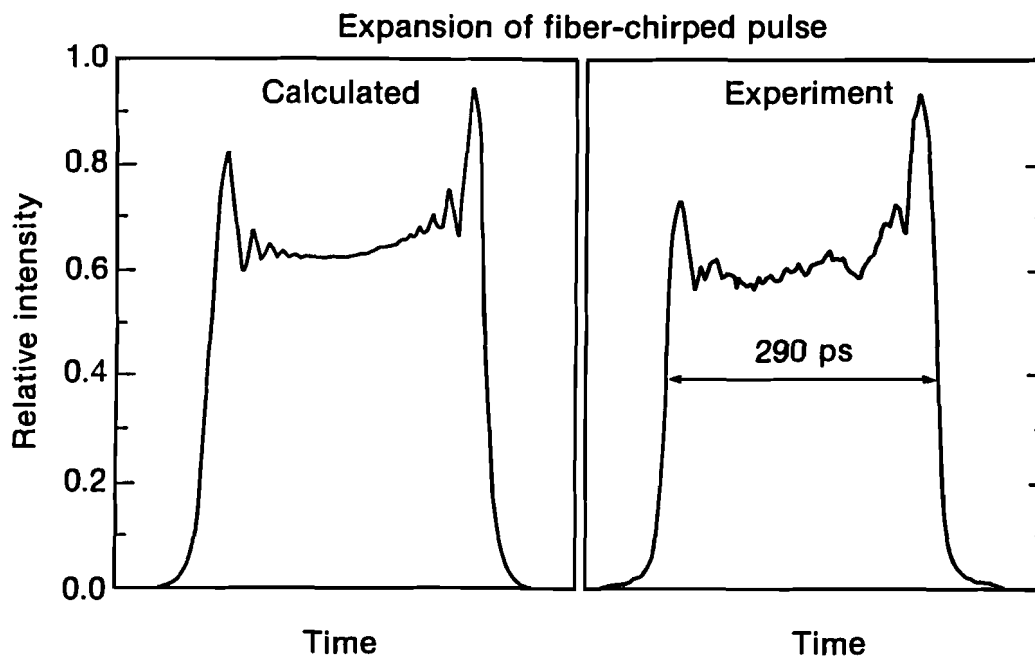


Fig. 2-7 Calculated and measured initial temporal pulse shape with a 290-ps pulse width and a 20-Å bandwidth. The peaked edges of the chirped pulse is a result of using expansion gratings [$\phi_e(w) = -3.8 \times 10^{-23} w^2 + 4 \times 10^{-37} w^3$].

shape of case (ii) with a gain-center offset about 5 Å. One of the peaked edge is suppressed by gain narrowing, but the other is not. The gain center of the regenerative amplifier is adjusted by tuning the frequency dependent loss associated with the voltage of the Q-switching Pockels' cell. SPM changes the phase but not the amplitude of the pulse and hence does not change the temporal shape.

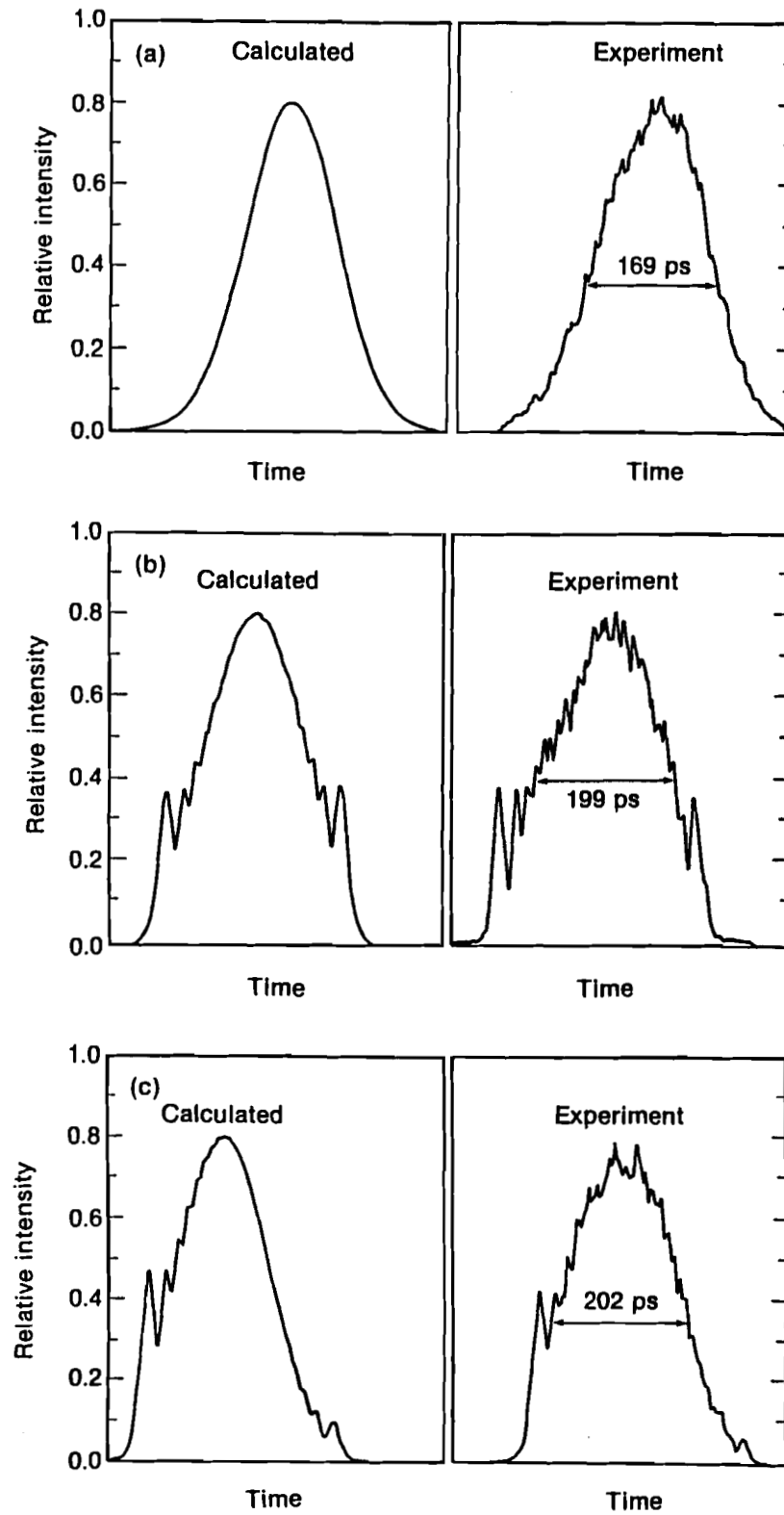


Fig. 2-8 Calculated and measured amplified temporal pulse shape. The total

power gain is $G_0=10^{45}$, and the amplifier bandwidth is 210 Å (FWHM). (a) The chirped pulse initially has a 445-ps pulse width and a 35-Å bandwidth. Gain narrowing shapes the pulse to Gaussian. (b) The chirped pulse initially has a 290-ps pulse width and a 20-Å bandwidth. It retains peaked edges because of less gain narrowing. (c) Same chirped pulse as in (b) except the gain center is offset 5 Å.

Figure 2-9 shows the calculated and measured power spectra of the amplified chirped pulse of case (ii) with gain center offset, which is shown in Fig. 2-8(c). Figure 2-9(a) shows the power spectrum of the chirped pulse switched out of the regenerative amplifier 5 round trips earlier than the peak of the pulse train. Figure 2-9(b) shows the power spectrum of a chirped pulse switched out of the regenerative amplifier 9 round trips after the peak of the pulse train, with the same energy as the pulse in Fig. 2-9(a). Spectral modulation due to SPM is clearly shown. The peak B-integral value is 5 for this calculation. There are other points which support the idea that the spectral distortion is due to SPM. In cases 2-9(a) and 2-9(b) the streak camera shows that both chirped-pulse shapes remain similar. Spectral windowing in expansion gratings cuts both peaked edges of the initial chirped pulse (Fig. 2-7), and reduces the degree of the spectral distortion due to SPM. By tuning the frequency offset to the opposite side, one can see the spectral distortion also move to the other side when SPM occurs.

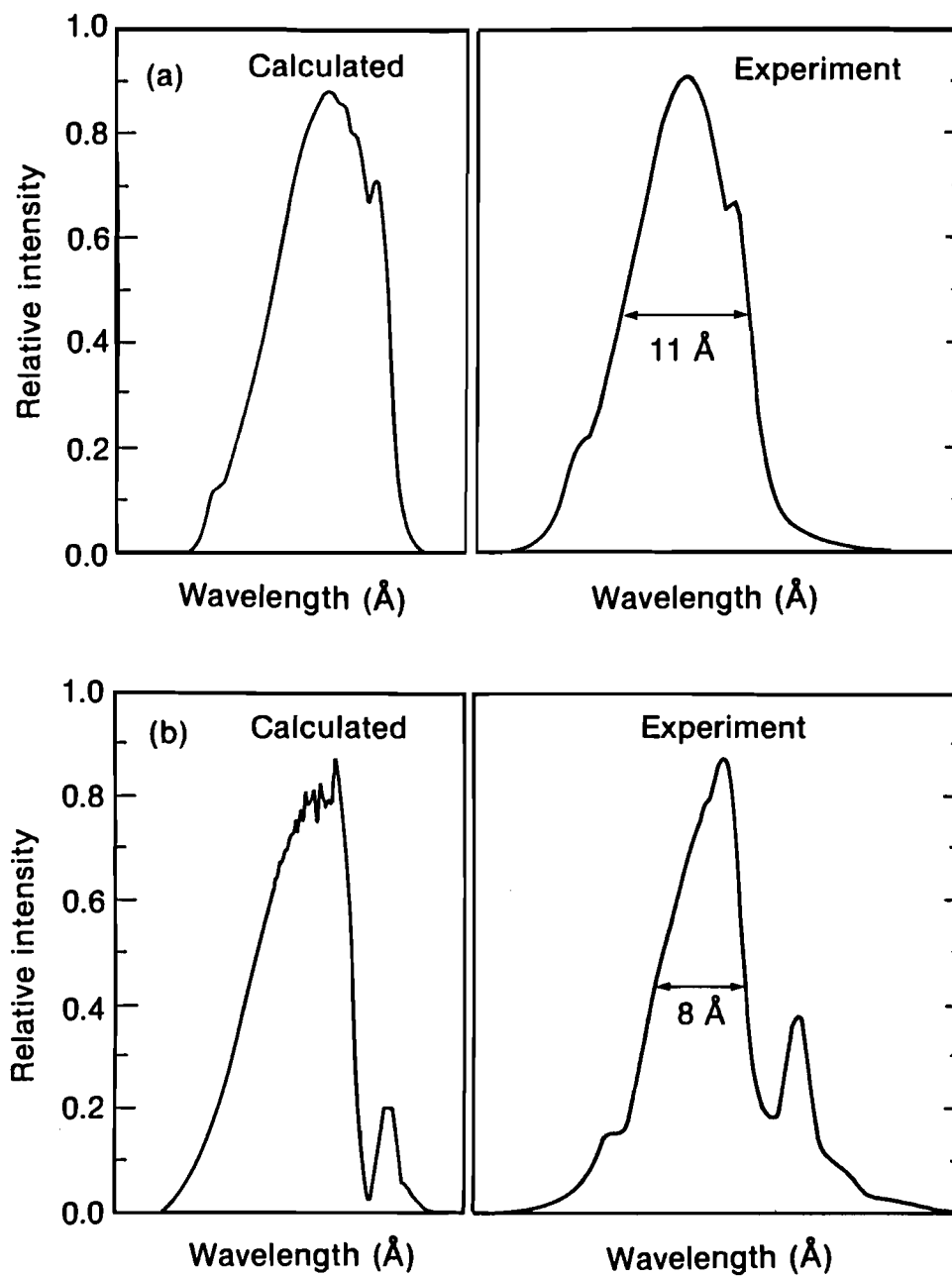


Fig. 2-9 Calculated and measured power spectra of amplified chirped pulses with gain center offset. (a) The chirped pulse is switched out of the regenerative amplifier in an earlier time. (b) The chirped pulse is switched out of the regenerative amplifier 15 round trips later than (a). Spectral modulation due to SPM ($B=5$) is clearly shown in (b).

F. CONCLUSIONS

In this chapter we have used the concept of instantaneous frequency to simplify the pulse propagation equations for CPA. As a result, the power gain and phase variations generated from the nonlinear amplification process become functions of time. An optical diffraction analogy illustrates the amplitude and phase modulations of the chirped pulse during amplification, and intuitively shows the distortion of the compressed pulse and its power spectrum.

In the CPA process the bulk of the amplitude modulation is typically due to spectral gain narrowing, and most of the phase modulation is from SPM. Gain narrowing, which may cause broadening of the final compressed pulse can be, however, employed as a pulse shaping tool. SPM not only broadens the compressed pulse but also enhances the background pedestal and should be avoided. In the gain saturation regime, both gain saturation and gain narrowing distort the pulse envelope and must be considered together. A frequency mismatch between the applied signal and the amplifiers may degrade the amplified pulse and potentially may cause phase modulation in gain saturation regime.

SPM in phosphate Nd:glass CPA laser systems that use fiber and expansion gratings to process the initial chirped pulses has been identified experimentally and theoretically. If the peaked edges of the chirped pulse are not well suppressed by spectral gain narrowing and frequency matching, they may undergo a high-frequency phase shift when SPM occurs. This high-frequency phase shift with its own wide-spread group velocity in compression gratings contributes to the background pedestal of the final compressed pulse.

The analysis presented here is valid for any CPA scheme, even those where an initial ultrashort pulse is expanded by a grating pair. The super-Gaussian order of the expanded pulse will, of course, change.

REFERENCES

1. D. Strickland and G. Mourou, "Compression of amplified chirped optical pulses," *Opt. Commun.* **56**, 219 (1985).
2. P. Maine, D. Strickland, P. Bado, M. Pessot, and G. Mourou, "Generation of ultrahigh peak power pulses by chirped pulse amplification," *IEEE J. Quantum Electron.* **QE-24**, 398 (1988).
3. G. P. Agrawal, in *Nonlinear Fiber Optics*, Boston: Academic Press, 1989, Ch. 2, 4, and 6.
4. O. E. Martinez, "3000 times grating compressor with positive group velocity dispersion: Application to fiber compensation in 1.3–1.6 mm regime," *IEEE J. Quantum Electron.* **QE-23**, 59 (1987).
5. M. Pessot, P. Maine, and G. Mourou, "1000 times expansion/compression of optical pulses for chirped pulse amplification," *Opt. Commun.* **62**, 419 (1987).
6. E. B. Treacy, "Optical pulse compression with diffraction gratings," *IEEE J. Quantum Electron.* **QE-5**, 454 (1969).
7. J. D. McMullen, "Analysis of compression of frequency chirped optical pulses by a strongly dispersive grating pair," *Appl. Opt.* **18**, 737 (1979).
8. A. E. Siegman, in *Lasers*, Mill Valley, CA: University Science, 1986, Ch. 5, 9, and 10.
9. J. C. Kieffer, P. Audebert, M. Chaker, J. P. Matte, H. Pepin, T. W. Johnston, P. Maine, D. D. Meyerhofer, J. Delettrez, D. Strickland, P. Bado, and G. Mourou, "Short-pulse laser absorption in very steep plasma density gradients," *Phys. Rev. Lett.* **62**, 760 (1989).

10. S. Augst, D. Strickland, D. D. Meyerhofer, S. L. Chin, and J. H. Eberly, "Tunneling ionization of noble gases in a high-intensity laser field," *Phys. Rev. Lett.* **63**, 2212, (1989).
11. Y.-H. Chuang, Z.-W. Li, D. D. Meyerhofer, and A. Schmid, "Nonresonant $\chi_{1111}^{(3)}$ obtained by nearly degenerate four-wave mixing using chirped-pulse technology," *Opt. Lett.* **16**, 7, (1991).
12. D. Strickland, "Development of an ultra-bright laser and an application to multi-photon ionization," Ph. D. Thesis, University of Rochester, 1988.
13. M. D. Perry, F. G. Patterson, and J. Weston, "Spectral shaping in chirped-pulse amplification," *Opt. Lett.* **15**, 381 (1990).
14. Y.-H. Chuang, D. D. Meyerhofer, S. Augst, H. Chen, J. Peatross, and S. Uchida, "Suppression of the pedestal in a chirped-pulse-amplification laser," *J. Opt. Soc. Am. B* **8**, 1226 (1991).
15. J. S. Coe, P. Maine, and P. Bado, "Regenerative amplification of picosecond pulses in Nd:YLF: gain narrowing and gain saturation," *J. Opt. Soc. Am. B* **5**, 2560 (1988).
16. M. Ferray, L. A. Lompré, O. Gobert, A. L'Huillier, G. Mainfray, C. Manus, A. Sanchez, and A. S. Gomes, "Multiterawatt picosecond Nd-Glass laser system at 1053 nm," *Opt. Commun.* **75**, 278 (1990).
17. M. Pessot, J. Squier, G. Mourou, and D. J. Harter, "Chirped-pulse amplification of 100-fsec pulses," *Opt. Lett.* **14**, 797 (1989).
18. L. M. Frantz and J. S. Nodvik, "Theory of pulse propagation in a laser amplifier," *J. Appl. Phys.* **34**, 2346 (1963).
19. A. Isevgi and W. E. Lamb, Jr., "Propagation of light pulses in a laser amplifier," *Phys. Rev.* **185**, 517 (1969).

20. A. E. Siegman, in *Lasers*, Mill Valley, CA: University Science, 1986, Ch. 14.
21. D. W. Hall, R. A. Haas, W. F. Krupke, and M. J. Weber, "Spectral and polarization hole burning in neodymium glass lasers," *IEEE J. Quantum Electron.* **QE-19**, 1704, (1983).
22. D. W. Hall, W. F. Hagen, and M. J. Weber, "Modeling broad-band and multiple-frequency energy extraction from glass laser amplifiers," *IEEE J. Quantum Electron.* **QE-22**, 793, (1986).
23. W. Zinth, A. Laibereau and W. Kaiser, "Generation of chirp-free picosecond pulses," *Opt. Commun.* **22**, 161, (1977).

CHAPTER III

GENERATION OF HIGH-CONTRAST ULTRASHORT PULSES

In this chapter the pedestal (pre-pulse and post-pulse) associated with a chirped pulse amplification (CPA) laser is studied. Four components have been identified that contribute to the pedestal. Pulses are spectrally shaped by gain-narrowing in a frequency-matched, regenerative amplifier while self-phase modulation (SPM) is avoided. The intensity contrast is further improved through the use of a saturable absorber, resulting in Gaussian pulses of ~ 0.9 -ps duration with an intensity contrast exceeding $10^5:1$. This work makes possible the study of high-intensity ultrashort laser plasma interactions with a fiber-grating CPA system.

A. INTRODUCTION

As mentioned in Chapter I, the study of high-density plasma physics¹ and ultrafast x-ray emission,^{2,3} by means of high-power, ultrashort laser pulses is of great current interest. Detailed knowledge of the temporal shape of the pulse is crucial. In particular, high-density plasma physics experiments require a laser pulse with a high-intensity contrast. The peak intensity may be well above 10^{16} W/cm², whereas the pre-pulse intensity should be limited to $\sim 10^{11}$ W/cm² if one is to avoid generating a low density, preformed plasma.

It is well known that the fiber-grating compression technique produces a pulse that carries a significant amount of energy and remains imperfectly compressed^{4,5}. This uncompressed portion is commonly referred to as the

pedestal. Pedestal reduction is discussed in many papers. Nonlinear birefringence can cause a fiber act as an intensity discriminator and partially suppress the pedestal.⁶ Careful adjustment of the compression gratings can help reduce the third order nonlinear chirp that arises from the fiber.⁷ Spectral windowing⁸ can nearly eliminate the pedestal, but the temporal shape of the pulse may still not be Gaussian. Recently, Perry⁹ et al. used the gain-narrowing of the regenerative amplifier to do spectral shaping in a chirped-pulse-amplification (CPA) system. They successfully shaped the spectrum to a near-Gaussian form, making the pulse also near-Gaussian. For this technique an intensity contrast of greater than 700:1 was reported.

This chapter explores the pedestal that is associated with a CPA laser. Four components have been identified that contribute to the pedestal of a compressed pulse. The square-top pulse envelope and the nonlinear frequency chirp that are generated in the optical fiber lead to the first two effects: (a) pulse wings that make the pulse wider than a true Gaussian at low intensities^{10,11} and (b) satellite pulses. The sinc²-type pulse wings are a direct result of compressing a square-top chirped pulse. This is because, as shown in Chap. II, the envelope of a compressed pulse is the Fourier transform of the envelope of a linearly chirped pulse. Low intensity, long duration satellite pulses that locate at the two edges of the original chirped pulse are a result of a negative frequency chirp¹² or an unshifted frequency component.¹³ The other two effects originate in the regenerative amplifier: (c) a large 200-ps background pedestal that is due to self-phase modulation (SPM) and (d) etalon effects. The details of how the SPM distorts the linear chirp and form the pedestal was introduced in Chap. II.

The pedestal contributions of the regenerative amplifier are removed by operation below saturation, removal of etalon effects, and adjustment of the gain center to that of the chirped pulse after the fiber. The pulse wings are suppressed by spectral gain-narrowing in the regenerative amplifier,⁹ and the satellite pulses are suppressed by a saturable absorber after pulse compression. Gaussian pulses of duration less than 0.9 ps with intensity contrasts exceeding $10^5:1$ have been produced. This work makes possible the study of high-intensity ultra-short laser plasma interactions with a fiber-grating CPA system. In Sec. B, the current CPA laser system is introduced. Section C presents experiments on pedestal suppression. This chapter is summarized in Sec. D.

B. LASER SYSTEM AND EXPERIMENTAL SETUP

A schematic diagram of the current CPA laser system is shown in Fig. 3-1. It consists of three parts: the pulse preparation stage, the amplifier chain, and the compression stage. Figure 3-1(a) shows the pulse preparation stage. A cw-pumped mode-locked Nd:YLF oscillator generates a 100-MHz train of 50-ps pulses at a wavelength of 10530 Å. The pulses are coupled into a 0.8-km single-mode optical fiber with a 9- μm core and then are sent through a pair of expansion gratings. The pulse undergoes SPM and group-velocity dispersion in the fiber and further dispersion by the expansion grating pair. This leads to chirped pulses with a 37-Å bandwidth and a 300-ps duration. A cw autocorrelator monitors the compressibility of the chirped pulses produced in the fiber. A small grating pair, matched to the high-power-compression gratings, is used to compress the pulse.

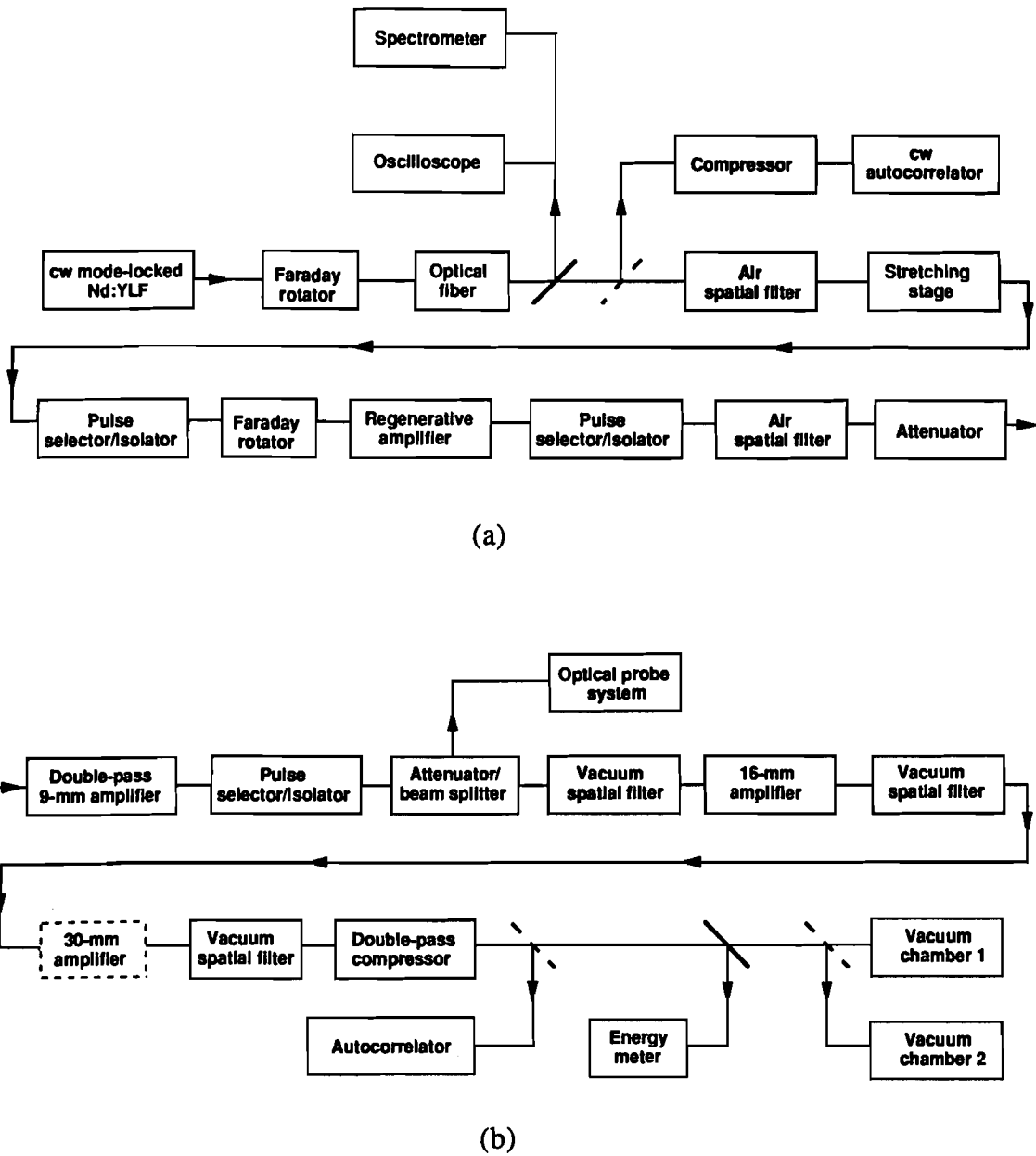


Fig. 3-1 Schematic diagram of the current chirped-pulse-amplification laser system: (a) Pulse preparation stage. The regenerative amplifier serves to amplify and shape the laser pulse; (b) Amplifier chain and compression stage.

A single nanojoule energy-level pulse is selected by a Pockels cell and seeded into a Q-switched, end-mirror-dumped regenerative amplifier. The amplifier uses a 7-mm-diameter phosphate Nd:glass rod (Kigre Q98). (A carefully designed regenerative amplifier not only amplifies the laser pulse but also shapes the laser spectrum.⁹ For this reason, the regenerative amplifier is considered part of the pulse preparation stage.) A 1-mJ pulse is selected from the pulse train, which is transmitted through the 50% reflective end mirror in the regenerative amplifier. The spatial profile of the beam is improved with an air spatial filter. An attenuator consisting of a half-wave plate between two polarizers is used to control the energy input to the amplifier chain.

The amplifier chain and the compression stage are shown in Fig. 3-1(b). All the amplifiers contain Nd:glass with a maximum gain at 10530 Å. The amplifier chain consists of a double-pass 9-mm-diameter amplifier (Kigre Q-98, 235 mm long), and a single-pass 16-mm-diameter amplifier (Hoya LHG-8, 360 mm long). A single pass 30-mm-diameter amplifier (Hoya LHG-8, 360 mm long) will be added when compression gratings with a higher damage threshold are installed. One Pockels cell after the 9-mm amplifier further isolates the pulse and suppresses any feedback pulse that might result from reflections off optical elements. An additional attenuator increases the system's dynamic range to 10^6 . A vacuum spatial filter after each amplifier is used to upcollimate, to relay the image, and to filter the pulse spatially. The energy of the chirped pulse after the 16-mm amplifier can be as high as a joule with a repetition rate of 1 shot per 70 seconds (limited by the thermal lensing in the 16-mm amplifier rod).

The compression stage currently consists of two 1700 lines/mm gold-coated holographic gratings with dimensions 80 x 110 mm. The gratings are used

in the near Littrow, double-pass configuration with a separation distance of 164 cm. The laser pulse is compressed to 1.6 ps with a bandwidth of 12 Å when no saturable absorber is used. The laser beam has a 36-mm diameter currently limiting the maximum energy to 300 mJ because of the damage threshold of the compression gratings. An autocorrelator and an energy meter are used to measure the final pulse width and pulse energy after compression.

The laser spectrum and pulse width are almost un-affected by our amplifier chain (after the regenerative amplifier) because of the relatively low amount of gain compared with that in the regenerative amplifier. For the experiments on pedestal suppression the laser pulse goes directly from the pulse preparation stage to the compressor. This allows the laser to operate at a repetition rate of 1 Hz. The main diagnostic for this experiment is an autocorrelator, as shown in Fig. 3-2. The wedged beam splitter and slits are used to prevent all secondary reflections within the autocorrelator from reaching the photomultiplier. The PIN diode measures shot-to-shot laser energy fluctuations. The autocorrelation signal is obtained by division of the photomultiplier signal by the square of the PIN diode signal. This assumes a non-depletion condition for the second-harmonic generation. Each data point in the autocorrelation trace represents an average over 10 shots. The standard deviation is shown by the error bars. This setup becomes a single-shot autocorrelator when the slits are removed and the photomultiplier is replaced by a linear array detector. We use this single-shot autocorrelator to begin the initial pulse width measurement and to align the compression gratings, and then use multiple shots to obtain a detailed autocorrelation trace.

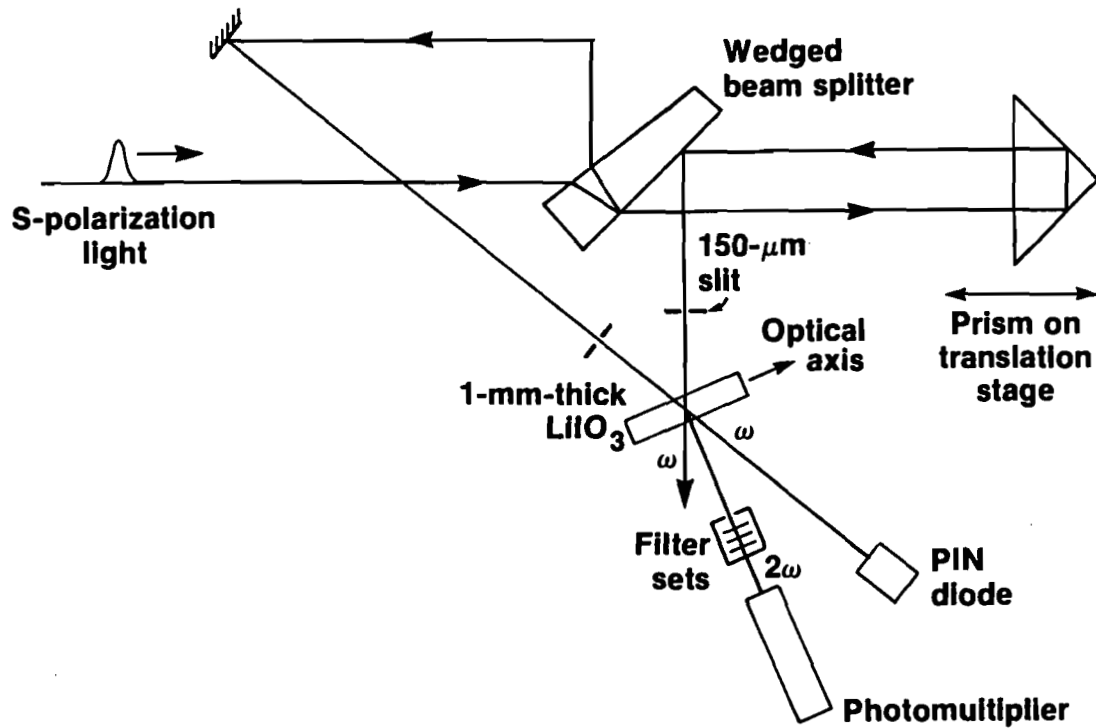


Fig. 3-2 Autocorrelator. The wedged beam splitter and slits are used to eliminate all etalon reflections from reaching the photomultiplier. The PIN diode detects shot-to-shot laser energy fluctuations. This setup becomes a single-shot autocorrelator when the slits are removed and the photomultiplier is replaced by a linear array detector.

C. EXPERIMENTS ON PEDESTAL SUPPRESSION

The pedestal was suppressed by spectral gain narrowing in the regenerative amplifier and by a saturable absorber after pulse compression. Improvements in the laser pulse shape begin with a careful adjustment of the regenerative amplifier in order to avoid SPM and etalon effects. Next, the spectral gain-narrowing of the frequency-matched regenerative amplifier shapes the pulse wings.⁹ Finally, a saturable absorber suppresses the satellite pulses.

C.1 Spectral Shaping

The pulse wings and satellite pulses of a compressed pulse come from the square-top envelope and nonlinear chirp that are generated in the fiber.^{10,11} A typical power spectrum of a chirped pulse after the fiber in our laser system is shown in Fig. 3-3(a). The bandwidth is 37 Å and the line center is at 10530 Å, the wavelength of our Nd:YLF oscillator. The results reported in Ref. 10 show that the linear chirp is located near the center part of the spectrum, while the nonlinear chirp is located near the edges. Figure 3-3(b) shows the autocorrelation trace of the compressed pulse after the fiber without further amplification. This figure shows a 1.6-ps pulse with broad pulse wings. An additional feature that can be seen in Fig. 3-3(b) is the long satellite pulses due to negative frequency chirp and frequency-unshifted light.

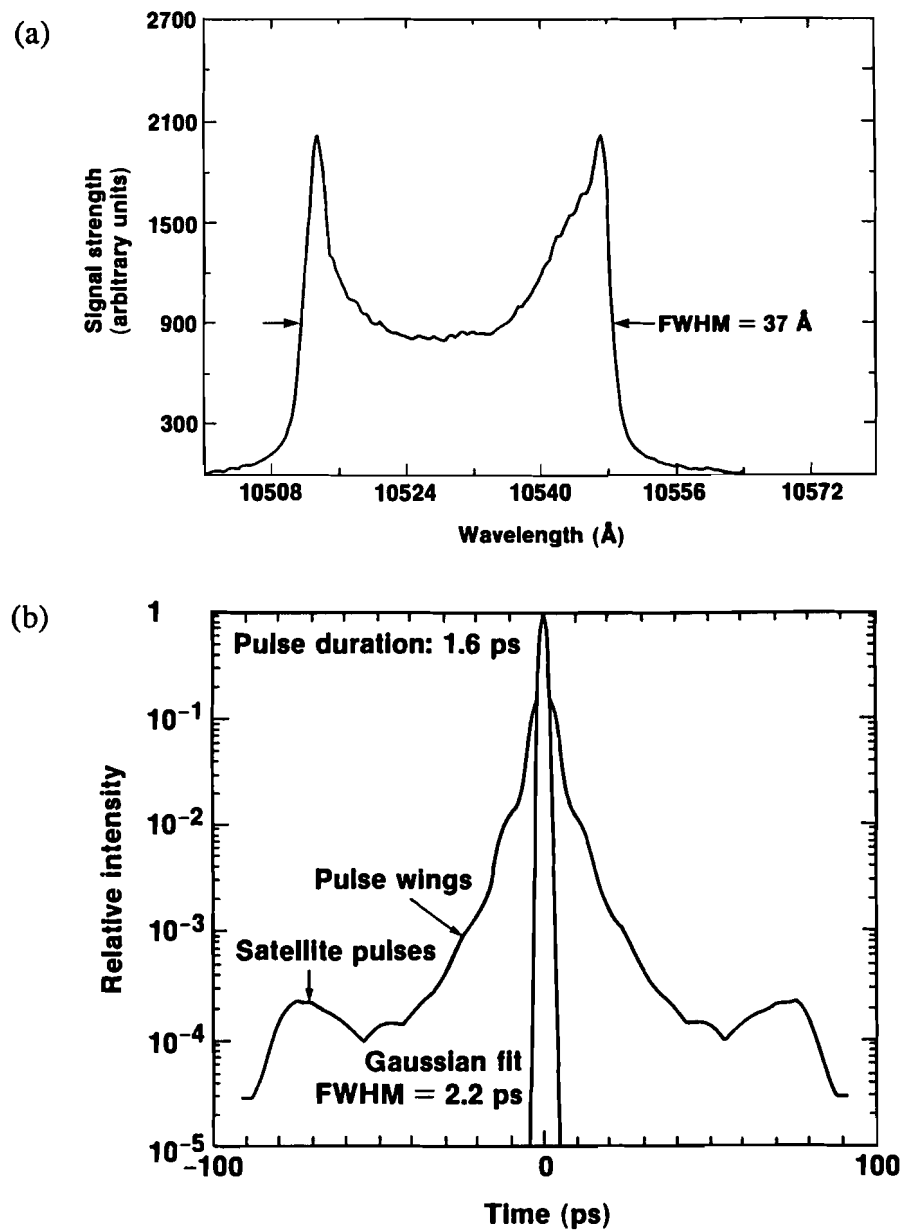


Fig. 3-3 (a) Spectrum of the chirped pulse leaving the fiber, FWHM = 37 Å.
 (b) Autocorrelation trace of the compressed pulse before amplification, FWHM = 1.6 ps, assuming a Gaussian profile. The pulse wings and the satellite pulses are the results of compressing a square-top chirped pulse with the nonlinear chirp locating at the leading and trailing edges.

Frequency mismatch and SPM in amplification process further enhance the pedestal of the final compressed pulse. This was discussed in Chapter II. The end-mirror-dumped regenerative amplifier produces a train of pulses, one of which is selected for injection into the amplifier chain. Pulses were sampled at various times with respect to the peak of the pulse train, and it was found that pulses near and after the peak of the pulse train are strongly spectrum modulated. The distortion in the pulse appears to be due to the combination of SPM¹⁴ with a mismatch in the gain-center wavelength of the regenerative amplifier and the Nd:YLF oscillator. Figure 3-4(a) shows the autocorrelation trace of a compressed pulse which was extracted at the peak of the pulse train. The bandwidth of the injected chirped pulse was only 20 Å, and there was a frequency mismatch of 4 Å between the line center of the chirped pulse and that of the regenerative amplifier. An overwhelming 200-ps-long background pedestal is generated. One can reduce this type of pedestal by switching out a pulse before the peak of the pulse train. This would reduce the total B integral seen by the pulse. Figure 3-4(b) shows the autocorrelation trace of the compressed pulse which is 5 pulses (~50 ns) earlier than the peak of the pulse train. The Gaussian curve-fits in Fig.3-4 show the ideal pulses, the goal of this experiment.

There are many spectral-shaping methods that can be used to reduce the pulse wings. Spectral windowing⁸ can be used within the expansion gratings. A bandpass filter can be used to shape the spectrum and reduce the nonlinear chirp near the edges of the chirped pulse. One can also reduce the nonlinear chirp by adjusting the angle of incidence and separation distances between the compression gratings,¹⁵ though this can lead to astigmatism in the compressed

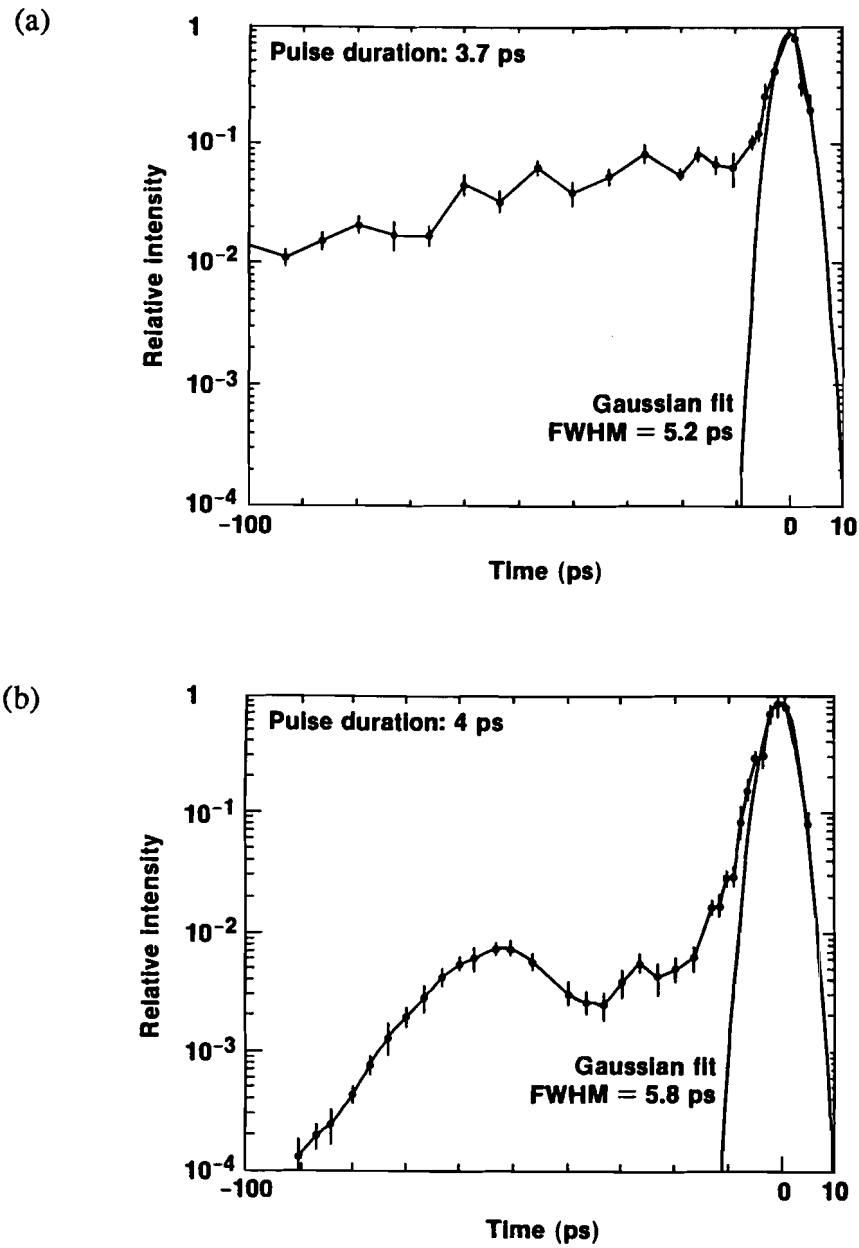


Fig. 3-4 Autocorrelation traces of the compressed pulse shows the pedestal enhanced by SPM and gain-center mismatch. (a) With SPM and gain-center mismatch. (b) Without SPM. The Gaussian curve-fits show the ideal pulses. Each data point represents the average of 10 shots.

pulse.¹⁶ In this experiment we used spectral gain narrowing in the frequency matched regenerative amplifier for spectral shaping.⁹ With SPM being carefully avoided the laser spectrum is forced to become Gaussian. A further improvement involved adjusting the Brewster-plate-polarizer angle and the Q-switch voltage inside the regenerative amplifier cavity in order to match the spectral line center of the Q-switched pulse to that of the seed pulse. To this stage the pulse wings are suppressed, leaving the etalon effects as shown in Fig. 3-5. Etalon effects came from optical elements with parallel surfaces such as mirrors, Brewster-plate polarizers, beam splitters, etc. They were removed through the use of wedged or thick optics.

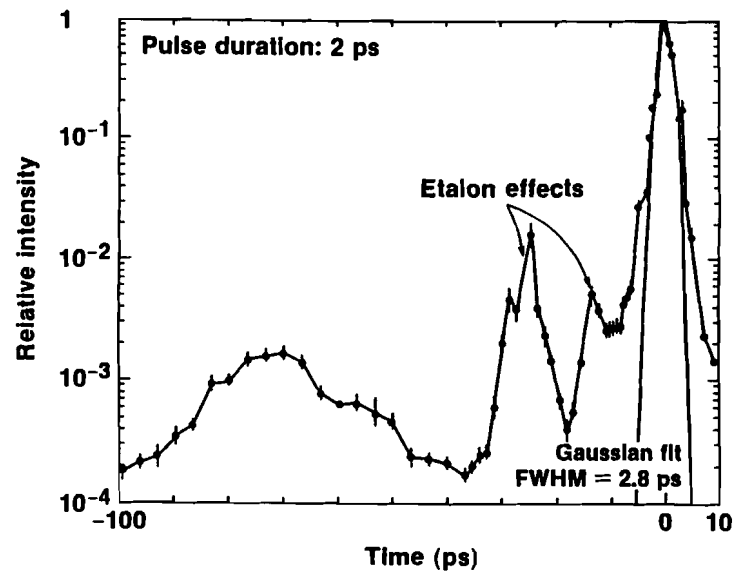


Fig. 3-5 Autocorrelation trace of the compressed pulse shows the etalon effects.

The spectrum of a pulse switched out of the regenerative amplifier with a bandwidth of 12 Å is shown in Fig. 3-6(a). This spectrum has a Gaussian form. The corresponding autocorrelation trace of the compressed pulse with a width of 1.6 ps is shown in Fig. 3-6(b). The pulse profile is nearly Gaussian for three orders of magnitude. Low-intensity, long-duration-satellite pulses are also clearly shown in Fig. 3-6(b). With this spectral-shaping scheme, the final problem is the elimination of the last structure in the pedestal, i.e., the satellite pulses.

C.2 Temporal Filtering

There are two low-intensity, long-duration satellite pulses. We have used the third order correlation technique¹⁷ to find that these two satellite pulses are almost symmetrically located 80 ps on either side of the main peak with an intensity contrast of order 10^3 . This part of the pedestal originates from the low intensity wings of the oscillator pulse that either get a negative frequency chirp in the fiber¹² or go directly through the fiber without SPM.¹³ The satellite pulse intensities decrease when the power spectrum generated from the SPM in the fiber is made broader.

Saturable absorbers¹⁸ are used to filter the low-intensity satellite pulses temporally. Two kinds of saturable absorber are used in this experiment, Kodak Q-switching dyes #9860 and #5. Dye #9860, with pure nitrobenzene as a solvent (approximately 5×10^{-5} M), is contained in a 2-cm-long dye cell. The relaxation time of this saturable absorber is 4.2 ps, which is much shorter than the time delay between the satellite pulses and the main peak (see Fig. 3-6 (b)). This dye cell is placed between two lenses ($f = 140$ mm) after the compression gratings, so the

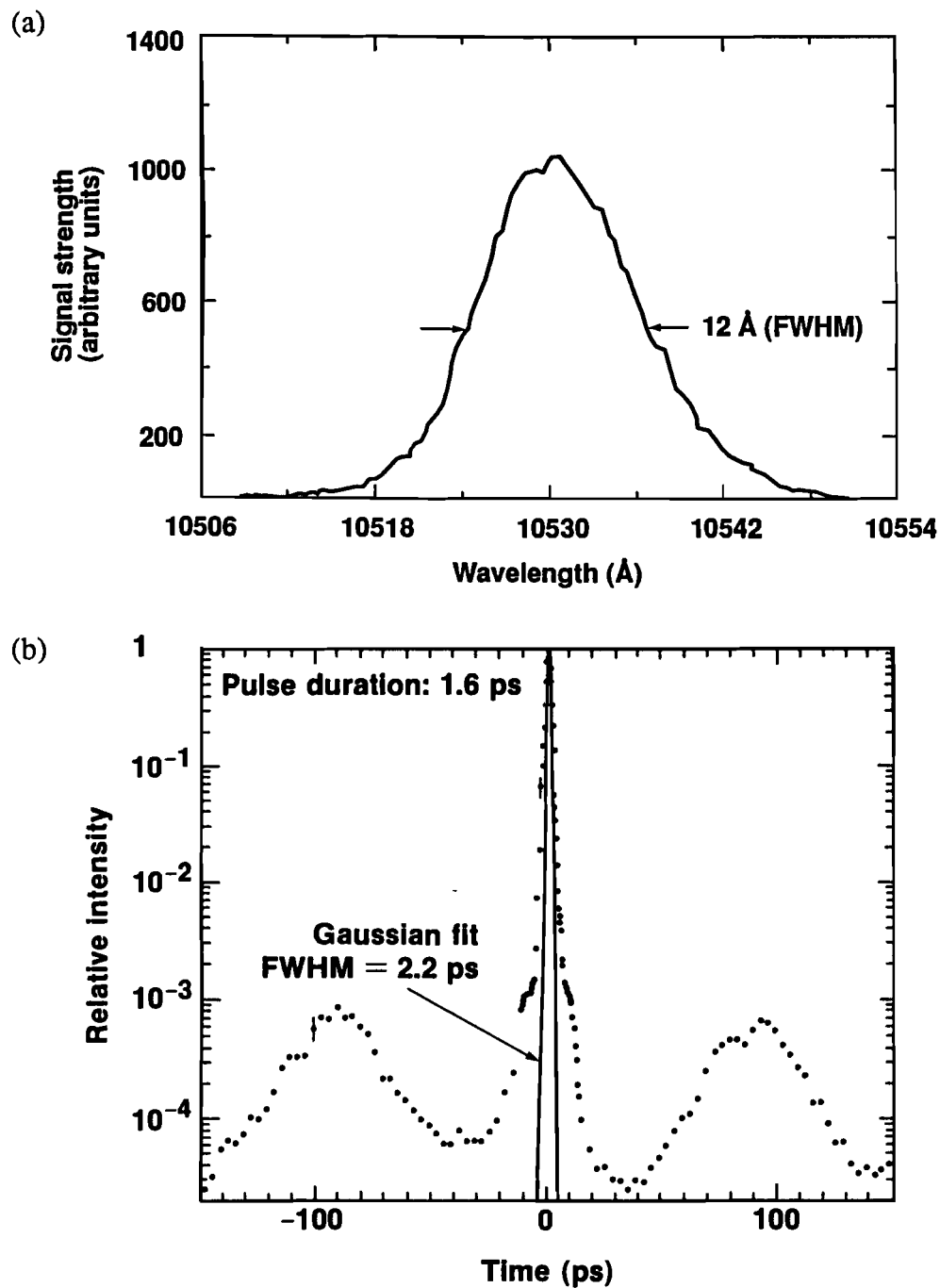


Fig. 3-6 (a) Spectrum of the pulse leaving the regenerative amplifier, FWHM = 12 Å. The Gaussian profile is a result of spectral gain narrowing. The spectral line center is the same as in Fig. 3-3(a). (b) Autocorrelation trace of the compressed pulse, FWHM = 1.6 ps, assuming a Gaussian profile.

peak laser intensity will exceed the saturation intensity of the dye. The low-intensity transmission is less than 10^{-4} , while the transmission for the main peak is $\sim 30\%$. Figure 3-7 shows the experimental results with this dye cell in the system (compare to Fig. 3-6, without the saturable absorber). The spectrum is broadened to 36 \AA and is mainly red shifted, as shown in Fig. 3-7(a). The autocorrelation trace of a 0.9-ps pulse, with a Gaussian fit over 5 orders of magnitude, is shown in Fig. 3-7(b). The satellite pulses are no longer present in this autocorrelation trace. The baseline is the noise from the detector. The intensity contrast is now greater than 10^5 , with this value limited by the dynamic range of our autocorrelator. A rescaled autocorrelation trace of Fig. 3-7(b) with a Gaussian fit is shown in Fig. 3-8.

The dye cell is currently placed after the compression gratings with the whole amplifier system firing and is used only when a high-intensity-contrast pulse is required. A 200-cm lens was used to measure the focal characteristics of the beam both with and without the saturable absorber in place. The focal-spot area was larger by approximately a factor of 2 with the saturable absorber in place. This decrease in focusability is probably due to nonuniformities in the near-field pattern of the beam entering the saturable absorber. The nonlinearity of the saturation process can enhance the nonuniformities. It is also possible that there is self-focusing accompanying the SPM that degrades the focal spot. The factor-of-2 degradation of the focal-spot area appears to be an acceptable trade-off for the improved temporal quality.

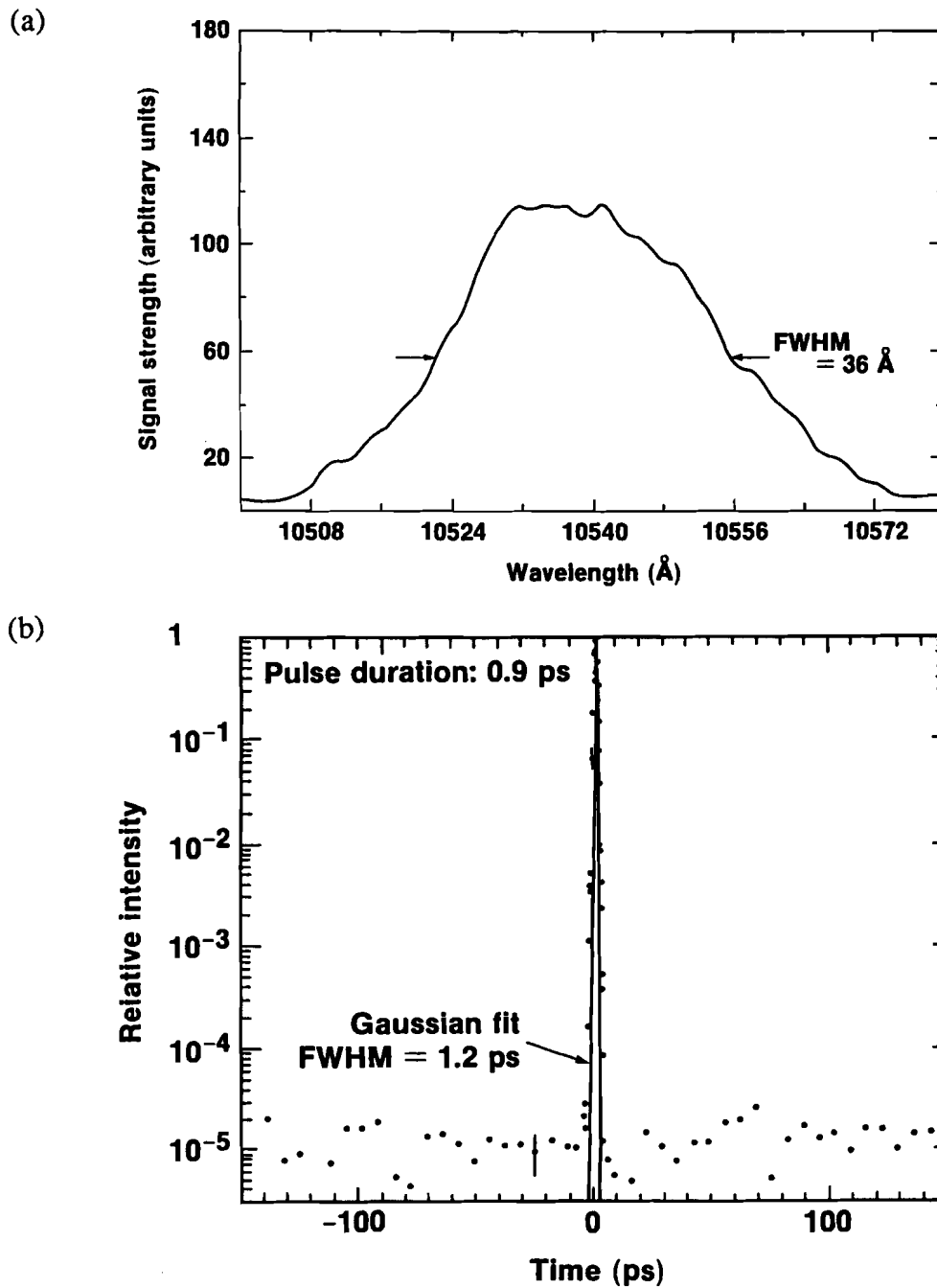


Fig. 3-7 (a) Spectrum of the pulse with a saturable absorber in the system, FWHM = 36 \AA ; (b) Autocorrelation trace of the compressed pulse, FWHM = 0.9 ps assuming a Gaussian profile. The baseline represents the noise level of our detector and data-acquisition system. The intensity contrast is now greater than 10^5 , the limit of our autocorrelator dynamic range.

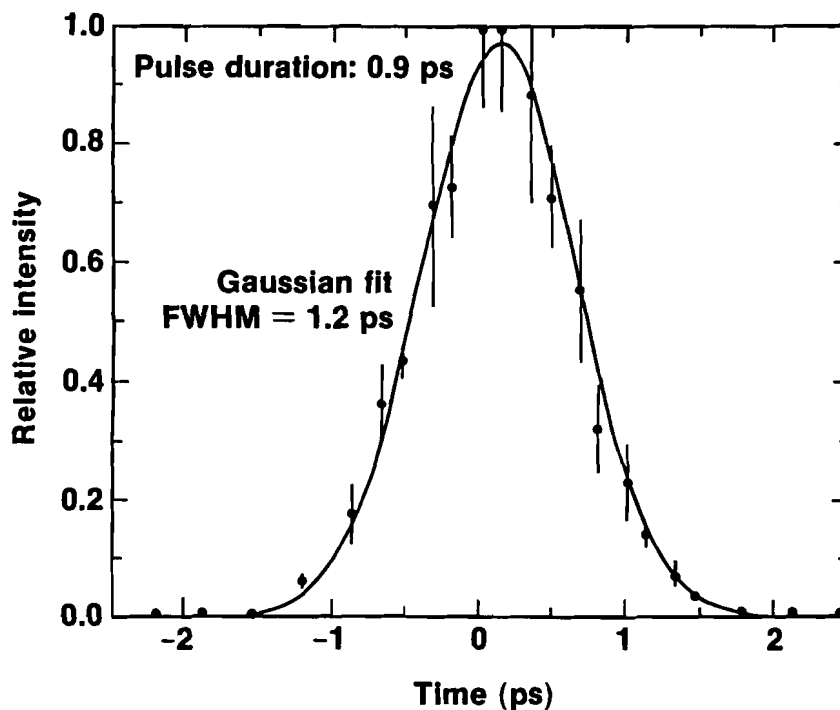


Fig. 3-8 Rescaled view of Fig. 3-7(b). A detailed autocorrelation trace of a 0.9-ps pulse with a Gaussian fit is shown.

The second saturable absorber, dye #5 with 1,2-dichloroethane as the solvent (approximately 5×10^{-5} M), is contained in a 1-cm dye cell. The relaxation time of this saturable absorber is 2.7 ps, even shorter than that of dye #9860. This dye cell is put in the same position as dye #9860. The low-intensity transmission is less than 10^{-4} , while the transmission for the main peak is $\sim 30\%$. The experimental result had the same characteristics as those for dye #9860 except the pulse width was slightly longer at 1.1 ps.

D. CONCLUSION

We have discussed four different contributions to the pedestal associated with a CPA laser system and have investigated techniques to reduce them, leading to the production of high-intensity contrast ($>10^5:1$) 0.9-ps Gaussian pulses. The pedestal consists of: (a) pulse wings, (b) satellite pulses, (c) a background pedestal resulting from SPM during amplification, and (d) etalon effects. The pulse wings and satellite pulses result from the square top envelope and the nonlinear chirp generated in the optical fiber. The pulse is switched out before gain saturation so that further frequency modulation in the regenerative amplifier is avoided. The pulse wings are suppressed by spectral gain narrowing in the frequency-matched regenerative amplifier. A saturable absorber is used to filter the satellite pulses and further reduce the pedestal.

These results suggest a method for increasing the energy and temporal and focal qualities in a CPA laser. The laser pulse from the Nd:YLF oscillator will be first chirped by the fiber and then injected directly into the regenerative amplifier without further stretching. The resulting 1-mJ level pulse will then be compressed by the first compression grating pair and will pass through the saturable absorber so that the pedestal is removed. This low pedestal pulse will be restretched and chirped in an expansion grating pair and be injected into the amplifier chain. After amplification the chirped pulse will be perfectly compressible in the final compression grating pair, since the expansion- and compression-grating pairs have opposite functions and will be separated by the same distance. Without suffering any higher-order chirp, this pulse can be stretched to an arbitrary chirp ratio in order to gain more energy and to reach the same intensity-ratio increase

after compression. The limiting factors are the size of the gratings and the space required for grating separation.⁴

With this pedestal reduction, high-intensity contrast picosecond pulses with intensities exceeding 10^{16} W/cm² can be produced with the current system, with higher intensities available with larger gratings. The results of this work make possible the study of high-intensity ultra-short laser plasma interactions with a fiber-grating CPA system. It is important to note, though, that chirped pulses with Gaussian envelopes can undergo SPM if the total B integral is of order 2, and this factor must be taken into account in the design of future high-power CPA systems.

REFERENCES

1. M. M. Murnane, H. C. Kapteyn, and R. W. Falcone, "High-Density Plasmas Produced by Ultrafast Laser Pulses," *Phys. Rev. Lett.* **62**, 155 (1989).
2. O. L. Landen, E. M. Campbell, and M. D. Perry, "X-Ray Characterization of Picosecond Laser Plasmas," *Opt. Commun.* **63**, 253 (1987).
3. J. A. Cobble, G. A. Kyrala, A. A. Hauer, A. J. Taylor, C. C. Gomez, N. D. Delamater, and G. T. Schappert, "Kilovolt x-ray spectroscopy of a subpicosecond-laser-excited source," *Phys. Rev. A* **39**, 454 (1989).
4. P. Maine, D. Strickland, P. Bado, M. Pessot, and G. Mourou, "Generation of Ultrahigh Peak Power Pulses by Chirped Pulse Amplification," *IEEE J. Quantum Electron.* **QE-24**, 398 (1988).
5. G. P. Agrawal, in Nonlinear Fiber Optics, (Academic Press, Boston, 1989), Chaps. 4 and 6.
6. R. H. Stolen, J. Botineau, and A. Ashkin, "Intensity Discrimination of Optical Pulses with Birefringent Fibers," *Opt. Lett.* **7**, 512 (1982); B. Nikolaus, D. Grischkowsky, and A. C. Balant, "Optical Pulse Reshaping Based on the Nonlinear Birefringence of Single-mode Optical Fibers," *Opt. Lett.* **8**, 189 (1983); N. J. Halas and D. Grischkowsky, "Simultaneous Optical Pulse Compression and Wing Reduction," *Appl. Phys. Lett.* **48**, 823 (1986).
7. H. Kubota and M. Nakazawa, "Compensation of Nonlinear Chirp Generated by Self-Steepening Using Third Order Dispersion of a Grating Pair," *Opt. Commun.* **66**, 79 (1988).

8. J. P. Heritage, R. N. Thurston, W. J. Tomlinson, A. M. Weiner, and R. H. Stolen, "Spectral Windowing of Frequency-modulated Optical Pulses in a Grating Compressor," *Appl. Phys. Lett.* **47**, 87 (1985).
9. M. D. Perry, F. G. Patterson, and J. Weston, "Spectral Shaping in Chirped-pulse Amplification," *Opt. Lett.* **15**, 381 (1990).
10. J. P. Heritage, A. M. Weiner, R. J. Hawkins, and O. E. Martinez, "Stabilized Pulse Compression by Multiple-Order Stimulated Raman Scattering with Group Velocity Dispersion," *Opt. Commun.* **67**, 367 (1988).
11. H. Roskos, A. Seilmeier, W. Kaiser, and J. D. Harvey, "Efficient High-Power Optical Pulse Compression with Logarithmic Wing Analysis," *Opt. Commun.* **61**, 81 (1987).
12. J. S. Coe, P. Maine, and P. Bado, "Regenerative Amplification of Picosecond Pulses in Nd:YLF: Gain Narrowing and Gain Saturation," *J. Opt. Soc. Am. B* **5**, 2560 (1988).
13. W. J. Tomlinson, "Curious Features of Nonlinear Pulse Propagation in Single-Mode Optical Fibers," *Optics News* **15**, 7 (1989).
14. W. Zinth, A. Laibereau and W. Kaiser, "Generation of Chirp-Free Picosecond Pulses," *Opt. Commun.* **22**, 161 (1977).
15. J. D. McMullen, "Analysis of Compression of Frequency Chirped Optical Pulses by a Strongly Dispersive Grating Pair," *Appl. Opt.* **18**, 737 (1979).
16. O. E. Martinez, "Grating and Prism Compressors in The Case of Finite Beam Size," *J. Opt. Soc. Am. B* **3**, 929 (1986).
17. G. Albrecht, A. Antonetti, and G. Mourou, "Temporal Shape Analysis of Nd³⁺:YAG Active Passive Mode-locked Pulses," *Opt. Commun.* **40**, 59 (1981).

18. B. Kopainsky, W. Kaiser, and K. H. Drexhage, "New Ultrafast Saturable Absorbers For Nd: Lasers," *Opt. Commun.* **32**, 451 (1980).

CHAPTER IV

FREQUENCY DOUBLING OF PICOSECOND PULSES*

The efficient second harmonic generation (SHG) of picosecond pulses is studied. A type-II KDP crystal is used for frequency doubling of 1053-nm, 1.6-ps pulses. When a 1.46-ps delay between the extraordinary and ordinary pulses is introduced at the input of the doubling crystal, the energy conversion efficiency increases from ~40 to ~75%.

A. INTRODUCTION

As mentioned in early chapters, high-power ultrashort laser pulses are the basic tools for studying fundamental atomic and plasma physics, and for investigating x-ray applications.¹ Frequency up-conversion further extends the capability of these pulses. Advantages of the frequency up-conversion of ultrashort pulses for laser-plasma interactions are twofold. First, the nonlinear nature of the frequency up-conversion may increase the intensity contrast of the ultrashort pulse.² High-contrast ultrashort pulses are desired for the study of high-density plasmas in order to produce short-pulse x-rays. Second, short-wavelength laser pulses offer better absorption conditions in laser-plasma interactions.^{3,4} A higher absorption efficiency is also desired for efficient x-ray production from a moderate-size laser system.

*This experiment was performed in collaboration with a group from the Australian National University and the results were published in Optics Letters ("Highly efficient conversion of picosecond Nd laser pulses with the use of group-velocity-mismatched frequency doubling in KDP," Y. Wang, B. Luther-Davies, Y.-H. Chuang, R. S. Craxton, and D. D. Meyerhofer, Opt. Lett. 16, 1862 (1991)).

The first second harmonic generation (SHG) experiment was reported by Franken et al. in 1961.⁵ In the following year Armstrong et al.⁶ presented a theoretical analysis and considered SHG as a three-wave parametric interaction with two pump waves and one SHG wave. They pointed out that phase matching of these three waves is required in order to achieve high conversion efficiency. In later SHG experiments the phase matching condition was obtained, for example, by changing the crystal temperature, pump wavelength or angular orientation of the birefringent doubling crystal. Conversion efficiencies from 80% to 92% for long pump pulses with narrow bandwidth were reported.⁷⁻⁹ For ultra-short pulses (with broad bandwidth), the frequency dependence of the wavevector is

$$k = k_0 + \frac{\partial k}{\partial \omega}(\omega - \omega_0) + \frac{1}{2} \frac{\partial^2 k}{\partial \omega^2}(\omega - \omega_0)^2 + \dots, \quad (4-1)$$

where k_0 is the wavevector at the central frequency ω_0 . The conversion efficiency is usually low even when the central-frequency wavevectors of the three mixing waves are well matched. This is because these waves have different group velocities, $(\partial k/\partial \omega)^{-1}$, in the dispersive conversion crystal.¹⁰⁻¹² For example, in a type II doubling crystal the input beam is decomposed into an ordinary wave (o-wave) and an extraordinary wave (e-wave). These two pump waves and the SHG wave will have different group velocities v_o , v_e , and v_2 , respectively. In an extreme case, the three mixing waves may spatially separate from each other after propagating a certain distance within the conversion crystal, and greatly reduce the total conversion.

Two schemes have been proposed to increase the up-conversion efficiency for ultrashort pulses. One method introduces a spectral angular dispersion by using gratings (or prisms) to match all wavevectors.^{13,14} The other method

requires the introduction of a pre-delay between two pump waves at the entrance of the type II doubling crystal to compensate the group velocity delay.^{2,15}

In this chapter we report on the efficient up-conversion of 1.6-ps laser pulses at 1053 nm to their second harmonic at 527 nm using the pre-delay scheme.² The overall energy conversion efficiencies are up to 75%. These efficiencies were measured at average beam intensities of ~ 2.5 GW/cm² for a 1-cm-diameter beam. The chirped-pulse-amplification (CPA) laser system^{16,17} used in this experiment was introduced in Chapter III (see Fig. 3-1). To complete the study of frequency up-conversion for picosecond pulses, we report this work in the following order. First, we present the experimental and calculated results using a single type-II KDP crystal without pre-delay, which gives $\sim 40\%$ conversion efficiency. We then show an increase in the conversion efficiency from $\sim 40\%$ to $\sim 75\%$ by introducing the pre-delay crystal. Besides central wavevector matching and group velocity matching, we further consider the sensitivity of polarization mismatch for picosecond pulses. For type-II frequency conversion the laser is equally decomposed into two optical axes leading to an optimum polarization angle of 45° (to the ordinary axis of the doubling crystal). A lower conversion efficiency (60% under the pre-delay scheme) is obtained with a non-optimum polarization angle of 51° , which is equivalent to $\sim 1\%$ (energy) depolarization of the input beam. A final experiment in which a polarization-angle scan was carried out using a single KDP crystal shows the conversion efficiency falling off with polarization angle as predicted.

B. METHODS

The frequency doubling scheme² used in this experiment is shown in Fig. 4-1. It includes two crystals, one for predelay and one for doubling. The predelay crystal is a 15-mm thick 53° cut KD*P crystal with its o and e directions aligned at 90° to those of the doubling crystal. This crystal is detuned so that no second harmonic generation occurs. Based on published refractive index data (Ref. 18), this KD*P crystal introduces a 1.46-ps predelay. The doubling crystal is a 25-mm-thick type-II KDP crystal with sol-gel AR coatings on its input face for 1.06 μm and on its output face for 0.53 μm. From the refractive indices reported in Ref. 19, the calculated group velocities of the pump o and e waves, and the second harmonic are $v_o = 1.966 \times 10^{10}$ cm/s, $v_e = 2.019 \times 10^{10}$ cm/s, and $v_2 = 1.988 \times 10^{10}$ cm/s, respectively. This KDP crystal gives the o-wave a 3.3-ps group velocity delay relative to the e-wave. When a laser pulse passes the first predelay crystal its p-polarization leads the s-polarization by 1.46 ps as shown in Fig. 4-1. In the doubling crystal, the s-polarization catches up with the p-polarization and moves to the leading position at the output. This results in a *shortened*, high-peak-intensity second harmonic pulse located in time between the two residual pump waves.²

The autocorrelation trace of the laser pulse is shown in Fig. 3-5(b) (Chap. III). It is a near-Gaussian 1.6-ps pulse with less than 5% energy in the pedestal. The laser beam profile was modified for these experiments by placing a 1-cm-diameter hard aperture in front of the vacuum spatial filter in order to produce a uniform beam profile. Fig. 4-2 shows the schematic layout of frequency-doubling experiments. A PIN diode measuring the leakage light from the compression

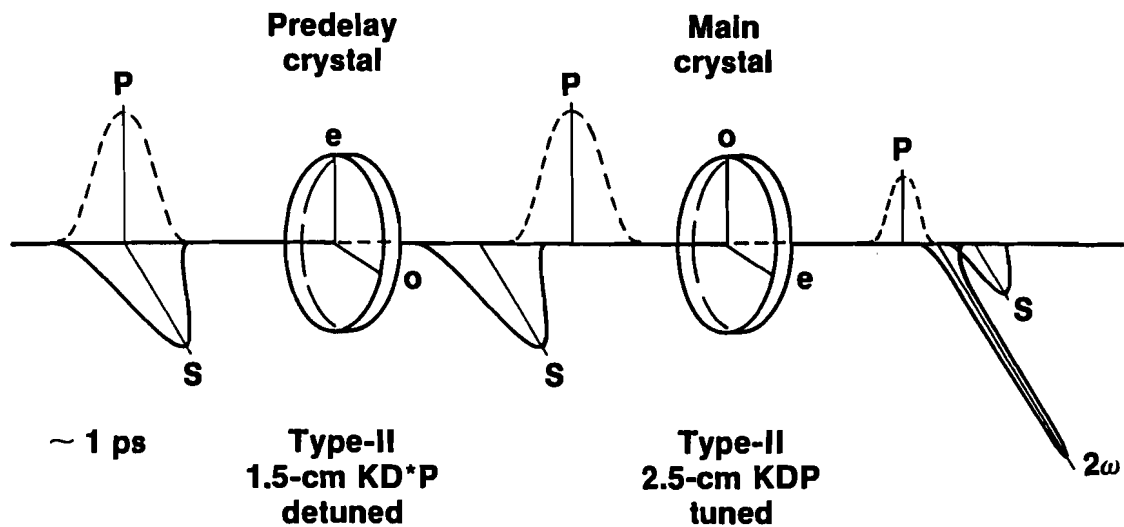


Fig. 4-1 Frequency doubling scheme for picosecond pulses with the use of a predelay crystal.

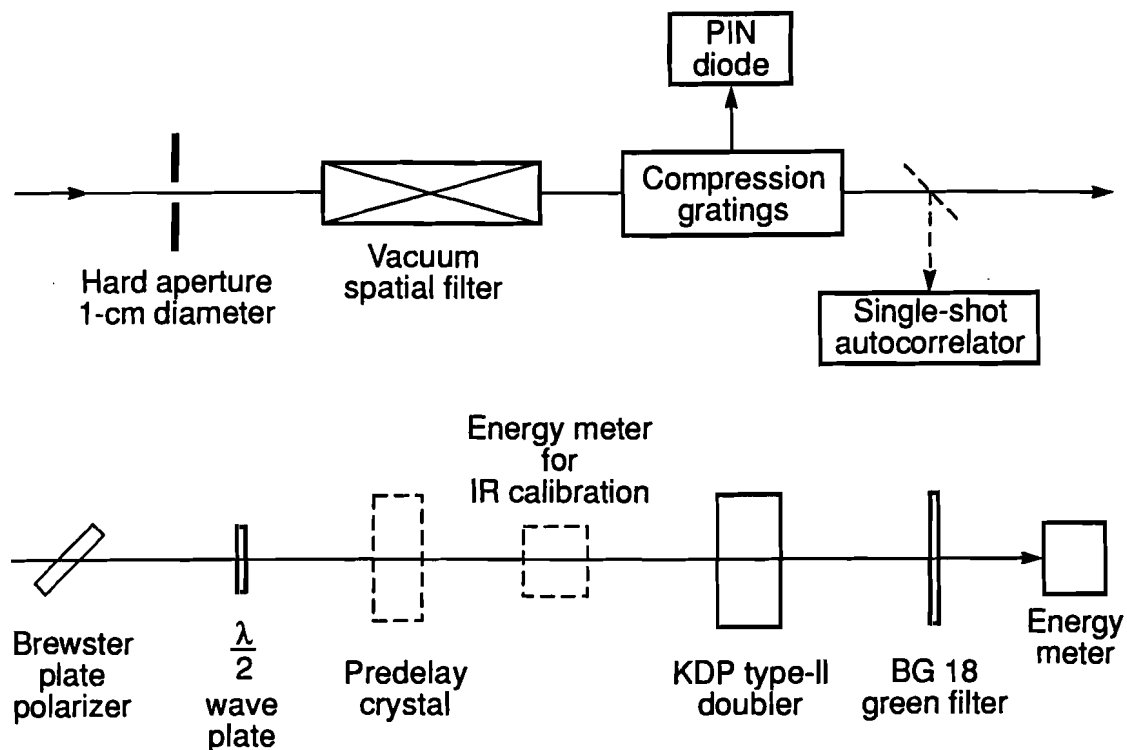


Fig. 4-2 Schematic layout of frequency doubling experiments.

gratings served as a system energy monitor. A single-shot autocorrelator provided an off-line diagnostic of the pulse width. The Brewster-plate polarizer was used to improve the polarization contrast, and the half-wave plate was used to rotate the polarization angle for frequency doubling experiments. The pre-delay KD*P crystal was located immediately after the half-wave plate. It was removed when single-crystal frequency conversion experiments were being performed. The laser pulse energies were controlled by tuning a half-wave plate between two polarizers (not shown in Fig. 4-2) and were measured by a pyroelectric calorimeter.

The energy conversion efficiencies were measured as follows. The energies of fundamental IR pulses were measured by the PIN diode, which was calibrated by an energy meter in front of the doubling KDP crystal over a wide range of laser energy. The energies of the second harmonic pulses were measured by the same energy meter at the output of the doubling KDP crystal. A 2-mm-thick BG 18 green filter (optical density > 8 at 1054 nm) was used to block the IR light from the energy meter. The measured conversion energies were then corrected by the transmittance of the filter at the second harmonic. The energy conversion efficiency was obtained as the second harmonic energy at the output of the KDP doubling crystal divided by the total IR energy at the input. From repeating shots, we estimate the uncertainty of the conversion efficiency to be $\pm 5\%$.

The beam profiles were measured for each experimental run. They changed slightly between runs due to changes in alignment. Kodak TMAX 400 film was placed in front of the doubling crystal to record the beam patterns. The images were digitized and converted into intensity data using the known film response calibrated from the same laser conditions (1.6 ps at near 1053 nm). Figure 4-3 (a)

is an example which shows the intensity contours of the laser beam used for frequency conversion with pre-delay. Figure 4-3(b) shows two radial line-outs of the beam distributions, in the x and y directions. The dashed line is a simple averaged profile used in calculations to approximate the real beam distribution. The total energy under the dashed line is equal to the measured total energy.

All theoretical predictions in this chapter were provided by Dr. R. S. Craxton at the Laboratory for Laser Energetics (LLE), University of Rochester. The theoretical approach begins from the frequency doubling equations for monochromatic signals. The electric fields of three interacting waves are given by the real part of $E_j \exp(i\omega_j t - ikz)$ for $j = o, e,$ and 2 , with E_j slowly varying along the z -direction. For convenience the modified variables $\hat{E}_j = n_j^{1/2} E_j$ are used, where n_j is the refractive index of wave j . The energy flux is then proportional to $|\hat{E}_j|^2$. The general equations governing frequency doubling for monochromatic signals are²⁰

$$d\hat{E}_o/dz = -(1/2)\gamma_o\hat{E}_o - iK\hat{E}_2\hat{E}_e^* \exp(-i\Delta k \cdot z) \quad (4-2)$$

$$d\hat{E}_e/dz = -(1/2)\gamma_e\hat{E}_e - iK\hat{E}_2\hat{E}_o^* \exp(-i\Delta k \cdot z) \quad (4-3)$$

$$d\hat{E}_2/dz = -(1/2)\gamma_2\hat{E}_2 - 2iK\hat{E}_o\hat{E}_e \exp(i\Delta k \cdot z), \quad (4-4)$$

where K is related to the fundamental constant d_{36} by

$$K = \frac{\omega_o}{c_0} (n_o n_e n_2)^{-1/2} \frac{d_{36}}{\epsilon_0} \sin(2\theta_m + \rho_e + \rho_2), \quad (4-5)$$

γ_j are absorption coefficients, and $\Delta k = k_2 - (k_o + k_e)$ is the wavevector mismatch. In Eq. (4.5) θ_m is the corresponding phase-matching angle, and ρ_e and ρ_2 are the small walkoff angles of the input e-wave and the SHG wave, respectively. Note that the d_{36} used in Eq. (4-5) is 0.5 times the d_{36} of Ref. 23. Equation (4-5) is consistent with the more standard definition of d_{36} used in Ref. 22.

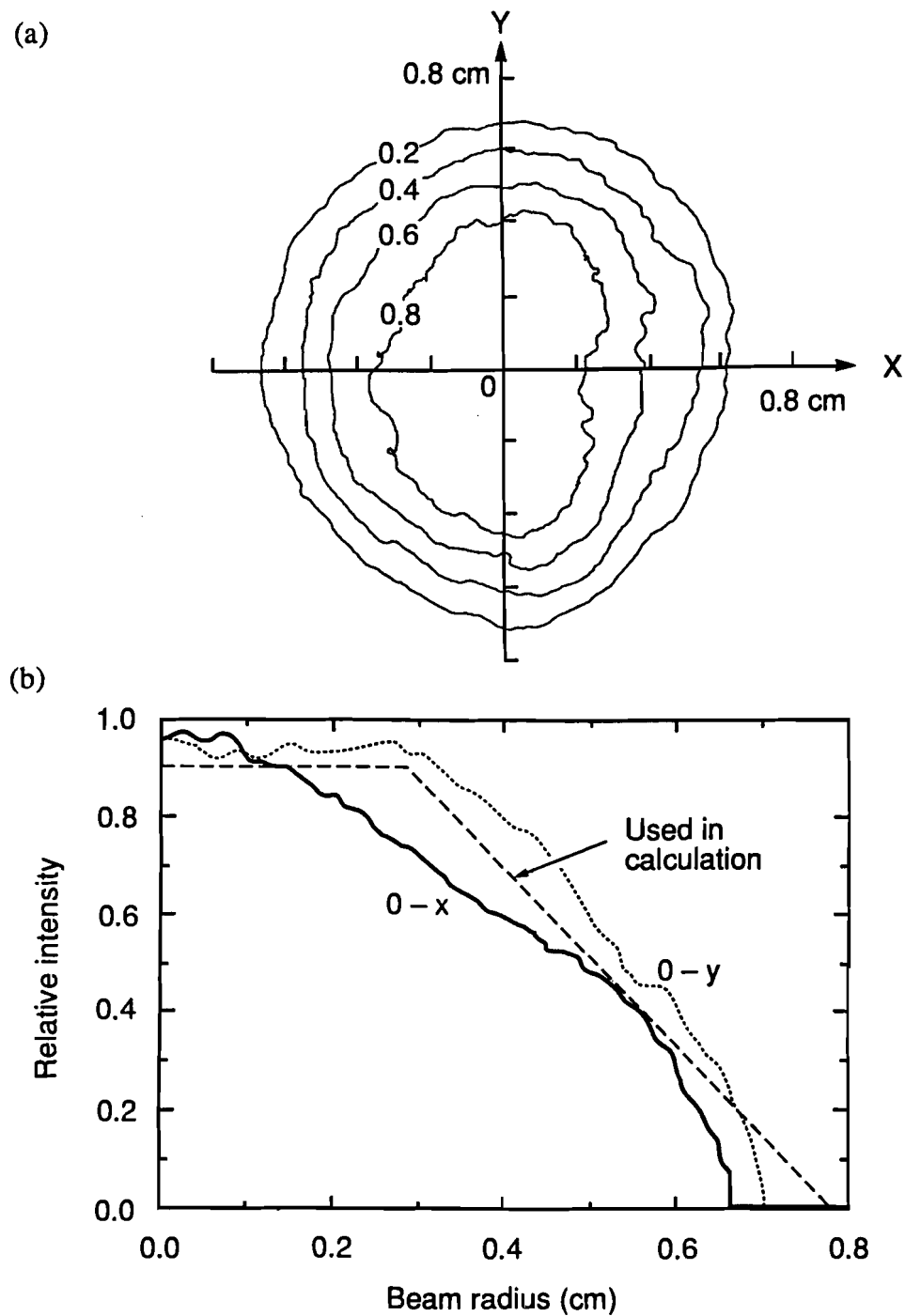


Fig. 4-3 The laser beam profile. (a) Intensity contours relative to the maximum intensity. (b) Line-out of the beam profiles in two perpendicular directions. The dashed line was used as an average in the calculations (which assumed cylindrical symmetry).

Numerical data used in calculations are as follows. The nonlinear constant for KDP was²⁰⁻²² $d_{36}/\epsilon_0 = 0.39$ pm/V (0.78 pm/V in the notation of Ref. 23). The constant $K=1.106 \times 10^{-6}$ V⁻¹ was used. The phase-matching angle was $\theta_m = 59.2^\circ$. The walkoff angles were $\rho_e = 0.0201$ rad and $\rho_2 = 0.0245$ rad. Refractive indices came from Ref. 18 for KD*P and Ref. 19 for KDP. Energy absorptions in KDP at 1054 nm were 5.8 m⁻¹ for the o-wave and 2.0 m⁻¹ for the e-wave (propagating at θ_m).²³ Other KDP properties particularly related to the frequency up-conversion at 1054 nm are available in Ref. 23.

A broadband ultra-short pulse is described by a summation of monochromatic modes, where each mode has a distinct frequency. The electric fields of three interacting waves are then given by

$$E_j(\mathbf{r}, t) = \text{Re} \left\{ \sum_{m=-M}^M E_{j,m}(z) \exp[i\omega_{j,m}t - i\mathbf{k}_j(\omega_{j,m}) \cdot \mathbf{r}] \right\}, \quad (4-6)$$

for $j = o, e,$ and 2 . Mixing any two monochromatic modes, one from the o-wave and the other from the e-wave, with the same sum frequency gives a new monochromatic mode of the SHG signal. The final SHG pulse is obtained by summing all the SHG modes. Therefore, broadband frequency conversion may be described using the multimode equations

$$\frac{\partial \hat{E}_{o,m}}{\partial z} = -\frac{1}{2} \gamma_o \hat{E}_{o,m} - iK \sum_n \hat{E}_{2,m+n} \hat{E}_{e,n}^* \exp(-i\Delta \mathbf{k}_{mn} \cdot \mathbf{z}) \quad (4-7)$$

$$\frac{\partial \hat{E}_{e,m}}{\partial z} = -\frac{1}{2} \gamma_e \hat{E}_{e,m} - iK \sum_n \hat{E}_{2,m+n} \hat{E}_{o,n}^* \exp(-i\Delta \mathbf{k}_{nm} \cdot \mathbf{z}) \quad (4-8)$$

$$\frac{\partial \hat{E}_{2,m}}{\partial z} = -\frac{1}{2} \gamma_2 \hat{E}_{2,m} - 2iK \sum_n \hat{E}_{o,m-n} \hat{E}_{e,n} \exp(i\Delta \mathbf{k}_{m-n,n} \cdot \mathbf{z}), \quad (4-9)$$

where $\hat{E}_{j,m=n_j}^{1/2} E_{j,m}$, and $\Delta k_{mn} = k_2(\omega_{2,m+n}) - k_e(\omega_{e,n}) - k_o(\omega_{o,m})$. The input pump pulses were assumed Gaussian with a pulse width of 1.6 ps (FWHM). The spectra of these pulses were also assumed Gaussian. There are $2M+1$ frequency modes in this calculation and $M = 50$ was used. The spatial profiles were approximated by a simple shape shown in Fig. 4-3(b).

Besides Craxton's method using multimode equations as stated above, another theoretical approach based on Wang and Dragila's model, which advanced the electric field in time domain, was also used for the calculation of ultrashort-pulse frequency conversion.^{2,24} Both codes gave exactly the same results.

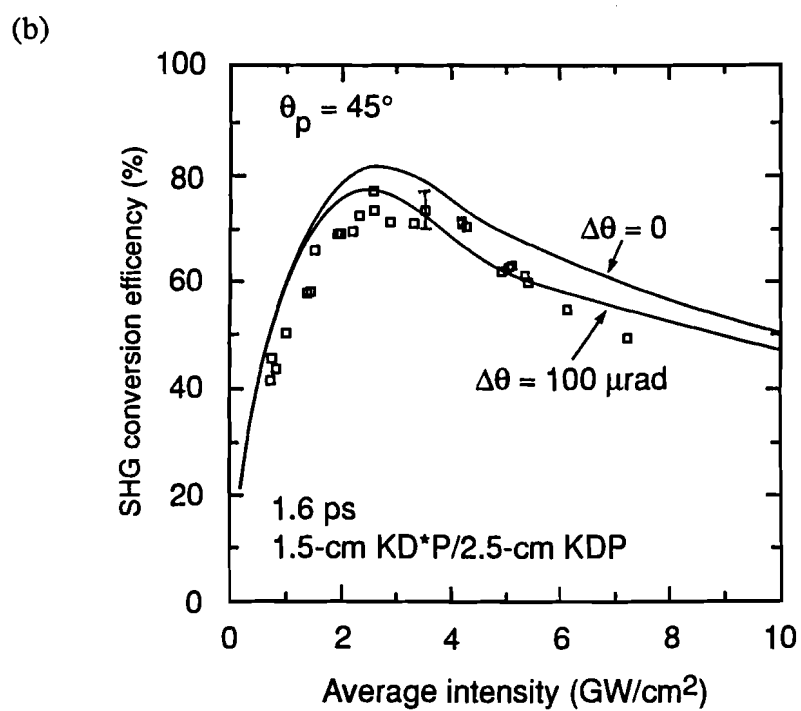
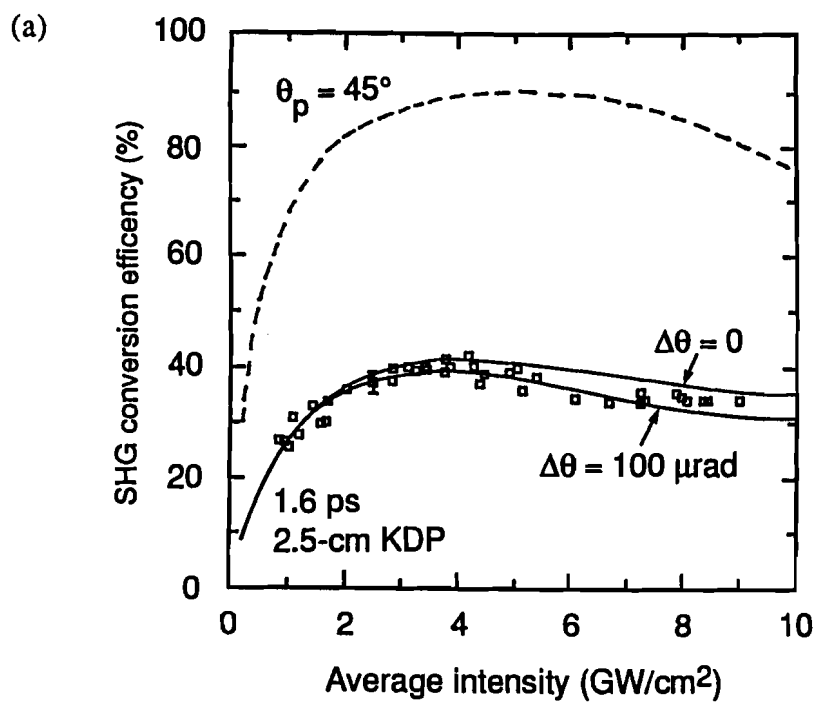
C. RESULTS

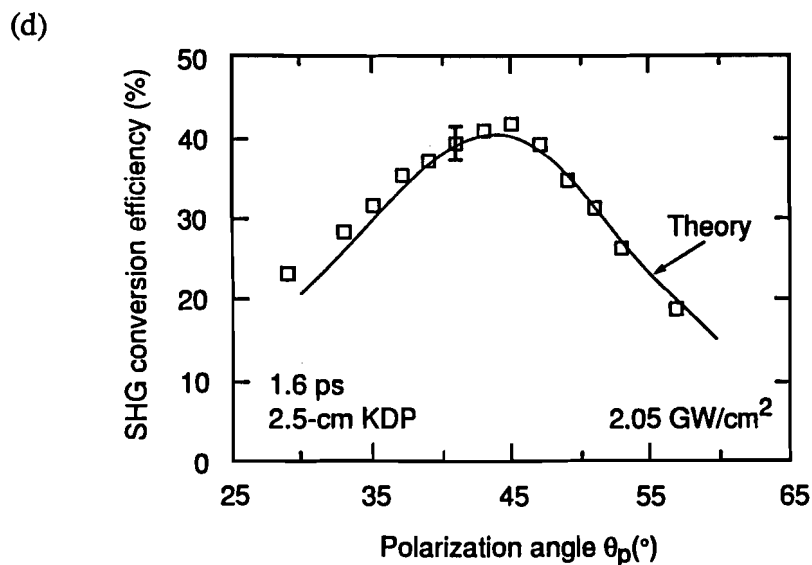
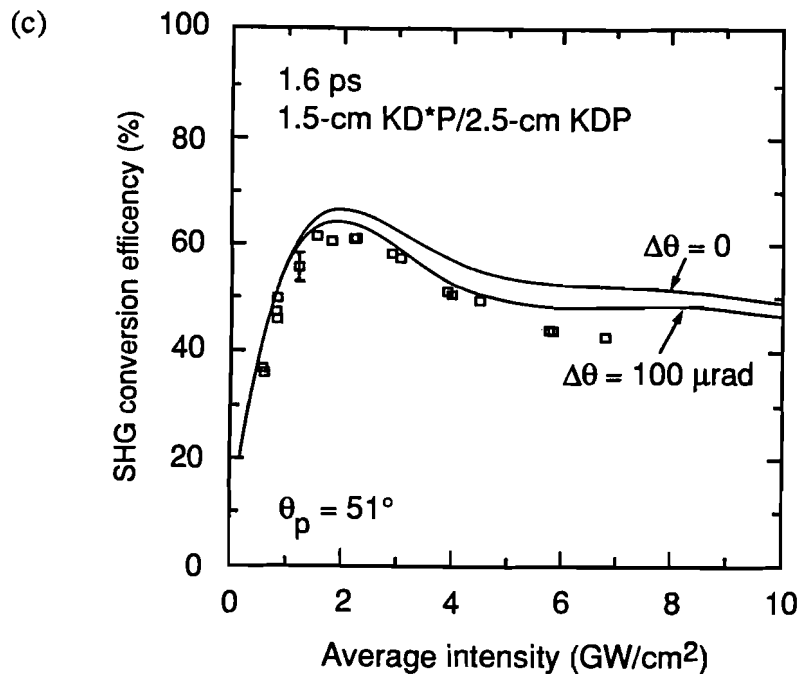
The measured and calculated frequency up-conversion efficiencies for ultrashort pulses are shown in Fig. 4-4. In all cases the KDP crystal was tuned for optimum phase matching. However, due to the finite size of the laser beam ($D \approx 1$ cm) a $100\text{-}\mu\text{rad}$ ($\Delta\theta \approx \lambda/D$) angular detuning is expected. Figure 4-4(a) shows the results of the doubling efficiency without pre-delay (i.e. the first crystal in Fig. 4-2 is removed). The dashed curve, as a reference, shows the calculated conversion efficiency of monochromatic plane waves (with absorption) that we should have got without group velocity mismatch. With group velocity mismatch the conversion efficiency of 1.6-ps pulses drops to be about 40% near the peak, and is relatively insensitive over a wide range of laser intensity. The agreement between experiment and theory (with a 0-100 μrad angular detuning) is excellent over the entire range covered. This level of conversion efficiency is also consistent with the data reported in Ref. 25 (4-ps pulses, $\sim 40\%$ conversion efficiency). Figure 4-4(b) shows the results of frequency doubling with pre-delay. With the addition of

predelay the conversion efficiency rises to 75% at a laser intensity near 2.5 GW/cm². The data matches the theory very well over the whole intensity range.

We encountered one difficulty in our first attempt at high efficiency frequency doubling. The laser pulses experienced depolarization during the amplification and compression processes leading to a loss of SHG efficiency. A Brewster-plate polarizer was then introduced to improve the polarization contrast as shown in Fig. 4-2. To understand the role of polarization matching we further placed a half-wave plate to detune the polarization. Figure 4-4(c) shows the doubling results with a non-optimum polarization angle of 51° to o-direction, which is equivalent to ~1% depolarization. The peak conversion efficiency (with the predelay) dropped from ~75% to ~60%. This was consistent with the theoretical prediction.

We carried out a further experiment to investigate the sensitivity of the conversion efficiency to the polarization angle. For simplicity, this experiment was only performed without the predelay. We fixed the laser intensity at 2.1 ± 0.2 GW/cm². The results are shown in Fig. 4-4(d). The agreement between the experiment and the theory is, again, excellent.





4-4 Second harmonic energy conversion efficiency. (a) Without pre-delay, ~40% conversion efficiency is obtained. (b) With pre-delay, the conversion efficiency increases to ~75%. (c) A lower conversion efficiency (with pre-delay) is obtained with a non-optimum polarization angle of 51° . (d) The conversion efficiency (of single KDP doubler) falls off with polarization angle as predicted.

D. SUMMARY

Experiments on frequency doubling of picosecond pulses using a pre-delay scheme² have been presented. A KD*P crystal was used to give the pre-delay in this experiment for its well known properties and low absorption losses at 1053 nm. A type-II KDP crystal was used as an frequency doubler. When a pre-delay between o and e waves was introduced in front of the doubling crystal the conversion efficiency increased from ~40% (without pre-delay) to ~75% (with pre-delay). The agreement between the experiment and theory is excellent. Experiments on the sensitivity of polarization angle mismatch for frequency doubling were also reported. Depolarization or polarization mismatch of the laser pulse decreases the conversion efficiency, consistent with theoretical predictions.

This simple and effective conversion scheme is well suited for picosecond high power lasers. Further experiments should include a second-harmonic pulse-shape measurement to investigate the pulse shortening and pedestal reduction predicted in Ref. 2. Frequency tripling using two type II crystals (Ref. 9 and 20) for picosecond pulses should also be considered since partial compensation for the group velocity delay is automatically provided in this scheme. The capability of operating high-power picosecond lasers at several different frequencies should thus be possible in the near future.

REFERENCES

1. See references 7 to 21 in Chapter I.
2. Y. Wang and R. Dragila, "Efficient conversion of picosecond laser pulses into second-harmonic frequency using group-velocity dispersion," *Phys. Rev. A* **41**, 5645 (1990).
3. C.E. Max, "Physics of the Coronal Plasma in Laser Fusion Targets," in Laser Plasma Interaction, R.Balian and J.C. Adam, eds., North Holland (1982).
4. W. Kruer, The Physics of Laser Plasma Interactions, Addison-Wesley, NY, Chap. 5 (1987).
5. P. A. Franken, A. E. Hill, C. W. Peters, and G. Weinreich, "Generation of optical harmonics," *Phys. Rev. Lett.* **7**, 118 (1961).
6. J. A. Armstrong, N. Bloembergen, J. Ducuing, and P. S. Pershan, "Interactions between light waves in a nonlinear dielectric," *Phys. Rev.* **127**, 1918 (1962).
7. J. Reintjes and R. C. Eckardt, "Efficient harmonic generation from 532 to 266 nm in ADP and KD*P," *Appl. Phys. Lett.* **30**, 91 (1977).
8. Y. A. Matveets, D. N. Nikogosyan, V. Kabelka, and A. Piskarskas, "Efficient second harmonic generation in a KDP crystal pumped with picosecond YAG:Nd³⁺ laser pulses of 0.5 Hz repetition frequency," *Sov. J. Quantum Electron.* **8**, 386 (1978).
9. W. Seka, S. D. Jacobs, J. E. Rizzo, R. Boni, and R. S. Craxton," *Opt. Commun.* **34**, 469 (1980).

10. J. A. Armstrong, S. S. Jha, and N. S. Shiren, "Some effects of group-velocity dispersion on parametric interactions," *IEEE J. Quantum Electron.* **QE-6**, 123 (1970).
11. I. V. Tomov, R. Fedosejevs, and A. A. Offenberger, "Up-conversion of subpicosecond light pulses," *IEEE J. Quantum Electron.* **QE-18**, 2048 (1982).
12. R. C. Eckardt and J. Reintjes, "Phase matching limitations of high efficiency second harmonic generation," *IEEE J. Quantum Electron.* **QE-20**, 1178 (1984).
13. V. D. Volosov, S. G. Karpenko, N. E. Kornienko, and V. L. Strizhevskii, "Method for compensating the phase-matching dispersion in nonlinear optics," *Sov. J. Quantum Electron* **4**, 1090, (1975).
14. O. E. Martinez, "Achromatic phase matching for second harmonic generation of femtosecond pulses," *IEEE J. Quantum Electron.* **25**, 2464 (1989); G. Szabo and Z. Bor, "Broadband frequency doubler for femtosecond pulses," *Appl. Phys. B* **50**, 51 (1990).
15. M. S. Pronko, R. H. Lehmberg, S. Obenschain, C. J. Pawley, C. K. Manka, and R. Eckardt, "Efficient second harmonic conversion of broad-band high-peak-power Nd:glass laser radiation using large-aperture KDP crystals in quadrature," *IEEE J. Quantum Electron.* **26**, 337 (1990).
16. P. Maine, D. Strickland, P. Bado, M. Pessot, and G. Mourou, "Generation of ultrahigh peak power pulses by chirped pulse amplification," *IEEE J. Quantum Electron.* **QE-24**, 398 (1988).

17. Y.-H. Chuang, D. D. Meyerhofer, S. Augst, H. Chen, J. Peatross, and S. Uchida, "Suppression of the pedestal in a chirped-pulse-amplification laser," *J. Opt. Soc. Am. B* **8**, 1226 (1991).
18. K. W. Kirby and L. G. DeShazer, "Refractive indices of 14 nonlinear crystals isomorphic to KH_2PO_4 ," *J. Opt. Soc. Am. B* **4**, 1072 (1987).
19. F. Zernike, "Refractive indices of ammonium dihydrogen phosphate and potassium dihydrogen phosphate between 2000 Å and 1.5 μ," *J. Opt. Soc. Am.* **54**, 1215 (1964).
20. R. S. Craxton, "High efficiency frequency tripling schemes for high power Nd:glass lasers," *IEEE J. Quantum Electron.* **QE-17**, 1771 (1981).
21. R. C. Eckardt, H. Masuda, Y. X. Fan, and R. L. Byer, "Absolute and relative nonlinear optical coefficients of KDP, KD^*P , BaB_2O_4 , LiIO_3 , MgO:KiNbO_3 , and KTP measured by phase-matched second-harmonic generation," *IEEE J. Quantum Electron.* **26**, 922 (1990).
22. D. Eimerl, "Electro-optic, linear, and nonlinear optical properties of KDP and its isomorphs," *Ferroelectrics* **72**, **95** (1987).
23. R. S. Craxton, S. D. Jacobs, J. E. Rizzo, R. Boni, "Basic properties of KDP related to the frequency conversion of 1 μm laser radiation," *IEEE J. Quantum Electron.* **QE-17**, 1782 (1981).
24. Y. Wang, B. Luther-Davies, Y.-H. Chuang, R. S. Craxton, and D. D. Meyerhofer, "Highly efficient conversion of picosecond Nd laser pulses with the use of group-velocity-mismatched frequency doubling in KDP," *Opt. Lett.* **16**, 1862 (1991).

25. K. Yamakawa, C. P. J. Barty, H. Shiraga, and Y. Kato, "Generation of a high-energy picosecond laser pulse with a high-contrast ratio by chirped-pulse amplification," *IEEE J. Quantum Electron.* **27**, 288 (1991).

CHAPTER V

NONRESONANT $\chi_{1111}^{(3)}$ MEASUREMENTS

Picosecond, chirped-pulse technology is used to generate two spectrally separate, time-synchronized pulses for $\chi^{(3)}$ measurements by nearly-degenerate four-wave mixing. Near 1053 nm, nonresonant, relative measurements of $\chi_{1111}^{(3)}$ are carried out on three model substances: nitrobenzene, α -chloronaphthalene, and 4'-decyloxynaphthyl-1'-(4-decyloxy benzoate). Their $\chi^{(3)}$ values are normalized to CS₂. There are two possible error sources. One comes from the laser; two input pulses are not well compressed due to the nonlinear chirp. The other comes from laser-matter interactions other than the Stokes and anti-Stokes generation: two beam coupling and phase modulation.

A. INTRODUCTION

All-optical nonlinear effects based on the third-order susceptibility $\chi^{(3)}$ are often investigated by four-wave mixing techniques. Starting with the classic 1965 proof-of-principle experiments by Maker and Terhune,¹ these measurements have yielded $\chi^{(3)}$ values for many condensed compounds. When these measurements are carried out in a fully degenerate manner, i.e., when $\chi_{ijkl}^{(3)}(-\omega; \omega, \omega, -\omega)$ is probed, the experimental hardware requirements become simple and relatively inexpensive. This permits the widespread use of the technique. In a more complicated embodiment using excitation beams of two frequencies, ω_1 and ω_2 , $\omega_1 > \omega_2$, four-wave mixing takes on the form of coherent anti-Stokes Raman scattering (CARS) and coherent Stokes Raman scattering (CSRS), generating

new frequencies at either $2\omega_1 - \omega_2$ if the intensity is $I(\omega_1) \gg I(\omega_2)$, or at $2\omega_2 - \omega_1$ if the reverse intensity condition holds and phase-matching requirements are met. Compared to the fully degenerate case, CARS complicates the measurement by requiring two laser sources and by being sensitive to phase matching. The major strength of this technique is that the output signal is both spatially and spectrally separated from the input beams. Whenever $\chi^{(3)}$ magnitudes are anticipated to be low and thus in need of background-free detection, CARS is the method of choice.

Adair, Chase, and Payne² have in recent years adopted a nearly-degenerate (near 1.06 μm) version of CARS and derived with it the nonlinear refractive index n_2 for a large number of optical glasses and crystals. In their approach ω_1 is chosen to differ from ω_2 by no more than $\Delta\omega \equiv \omega_1 - \omega_2 = 60 \text{ cm}^{-1}$, thereby simplifying the phase-matching condition for narrow-bandwidth input beams, $\Delta k = \frac{\omega}{c} [2n(\omega) - n(\omega + \Delta\omega) - n(\omega - \Delta\omega)]$. The absence of any significant group velocity dispersion over a 60 cm^{-1} range in all samples considered guarantees a phase-matched collinear alignment of all input and output beams for $\Delta k \cong 0$.

We report here on nearly-degenerate CARS measurements fashioned after those of Adair et al.² by using a chirped-pulse-amplification (CPA) laser³⁻⁵ for generating picosecond pulses at both ω_1 and ω_2 . A spectral window in a CPA laser is used to choose these two spectral lines. With this technique two pulses are jitter-free and spatially identical. The alignment and synchronization are thus greatly simplified.

B. EXPERIMENTAL SETUP

This approach exploits the spectral pulse shaping ability of the CPA technology. As mentioned in Chap. II, CPA overcomes the intensity-related B-integral effects (self-focusing and damage) which limit the amplification of short, picosecond pulses in solid-state lasing media. In CPA, short pulses are temporally stretched due to group velocity dispersion, amplified to higher energies than could be achieved by amplifying the short pulse directly, and then compressed to a short pulse.

The spectral pulse shaping technique in a CPA laser is shown in Fig. 5-1 schematically. A pulse train of a mode-locked Nd:YLF laser near 1053 nm was fed through a fiber to produce a 40-Å, self-phase-modulated spectrum.⁶ The use of an antiparallel, double-pass pair of gratings for pulse stretching allows access to the Fourier transform of the laser pulse (in wavelength space). This allows for spectral pulse shaping by the use of appropriate masks.⁸ In our case, we use a hard edge stop W (see Fig. 5-1) to block the central 20 Å of the laser bandwidth. This creates two independent, chirped laser pulses, each with a bandwidth of ~7 Å at ±11 Å from the gain center of the regenerative amplifier. To minimize diffraction effects, a spatial filter before the diffraction gratings is used to place the Fourier transform on a plane exactly at the location of W.

These nJ-level, spectrally and temporally separated pulses are amplified in the regenerative amplifier to an energy of ~0.5 mJ. Due to the temporal separation these pulses do not encounter any nonlinear wave mixing during amplification. The transverse mode TEM₀₀ build-up in the regenerative amplifier forces these pulses to have identical beam profile. This gives the wave-mixing experiment a constant ratio of energy flux between pump waves at all transverse positions. The

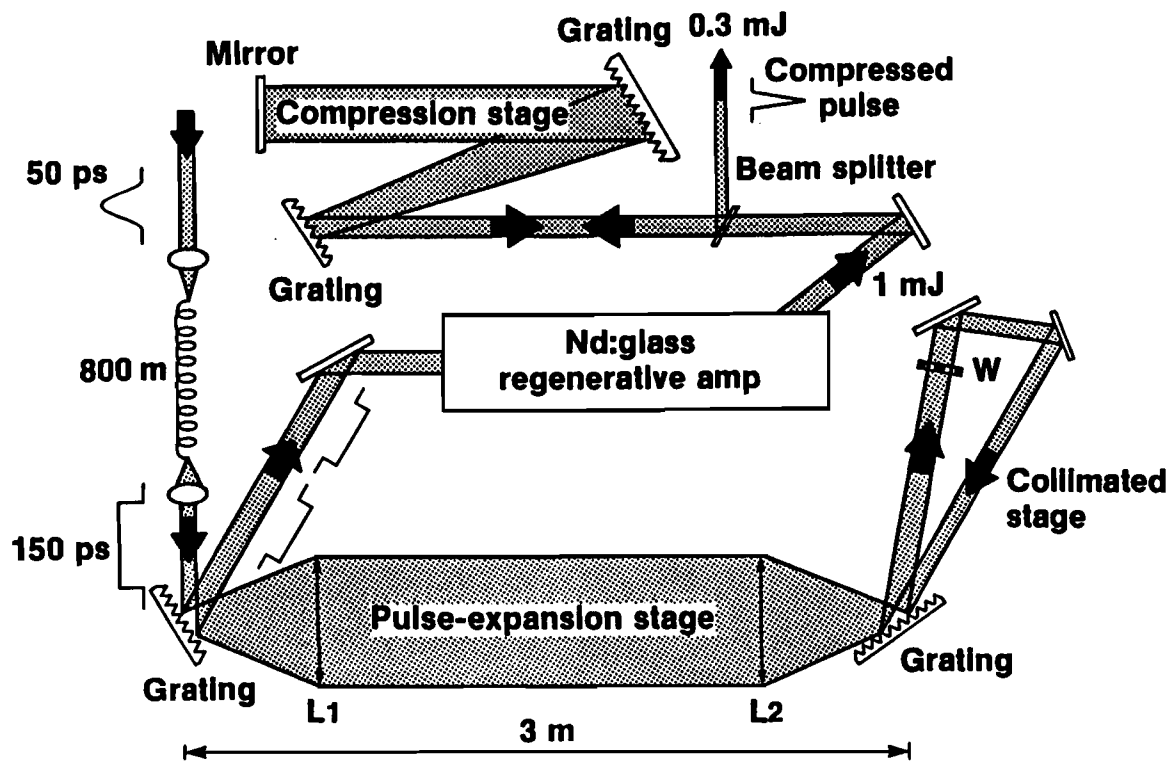


Fig. 5-1 Schematic representation of pulse expansion, spectral windowing, amplification and pulse compression used in nearly-degenerate four-wave mixing measurements.

symmetry of the injected pulses about the gain center of the regenerative amplifier ensures that the pulses undergo identical amplification. The resulting pulses each have a bandwidth of 8 Å and are separated by 17 Å.

Finally, the pulses are spatially filtered and undergo compression in a double pass, parallel grating configuration.⁷ The autocorrelation of the overlapped pulses is shown in Fig. 5-2. The 75 data points each represent 10-shot averages. The 17-Å spectral separation between the two pulses leads to a 2-ps temporal modulation of the combined pulse as expected. This beating must occur for any CARS technique. The envelope of the autocorrelation trace is fit with a 6.7-ps Gaussian. Because of losses during compression, the pulse reaching the sample carries 0.3 mJ energy.

CARS samples were enclosed in plane-parallel, 0.5-mm thick cells placed in the converging cone of a 1-m focal length lens. The beam spot size (0.5 mm) was recorded on calibrated IR film and measured by microdensitometry of the image. The beam exiting the cell, including the $\omega_1 + \Delta\omega$ signal, is recollimated and dispersed by a third, double-pass grating pair. The purpose of this grating arrangement is to spatially disperse pump, Stokes, and anti-Stokes signals for a neutral-density filter to attenuate the intense, undepleted signals at ω_1 and ω_2 to about the signal level of the $\omega_1 + \Delta\omega$ four-wave mixing signal. In this fashion, a cooled, IR-intensified optical multichannel analyzer in the image plane of a monochromator permits recording, within its dynamic range limits, all signals, $I(\omega_1)$, $I(\omega_2)$, and $I(\omega_1 + \Delta\omega)$. Since both $I(\omega_1)$ and $I(\omega_2)$ have identical polarization, this experiment is probing the tensor component $\chi_{1111}^{(3)}$ of the third-order susceptibility.

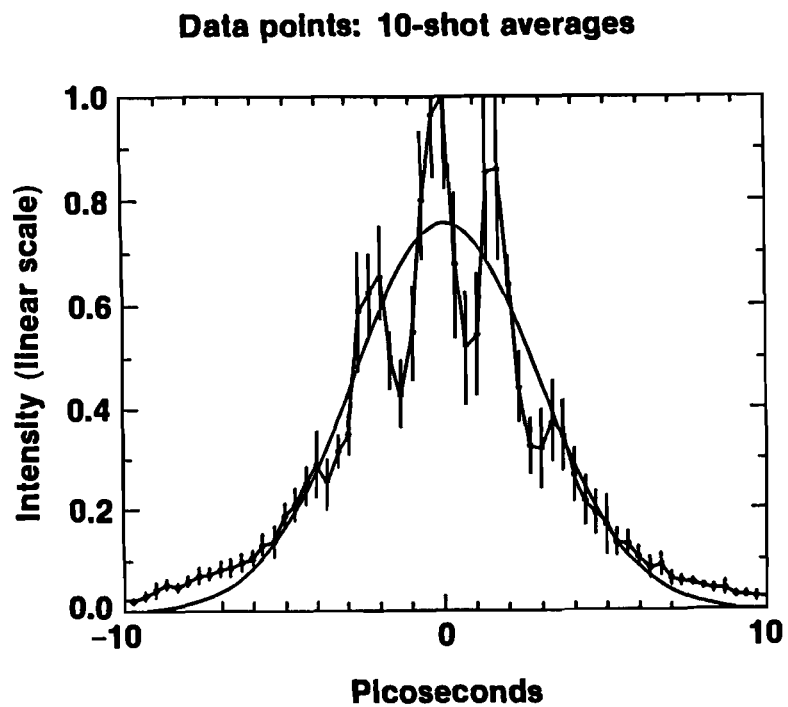


Fig. 5-2 Second-harmonic autocorrelation trace of compressed, spectrally-segmented pulse pair. Each data point is a 10-shot average. For comparison, first-order Gaussian (dotted line) is overlaid. The experimentally measured modulation frequency equals the beat-frequency between two, 17-Å separated waves.

C. EXPERIMENTAL RESULTS

Figure 5-3 shows the raw-data record of a single-shot measurement on CS_2 . The intense, undepleted signals at ω_1 and ω_2 were attenuated to a factor of 10 before entering the detector. Data in Fig. 5-4(a) show single-shot intensities of the anti-Stokes signal as a function of the pump intensity product $I^2(\omega_1) I(\omega_2)$ for a 0.5-mm CS_2 path, while those in Fig. 5-4(b) show the coherent Stokes signal plotted against $I^2(\omega_2) I(\omega_1)$. There is a one-to-one correspondence among data pairs in Figs. 5-4(a) and (b). The single-shot, systematic measurement error for these data is smaller than the plotted symbols. In assembling Fig. 5-4 only those measurements were selected for which the spectral width at both ω_1 and ω_2 fell within a preselected, spectral interval. Fluctuations in the spectral wings from shot to shot contribute to variations in the degree of compression and in the final, temporal pulse shape. The prime source for this spectral-width jitter will be investigated in next section. Over the ~one-order of magnitude intensity range plotted along the abscissa in Figs. 5-4(a) and (b), one finds the expected linear behavior. The solid lines in Fig. 5-4(a) and (b) are least-square fits to the data points. The non-zero offset at zero input intensity is attributed to both the CARS and Stokes signals riding on pump-pulse wings that have not been deconvoluted (see Fig. 5-3).

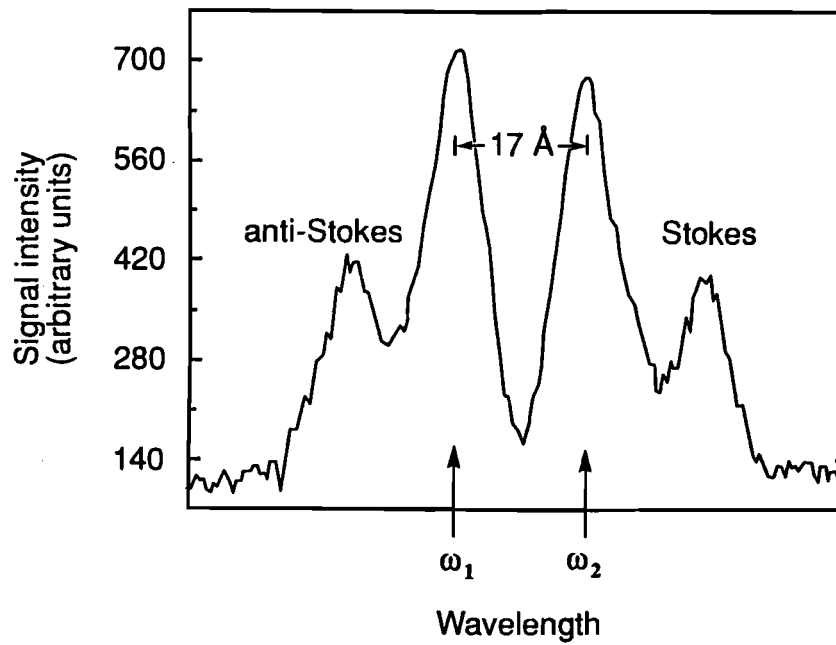


Fig. 5-3 Multichannel detector record from a single-shot, four-wave mixing event in CS_2 . Shorter wavelengths are to the left. The central two peaks represent $I(\omega_1)/10$ (left) and $I(\omega_2)/10$ (right). Clearly resolved (in full scale) are the coherent Stokes (furthermost right) and anti-Stokes (second from left) peaks.

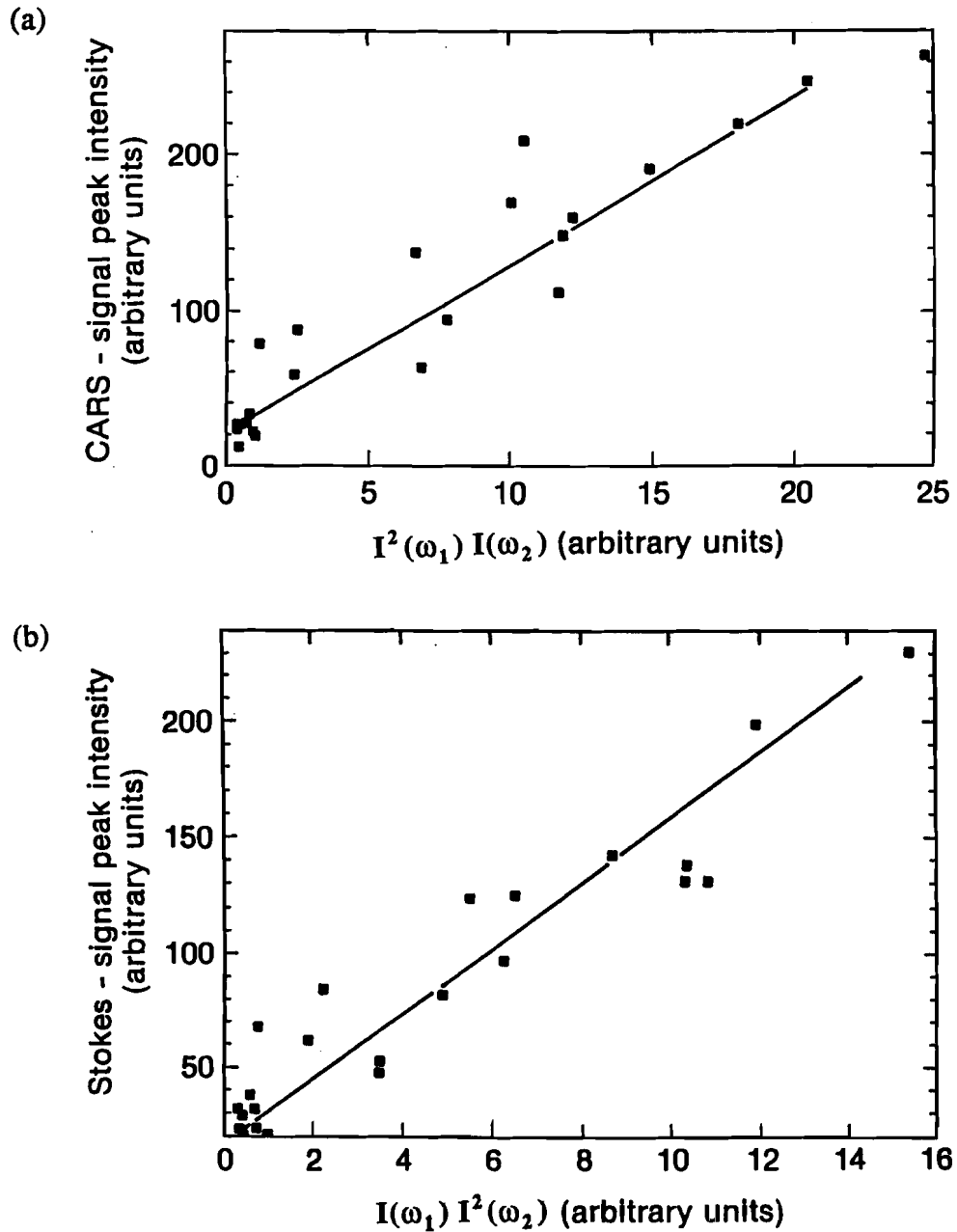


Fig. 5-4 (a) Nonresonant CARS signal magnitude plotted against the input wave intensity product $I^2(\omega_1) I(\omega_2)$. (b) Nonresonant CSRS signal magnitude plotted against the input wave intensity product $I^2(\omega_2) I(\omega_1)$. The data point in (a) and (b) map into each other, i.e., pairs of CARS and CSRS signals were taken simultaneously.

The monitoring of all pertinent intensities $I(\omega_1)$, $I(\omega_2)$, $I(\omega_1+\Delta\omega)$, and $I(\omega_2-\Delta\omega)$ on every shot facilitates relative sample-to-sample comparison, recording intensity fluctuations and checking for pump intensity depletion. This complete record permits comparing $\chi^{(3)}$ results from different samples with those of a standard such as CS_2 , without the need for irradiating, on each shot, both the sample and the standard. Of course, care must be taken in placing the samples in identical beam positions. In this manner, we measured the relative third-order susceptibility of several organic compounds.

Table I lists the relative CARS and CSRS results normalized to CS_2 for nitrobenzene, α -chloronaphthalene and 4'-octyloxynaphthyl-1'-(4-decyloxybenzoate). In each case the linear refractive index n of the material is accounted for. Refractive indices were measured at 1053 nm on an Abbe refractometer. The last compound is a liquid crystal synthesized at LLE out of a series of tolane and ester-linked naphthyl compounds, the nonlinear behavior of which will be published elsewhere.⁹ Maintaining alignment throughout the liquid-crystal bulk over the 500- μm sample path was difficult. We chose to measure $\chi^{(3)}$ in the sample's isotropic phase ($>90^\circ\text{C}$), realizing that a penalty in $\chi^{(3)}$ magnitude had to be paid by giving up the macroscopic mesophase alignment. CARS measurements of $\chi^{(3)}$ have been done on liquid-crystalline systems before.^{10,11} The values for nitrobenzene compare well with the relative value of 0.5 deduced from the 3-ns four-wave mixing data of Levenson and Bloembergen.¹² The values for chloronaphthalene can be compared with earlier, relative measurements by Saikan and Marowsky¹³ who found for 2-ns excitation near 440 nm a relative value of 0.3. The results show that within a factor of 2–3, these materials approach the $\chi^{(3)}$ values of CS_2 .

Table 1

Measured Relative Third-Order Nonlinear Susceptibilities $\chi^{(3)}/n^2$

Material	CS ₂	Nitrobenzene	Chloronaphthalene	OONDOB*
CARS	1	0.31 ± 0.07	0.46 ± 0.12	0.37 ± 0.06
CSRS	1	0.29 ± 0.07	0.42 ± 0.10	0.39 ± 0.06

*4'-octyloxynaphthyl-1'-(4-decyloxybenzoate) in isotropic phase

D. ERROR ANALYSIS

There are two possible error sources that cause the fluctuations of the Stokes and anti-Stokes generation. One comes from the laser fluctuation: the two pump pulses may not be well compressed and mixed by the compression grating pair due to the nonlinear frequency chirp, self-phase modulation, and spectral gain narrowing generated in CPA (see Chap. II). This can be improved immediately by adjusting the band-width of the self-phased-modulated spectrum generated from the optical fiber, avoiding self-phase modulation in amplification process, and carefully aligning the compression gratings. Masking a chirped pulse directly stretched from an ultrashort pulse is also a good choice for reducing the non-ideal pulse compression.³⁻⁵ The other comes from the interactions between the two pump pulses in the nonlinear medium other than the Stokes and anti-Stokes generation: two beam coupling,^{14,15} and phase modulations.

In considering the energy transfer between the light and the nonlinear material, we assume the nonlinear part of the refractive index n_{NL} can be described by the Debye relaxation equation in the integral form^{14,15}

$$n_{NL}(t) = \frac{n_2}{\tau} \int_{-\infty}^t I(t') \exp\left(-\frac{t'-t}{\tau}\right) dt', \quad (5.1)$$

where the relaxation time τ describes the time interval needed for the nonlinearity to develop. When the relaxation time τ is much shorter than the laser pulse duration, Eq. (5.1) gives the limiting result $n_{NL}(t) = n_2 I(t)$, which is consistent with the optical Kerr effect described in Chap. II. The order of magnitude of the relaxation time τ is as follows: femtosecond for electronic polarization, picosecond

for molecular orientation, nanosecond for electrostriction, millisecond for thermal effect.^{16,17} Using a procedure similar to that shown in Chap. II, we describe the mixed laser field on the moving pulse frame $t = \hat{t} - z/v_g$, as $E(t) = \text{Re}[E_0(t)\exp(i\omega_0 t)]$, where ω_0 is the center frequency of the continuum before the spectral window being used, \hat{t} is the usual laboratory time coordinate, and v_g is the group velocity. By neglecting the absorption, group velocity dispersion, and diffraction of the light in the nonlinear medium, the wave equation (A6) (see appendix) can be reduced in the form

$$\frac{\partial E_0}{\partial z} = -i \frac{2\pi}{\lambda_0} n_{\text{NL}}(t) E_0. \quad (5.2)$$

The laser light before entering the nonlinear material is $E_0(t) = A_1(t)\exp(iw_1 t) + A_2(t)\exp(iw_2 t)$, where $w_1 \equiv \omega_1 - \omega_0$ and $w_2 \equiv \omega_2 - \omega_0$ denote the frequency shifts relative to the fundamental frequency ω_0 .

We assume the electric field in the nonlinear material, including Stokes' and anti-Stokes' waves, can be written as

$$E_0(z, t) = A_1(z, t)e^{iw_1 t} + A_2(z, t)e^{iw_2 t} + A_s(z, t)e^{i(2w_2 - w_1)t} + A_{as}(z, t)e^{i(2w_1 - w_2)t}. \quad (5.3)$$

Using non-depletion conditions, $A_s, A_{as} \ll A_1, A_2$, we can approximately describe the laser intensity in the nonlinear medium as

$$I(z, t) = \frac{\epsilon c}{2} |E_0|^2 \approx \frac{\epsilon c}{2} \left[|A_1|^2 + |A_2|^2 + A_1 A_2^* e^{i(w_1 - w_2)t} + A_1^* A_2 e^{i(w_2 - w_1)t} \right]. \quad (5.4)$$

Substituting Eq. (5.4) into Eq. (5.1), assuming the amplitudes A_1 and A_2 are nearly invariant within the time scale τ , and carrying out the integral in Eq. (5.1), the nonlinear refractive index becomes

$$n_{\text{NL}}(t) = n_2(I_1 + I_2) + n_2 \frac{\epsilon c}{2} \left(\frac{A_1 A_2^* e^{i\Delta\omega t}}{1 + i\Delta\omega\tau} + \frac{A_1^* A_2 e^{-i\Delta\omega t}}{1 - i\Delta\omega\tau} \right), \quad (5.5)$$

where $I_{1,2} \equiv (\epsilon c/2)|A_{1,2}|^2$, and $\Delta\omega \equiv \omega_1 - \omega_2 = \omega_1 - \omega_2$.

Substituting Eq. (5.3) into Eq. (5.2), using Eq. (5.5), and collecting terms with the same frequency, we obtain a set of equations for the wave amplitudes

$$\frac{\partial A_1}{\partial z} = -i \frac{2\pi n_2}{\lambda_0} \frac{I_2}{1+i\Delta\omega\tau} A_1 - i \frac{2\pi n_2}{\lambda_0} [I_1 + I_2] A_1 \quad (5.6)$$

$$\frac{\partial A_2}{\partial z} = -i \frac{2\pi n_2}{\lambda_0} \frac{I_1}{1-i\Delta\omega\tau} A_2 - i \frac{2\pi n_2}{\lambda_0} [I_1 + I_2] A_2 \quad (5.7)$$

$$\frac{\partial A_s}{\partial z} = -i \frac{2\pi n_2}{\lambda_0} \frac{\epsilon c}{2} \frac{A_1^* A_2^2}{1-i\Delta\omega\tau} - i \frac{2\pi n_2}{\lambda_0} [I_1 + I_2] A_s \quad (5.8)$$

$$\frac{\partial A_{ss}}{\partial z} = -i \frac{2\pi n_2}{\lambda_0} \frac{\epsilon c}{2} \frac{A_2^* A_1^2}{1+i\Delta\omega\tau} - i \frac{2\pi n_2}{\lambda_0} [I_1 + I_2] A_{ss}. \quad (5.9)$$

Equations (5.6) to (5.9) provide the theoretical framework necessary for this analysis. The energy transfer between the two pump waves is described by the coupling equations (5.6) and (5.7). The Stokes and anti-Stokes waves are described by Eqs. (5.8) and (5.9), respectively. The common phase modulation for these four waves is shown in the last terms of Eqs. (5.6) to (5.9).

The two beam coupling equations (5.6) and (5.7) can be written in terms of I_1 and I_2 by using their complex conjugate equations. This gives¹⁴

$$\frac{\partial I_1}{\partial z} = - \frac{4\pi n_2}{\lambda_0} \frac{\Delta\omega\tau}{1+(\Delta\omega)^2\tau^2} I_1 I_2, \quad (5.10)$$

$$\frac{\partial I_2}{\partial z} = \frac{4\pi n_2}{\lambda_0} \frac{\delta\tau}{1+(\Delta\omega)^2\tau^2} I_1 I_2. \quad (5.11)$$

Adding Eq. (5.10) to Eq. (5.11) gives $\partial(I_1+I_2)/\partial z = 0$, the non-depletion condition. Letting $I_{\text{tot}}(t) \equiv I_1(z,t)+I_2(z,t) = I_1(0,t)+I_2(0,t)$, substituting the relation, $I_1(z,t) = I_{\text{tot}}(t)-I_2(z,t)$, into Eq. (5.11), and solving, we obtain

$$\frac{I_2(z,t)}{I_1(z,t)} = \frac{I_2(0,t)}{I_1(0,t)} \exp \left[\frac{4\pi n_2}{\lambda_0} \frac{\Delta\omega\tau}{1+(\Delta\omega)^2\tau^2} I_{\text{tot}}(t) z \right]. \quad (5.12)$$

Equation (5.12) shows the result of two beam coupling. The high-frequency (ω_1) pulse tends to transfer energy to the low-frequency (ω_2) pulse. When $\Delta\omega \cdot \tau$ approaches 0 or ∞ , there is no energy transfer between two pulses. When $\Delta\omega \cdot \tau = 1$ the energy transfer between two pulses is maximized. In $\chi^{(3)}$ measurements described in the previous section, two beam coupling is one of the mechanism that causes the spectral line fluctuation. To reduce the error, two beam coupling must be avoided. However, Eq. (5.12) shows a simple form for relaxation time measurement. By changing the spectral difference $\Delta\omega$ between two pump signals, one can obtain a set of output signal intensity ratios. The relaxation time τ is obtained as $\tau = 1/\Delta\omega$, when $\Delta\omega$ gives the maximum intensity ratio. For CS_2 the molecular re-orientation time is ~ 2 ps,^{18,19} the resonant condition occurs at $\Delta\omega = \omega_1 - \omega_2 = 1/\tau = 5 \times 10^{11}$ rad/sec, that is, when the wavelength difference between two pump waves is 3 Å.

If we assume the energy transfer between two pump signals is negligible, Eqs. (5.8) and (5.9) can be integrated to give

$$I_s = \left(\frac{2\pi n_2}{\lambda_0} \right)^2 I_1 I_2 z^2 \frac{1}{1 + (\Delta\omega)^2 \tau^2} \quad (5.13)$$

and

$$I_{as} = \left(\frac{2\pi n_2}{\lambda_0} \right)^2 I_1^2 I_2 z^2 \frac{1}{1 + (\Delta\omega)^2 \tau^2}. \quad (5.14)$$

For large values of $\Delta\omega \cdot \tau$ both Stokes and anti-Stokes waves are reduced by a factor of $1/[1 + (\Delta\omega)^2 \tau^2]$. This statement, however, is just true for a two-level atom far from resonance. The assumption of Debye-relaxation equation with a single decay time τ is only an approximation of the real physical process. Recently a model with several components of orientational response was considered.

Detailed theoretical and experimental descriptions are shown in Ref. 19 (and its references).

The frequency domain analysis shows another reason for the spectral line fluctuation of the pump waves and the scattering waves: the phase modulation $B = n_2(I_1 + I_2)(2\pi/\lambda_0)L$ enters into the power spectra of these waves. This phase modulation is clearly shown in the last term of Eqs. (5.6)-(5.9). The spectral line shapes of Stokes and anti-Stokes waves and the two pump waves are all distorted by this phase modulation. The total area beneath each line, however, is not changed by this phase modulation. It is equal to the time integral of each wave. Therefore in this experiment, the strength of each wave is obtained by integrating over its spectral lineshape instead of by its peak value.

E. DISCUSSION

A simple solution to synchronization jitter²⁰ among CARS input sources is presented. Spectral shaping of a linearly chirped pulse in the expansion gratings of a CPA laser was used to produce two pulses with different frequencies. A regenerative amplifier of appropriate bandwidth was used to amplify these two pulses. After amplification these two pulses were temporally mixed through compression gratings. With this technique two pulses are jitter-free and spatially identical. The alignment and synchronization are thus greatly simplified. In general, any ultra-short pulse source used in conjunction with expansion and compression grating pairs can serve as driver for this kind of four-wave mixing experiment. To reach other wavelength, sources such as Ti:sapphire could be used in a similar manner.

The energy transfer between two beams in this experiment is treated as a noise source. This two beam coupling phenomena, however, provides the relaxation time measurement by using the beating between the two lines. As the beating frequency resonates to the relaxation time of the nonlinear medium, the energy transfer between two signals is maximized. From the line ratio change one can measure the resonant condition and, as a result, the relaxation time.

The laser technique for producing two pump waves used in this experiment can be extended to produce synchronized multiple waves by changing the spectral window. These synchronized waves can be mixed by compression gratings for wave-mixing applications. They also can have different delays between each other by applying optical delay near the spectral window. This technique can be used for pump-probe experiments. The advantage is that each signal has its own distinguishable frequency but nearly same group velocity so that collinear pump-probe is possible. The identical beam profiles of pump and probe waves generated from the same regenerative amplifier also reduce the experimental uncertainty due to beam pattern fluctuation in usual two-beam pump-probe experiments.

REFERENCES

1. P. D. Maker and R. W. Terhune, *Phys. Rev.* **137**, A801 (1965).
2. R. Adair, L. L. Chase, and S. Payne, *J. Opt. Soc. Am. B* **4**, 875 (1987);
R. Adair, L. L. Chase and S. Payne, *Phys. Rev. B* **5**, 3337 (1989).
3. D. Strickland and G. Mourou, *Opt. Commun.* **56**, 219 (1985).
4. P. Maine, D. Strickland, P. Bado, M. Pessot, and G. Mourou, *IEEE J. Quantum Electron.* **QE-24**, 398 (1988).
5. Y.-H. Chuang, D. D. Meyerhofer, S. Augst, H. Chen, J. Peatross, and S. Uchida, "Suppression of the pedestal in a chirped-pulse-amplification laser," *J. Opt. Soc. Am. B* **8**, 1226 (1991).
6. D. Grischkowsky and A. C. Balant, *Appl. Phys. Lett.* **41**, 1 (1982).
7. E. B. Treacy, *IEEE J. Quantum Electron.* **QE-5**, 454 (1969).
8. A. M. Weiner, D. E. Leaird, J. S. Patel, and J. R. Wullert, *Opt. Lett.* **15**, 326 (1990).
9. K. Marshall, B. Puchebner, Z.-W. Li, Y.-H. Chuang, D. D. Meyerhofer, and A. Schmid, "Third-order nonlinear optical susceptibilities in naphthyl liquid-crystal systems," in preparation.
10. A. F. Bunkin, S. G. Ivanov, N. I. Koroteev, N. I. Rezov, and M. L. Sybeva, *Vestn. Mosk. Univ. Fiz. Astron. (USSR)* **18**, 35 (1977).
11. L. S. Aslanyan, N. N. Badalyan, A. A. Petrosyan, M. A. Khurshudyan, and Yu. S. Chilingaryan, *Opt. Spectrosc.* **53**, 54 (1982).
12. M. D. Levenson and N. Bloembergen, *J. Chem. Phys.* **60**, 1323 (1974).
13. S. Saikan and G. Marowsky, *Opt. Commun.* **26**, 466 (1978).
14. Y. Silberberg and I. Bar Joseph, "Instabilities, self-oscillation, and chaos in a simple nonlinear optical interaction," *Phys. Rev. Lett.* **48**, 1541 (1982).

15. Y. Silberberg and I. Bar-Joseph, "Optical instabilities in a nonlinear Kerr medium," *J. Opt. Soc. Am. B* **1**, 662 (1984).
16. R. W. Hellwarth, *Prog. Quantum Electron.* **5**, 1-68 (1977).
17. A. Owyong, Ph. D. Thesis, California Institute of Technology, 1971.
18. J-M. Halbout and C. L. Tang, "Femtosecond interferometry for nonlinear optics," *Appl. Phys. Lett.* **40**, 765 (1982).
19. C. E. Barker, R. Trebino, A.G. Kostenbauder, and A. E. Siegman, "Frequency-domain observation of the ultrafast inertial response of the optical Kerr effect in CS₂," *J. Chem. Phys.* **92**, 4740 (1990).
20. For an extensive discussion of oscillator phase jitter, see: M. J. W. Rodwell, D. M. Bloom, and K. J. Weingarten, *IEEE J. Quantum Electron.* **QE-25**, 817 (1989).

CHAPTER VI

AMPLIFICATION OF PHASE-MODULATED LIGHT FOR SSD

In this chapter the results of modelling the amplification of broadband laser pulses presented in Chap. II are extended to those pulses used in smoothing by spectral dispersion (SSD). The power gain is treated as a function of instantaneous frequency to simplify the analysis. Distortion of this phase-modulated pulse due to propagation and spectral gain narrowing is presented. Phase variations due to propagation and self-phase-modulation (SPM) are investigated to ensure the preservation of the initial phase modulation of the pulse. Local self-focusing of light, enhanced by the initial phase modulation, is shown to be critical for pulse amplification. For a pulse with a 3 \AA bandwidth and an angular dispersion $\Delta\theta/\Delta\lambda = 500 \text{ \mu rad/\AA}$, the local self-focusing length in Nd:glass can be shorter than one meter at an intensity $I = 5 \text{ GW/cm}^2$.

A. INTRODUCTION

In laser fusion, attention is currently being focussed on techniques to smooth the laser beam in order to form a uniform plasma. Broad-bandwidth and spatially incoherent laser pulses are proposed to average the interference between beamlets in time and space and achieve beam uniformity. One method is called induced spatial incoherence (ISI).^{1,2} A broad-bandwidth laser beam with short coherence time is divided into numerous independent beamlets by an orthogonal pair of reflecting, echelon-like mirrors. The echelons introduce time delays between the beamlets which are longer than the coherence time. The beamlets are

overlapped onto the target by a lens to form an instantaneous interference pattern which converges to a smooth intensity profile when averaged over time scales longer than the coherence time. Another method combining the phase-plate techniques^{3,4} and the phase-modulated broad-bandwidth laser is called smoothing by spectral dispersion (SSD).⁵ The bandwidth and the frequency modulation are obtained by passing a laser pulse through an electro-optic crystal. A pair of gratings is used to disperse the frequencies across the beam, without distorting the temporal pulse shape. After amplification the laser beam is broken up into beamlets using a phase plate and then focussed onto the target to form the time-averaged beam smoothing. In this chapter we deal with the amplification of the laser pulses treated by SSD technique.

In SSD the pulse leaving the second grating can be described by:⁵

$$E(t) = A \exp[i\omega_0 t + i\delta \sin(\omega_m t + \beta y)] = A \sum_n J_n(\delta) \exp\{i[\omega_0 t + n(\omega_m t + \beta y)]\}, \quad (6.1.1)$$

where δ and ω_m are the modulation amplitude and angular frequency of the electro-optical device, ω_0 is the fundamental angular frequency of the laser, and β , describing phase modulation across the transverse direction y , is related to the grating dispersion $\Delta\theta/\Delta\lambda$ by

$$\beta = 2\pi \frac{\Delta\theta}{\Delta\lambda} \frac{\omega_m}{\omega_0}. \quad (6.1.2)$$

As a result, different parts of the pulse (transverse and longitudinal) have different instantaneous frequencies. To amplify this pulse, care must be taken to preserve the initial frequency modulation, and not to distort the temporal profile.

When this phase-modulated pulse propagates through the amplifiers, there are three mechanisms that may lead to amplitude modulation. Angular dispersion

of the phase-modulated pulse tends to re-distribute the pulse energy during propagation and thus modulates the pulse amplitude. Spectral gain narrowing gives higher gain in any part of the pulse which has the instantaneous frequency near the linecenter of the gain medium and causes amplitude modulation.⁶ Gain saturation also causes amplitude modulation because the leading edge of the pulse undergoes higher gain than the trailing edge due to the depletion of the population inversion. These three mechanisms are not only coupled to each other but also depend on the phase variations of the pulse during propagation.

In addition to the evolution of the initial phase modulation, there are also three mechanisms that may cause phase modulation during amplification: diffraction, self-phase-modulation (SPM), and the phase-shift part of atomic response in gain medium.⁷ These three mechanisms are also coupled to each other and in turn depend on the amplitude modulation of the light pulse. When preserving the initial pulse frequency modulation through the gain medium is necessary, these phase variations should be minimized. Self-focusing, a result of phase variation in space, may damage the amplifier and must be avoided. As a result, the energy extraction efficiency of amplification process may be limited by these phase variations.

The purpose of this chapter is to provide an intuitive way of understanding the amplification of broadband SSD pulses. The instantaneous-frequency approximation derived in Chap. II and in the appendix are used. The major extension of the work in Chap. II is the inclusion of spatial effects. In Section B, we provide a set of basic equations that govern the amplification of broadband, phase-modulated pulses. In Section C, approximate solutions are obtained to analyze the amplitude and phase modulation during amplification process. The following topics

are studied: (a) amplitude modulation, (b) phase modulation, and (c) small scale self-focusing. The main results of this chapter are summarized in Section D.

B. BASIC EQUATIONS

The model considers a laser pulse, $E = E_0 e^{i\omega_0 t} = A e^{i(\omega_0 t - \phi)}$ traveling in the +z direction through a gain medium with a power-gain coefficient $\alpha(\omega) = \alpha_r(\omega) + i\alpha_i(\omega)$, where A and ϕ are real functions. The nonlinear dependence of the index of refraction on applied signal strength is given by the optical Kerr effect,⁷ $n = n_0 + n_{2E}\langle E^2 \rangle = n_0 + n_{2E} A^2/2 = n_0 + n_2 I$. The basic equation governing the light propagation in an amplifier including SPM is⁷ (also see appendix)

$$\frac{\partial E_0}{\partial z} = \frac{1}{2} [\alpha_r(\omega_i) + i\alpha_i(\omega_i)] E_0 - i \frac{1}{2k_0} \nabla_{\perp}^2 E_0 - i \frac{\beta_2}{2} |E_0|^2 E_0, \quad (6.2.1)$$

where $\omega_i \equiv \omega_0 - \partial\phi/\partial t$ is the instantaneous frequency of the laser pulse, $\beta_2 \equiv 2\pi n_{2E}/\lambda_0$, and λ_0 is the laser wavelength in vacuum. Note that z and t refer to coordinates in the moving pulse frame, which is defined by the transformation, $z = \hat{z}$ and $t = \hat{t} - \hat{z}/c$, where \hat{z} and \hat{t} are ordinary laboratory coordinates and c is the velocity of light in the amplifier. Equation (6.2.1) is similar to Eq. (2.3.5) in Chap.

II except that the term $\frac{1}{2k_0} \nabla_{\perp}^2 E_0$ is added to describe spatial effects in SSD.

In the gain-saturation regime, the power-gain coefficient α is a function of the the population inversion N of the gain medium. The simple two-level-atom model described in Chap. II provides the following relations for a homogeneously broadened gain medium^{6,7,8} (also see appendix and Eqs. (2.3.6) to (2.3.8))

$$\alpha_r[\omega_i(t)] \equiv \frac{\sigma_0 N}{1 + \left\{ \frac{2[\omega_i(t) - \omega_a]}{\Delta\omega_a} \right\}^2} \equiv \sigma[\omega_i(t)]N \quad (6.2.2)$$

$$\alpha_i[\omega_i(t)] \equiv -\frac{2[\omega_i(t) - \omega_a]}{\Delta\omega_a} \sigma[\omega_i(t)]N \quad (6.2.3)$$

with

$$\frac{\partial N}{\partial t} = -\frac{2^*}{\hbar\omega_0} \sigma[\omega_i(t)]NI, \quad (6.2.4)$$

describing the depletion of the population inversion, where $I = \epsilon c A^2/2$ is the laser intensity, ϵ and c are the dielectric constant and speed of light in the gain medium, ω_a and $\Delta\omega_a$ are the linecenter frequency and the full atomic linewidth, and 2^* is a dimensionless population saturation factor with values between 1 and 2, depending on the gain medium.⁷ For an inhomogeneously broadened gain medium, it is necessary to find an atomic model for the inhomogeneities and sum over them.⁹

Equations (6.2.1) to (6.2.4) provide the general framework for light pulses propagation in the amplifiers. For convenience, we choose $z = 0$ as the image-relay plane of the second grating. At this image plane the laser pulse can be described by Eq. (6.1.1) with both A and β divided by the total magnification of the spatial filters.¹⁰ In the following analysis we still keep the phase modulation at the image-relay plane in the form

$$\phi_0 = -\delta \sin(\omega_m t + \beta y). \quad (6.2.5)$$

C. ANALYSIS

In this analysis, we focus on the modulations of the laser pulse due to the evolution of the initial phase modulation described in Eq. (6.1.1) during amplification and propagation. Therefore we only consider the transverse dimension y and neglect the dependence on x . We first split the real part and imaginary part of Eq. (6.2.1) into two real equations and further describe them on a ray trajectory. We then make the approximation that the light rays follow straight lines within the amplifier, that is, the actions, such as diffraction and self-focusing, do not significantly bend the rays within the amplifier. This gives us a set of analytical solutions including the amplitude and phase of the laser pulse. We use this result to obtain the small phase variations, such as those due to SPM, as perturbation solutions. In the extreme case when local self-focusing of light induced by the initial phase modulation occurs, we then take account of both diffraction and self-focusing to complete this analysis.

Equation (6.2.1) can be split into two coupled equations describing the energy relation and the equation of motion, respectively:¹¹⁻¹³

$$\frac{\partial A^2}{\partial z} + \frac{1}{k_0} \nabla_{\perp} \cdot (A^2 \nabla_{\perp} \phi) = \alpha_r(\omega_i) A^2, \quad (6.3.1)$$

and

$$\frac{\partial \phi}{\partial z} + \frac{1}{2k_0} (\nabla_{\perp} \phi)^2 + \left(\frac{1}{2} \alpha_i(\omega_i) - \frac{1}{2k_0} \frac{\nabla_{\perp}^2 A}{A} - \frac{\beta_2}{2} A^2 \right) = 0. \quad (6.3.2)$$

Equation (6.3.1) can be understood in the usual form for the energy conservation, i.e., $\partial \rho / \partial t + \nabla \cdot (\rho \mathbf{v}) = \alpha \rho$, with A^2 playing the role as the energy density ρ , and z , k_0 , $\nabla_{\perp} \phi$, ∇_{\perp} corresponding to the time t , the particle mass m , the momentum \mathbf{p} , and the operator ∇ , respectively. Equation (6.3.2) has the same form as the

Hamilton-Jacobi equation $\partial S/\partial t + H = 0$ in classical mechanics,¹¹⁻¹³ where $H = p^2/2m + V$ is the Hamiltonian of a particle in a potential well V , and S is the Hamiltonian's principle function. In this case the phase variation ϕ plays the role as S , and

$$V \equiv \frac{1}{2}\alpha_i(\omega_i) - \frac{1}{2k_0} \frac{\nabla_{\perp}^2 A}{A} - \frac{\beta_2}{2} A^2 \quad (6.3.3)$$

describes the atomic response, diffraction, and self-focusing. For simplicity, the x -dependence is neglected in the SSD analysis, and the operator ∇_{\perp} becomes $\partial/\partial y$.

In order to solve the energy equation (6.3.1), we label the light rays using their y positions at $z = 0$ (an image plane of the grating), where the phase variation is known. The light rays are defined as the trajectories orthogonal to the wave-fronts.¹⁴ In the current case this leads to the ray trajectory defined by

$$\frac{dy}{dz} = \frac{k_y}{k_0} = \frac{1}{k_0} \frac{\partial \phi}{\partial y}, \quad (6.3.4)$$

where k_y is the y component of the wavevector. Using the particle analogy stated above, Eq. (6.3.4) can be understood as a velocity-momentum relation, $dy/dt = p/m$. We now assume that the solution of Eq. (6.3.4) is $y(z; y_0)$, where the parameter y_0 is the y position of the ray trajectory at $z = 0$, and is used to label the ray. By varying the parameter y_0 we can obtain a family of ray trajectories. In this family there exists a ray that connects any given point (y, z) back to the position $(y_0, 0)$. In other words, if we know the functional form of $y(z; y_0)$, we can invert the function to obtain $y_0(y, z)$. The parameter y_0 varies among rays, but is a constant along a ray. Since $y_0(y, z)$ is an invariant (a constant) along a ray trajectory, it has

a convective derivative equal to zero along a ray, i.e., $(\partial y_0/\partial z)dz + (\partial y_0/\partial y)dy = 0$.

This gives the slope of a ray as

$$\frac{dy}{dz} = -\left(\frac{\partial y_0}{\partial z}\right) / \left(\frac{\partial y_0}{\partial y}\right). \quad (6.3.5)$$

By using the invariant function $y_0(y,z)$ in Eq. (6.3.5) instead of using the phase variation $\phi(y,z)$ in Eq. (6.3.4) to find the ray trajectory, we can solve the energy relation (6.3.1) along a ray trajectory without knowing the exact functional form of this ray trajectory.

Equation (6.3.1) can be solved analytically along a ray trajectory. Using $d/dz = \partial/\partial z + (dy/dz)(\partial/\partial y)$ and the slope equations (6.3.5) and (6.3.4), we obtain

$$\frac{\partial y_0}{\partial y} \frac{d}{dz} \left[A^2 / \left(\frac{\partial y_0}{\partial y} \right) \right] = \frac{\partial A^2}{\partial z} + \frac{\partial A^2}{\partial y} \frac{dy}{dz} + A^2 \frac{\partial}{\partial y} \left(\frac{dy}{dz} \right) = \frac{\partial A^2}{\partial z} + \frac{1}{k_0} \left(\frac{\partial A^2}{\partial y} \frac{\partial \phi}{\partial y} + A^2 \frac{\partial^2 \phi}{\partial y^2} \right),$$

which is nothing but the left hand side of Eq. (6.3.1) in one transverse dimension.

We can now rewrite Eq. (6.3.1) in the form

$$\frac{d}{dz} \left[A^2 / \left(\frac{\partial y_0}{\partial y} \right) \right] = \alpha_r(\omega_i) \left[A^2 / \left(\frac{\partial y_0}{\partial y} \right) \right]. \quad (6.3.6)$$

The amplification can be given by a simple integration along the ray,

$$I(y,z,t) = \left[\left(\frac{\partial y_0}{\partial y} \right) / \left(\frac{\partial y_0}{\partial y} \right)_{z_1} \right] I(y_1, z_1, t) \exp \left\{ \int_{z_1}^z [\alpha_r(\omega_i)]_{y_0} dz' \right\}, \quad (6.3.7)$$

where $z = z_1$ is the entrance of the amplifier, y_1 is the corresponding y position in $z = z_1$ plane, and the integration of the power gain coefficient is along the ray where y_0 is an invariant. The intensity and phase profile at the entrance of the amplifier $z=z_1$ can be determined from solving for the free propagation of SSD

pulses from the image-relay plane $z=0$, that is, from solving $y_0(y_1, z_1, t) = y_0(y, z, t)$. This technique will be discussed in Subsection C.1.

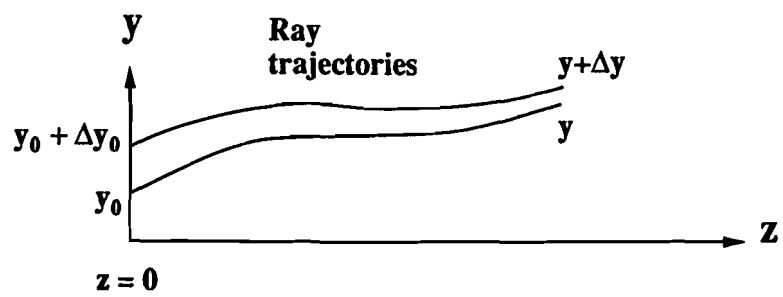
The energy relation between the position $z = 0$ and the current position z is shown in Fig. 6-1. Two neighboring rays with their initial positions at y_0 and $y_0+\Delta y_0$ are used to illustrate the energy flow. If we neglect the power gain in this illustration, we can intuitively obtain the energy-conservation relation $I(y_0, 0)\Delta y_0 = I(y, z)\Delta y$ or $I(y, z) = (\Delta y_0/\Delta y)I(y_0, 0)$ for an infinitesimal Δy_0 . This is nothing but a special case of Eq. (6.3.7) for $\alpha_r = 0$ and $z_1 = 0$. Once the functional form of the ray trajectory $y(z; y_0)$ is available, we can use Eq. (6.3.7) to predict the laser intensity $I(y, z)$ after propagation and amplification.

The ray trajectories can be obtained by solving Eq. (6.3.2). However, by knowing that the direct result of the Hamilton-Jacobi equation is the equation of motion, $\frac{d^2y}{dt^2} = -\frac{1}{m} \frac{\partial V}{\partial y}$, for the particle, we can rewrite Eq. (6.3.2) as

$$\frac{d^2y}{dz^2} = -\frac{1}{k_0} \frac{\partial V}{\partial y}, \quad (6.3.8)$$

for the ray trajectory y as a function of z with the initial condition $y = y_0$ at $z = 0$. One can also obtain Eq. (6.3.8) by taking the derivative of Eq. (6.3.2) with respect to y , and then using the slope relationship, $dy/dz = (\partial\phi/\partial y)/k_0$, and the following identity

$$\frac{d^2y}{dz^2} = \frac{\partial}{\partial z} \left(\frac{dy}{dz} \right) + \frac{dy}{dz} \frac{\partial}{\partial y} \left(\frac{dy}{dz} \right) = \frac{\partial}{\partial z} \left(\frac{dy}{dz} \right) + \frac{1}{2} \frac{\partial}{\partial y} \left(\frac{dy}{dz} \right)^2.$$



$$I(y, z)\Delta y = I(y_0, 0)\Delta y_0 \quad (\text{for no power gain})$$

$$\frac{\Delta y_0}{\Delta y} \rightarrow \frac{\partial y_0}{\partial y}$$

Fig. 6-1 The energy relation between the position $z = 0$ and the current position z is shown. Two neighboring rays with their initial positions at y_0 and $y_0 + \Delta y_0$ are used to illustrate the energy flow.

C.1. Amplitude Modulation

For simplicity we first assume that the light rays have the form of straight lines within the amplifier, that is, $d^2y/dz^2 = 0$. This assumption is valid only when α_i , $1/k_0$, and β_2 are all very small such that $V \rightarrow 0$, as shown in Eqs. (6.3.3) and (6.3.8). This assumption is an extension of the geometrical optics approximation that assumes $\lambda_0 \rightarrow 0$.¹⁴ From Eqs. (6.2.5) and (6.3.4) we obtain the initial slope of the ray at $z=0$, $y=y_0$ as $dy/dz = (\partial\phi_0/\partial y)/k_0 = -(\delta\beta/k_0)\cos(\omega_m t + \beta y_0)$. Since we assume that the light rays follow straight lines this slope is a constant along the ray. Direct integration gives the ray trajectory

$$y = y_0 - \frac{\delta\beta z}{k_0} \cos(\omega_m t + \beta y_0). \quad (6.3.9)$$

Varying the parameter y_0 we can obtain a family of rays that cover all the laser field. Inversion of Eq. (6.3.9) implicitly gives $y_0(y, z, t)$, the desired functional form for later analyses.

Using the slope equation (6.3.4) and Eq. (6.3.2) for $V = 0$, we obtain

$$\frac{\partial\phi(y, z, t)}{\partial y} = -\delta\beta \cos[\omega_m t + \beta y_0(y, z, t)] \quad (6.3.10)$$

and

$$\frac{\partial\phi(y, z, t)}{\partial z} = -\frac{1}{2k_0} \left(\frac{\partial\phi}{\partial y} \right)^2 = -\frac{\delta^2\beta^2}{2k_0} \cos^2[\omega_m t + \beta y_0(y, z, t)], \quad (6.3.11)$$

respectively. Note that the parameter y_0 becomes a function of y , z , and t from inverting Eq. (6.3.9). Integrating $d\phi/dz = (\partial\phi/\partial y)(dy/dz) + (\partial\phi/\partial z)$ along the ray gives the phase variation at position z ,

$$\phi(y, z, t) = -\delta \sin[\omega_m t + \beta y_0(y, z, t)] + \frac{\delta^2\beta^2 z}{2k_0} \cos^2[\omega_m t + \beta y_0(y, z, t)], \quad (6.3.12)$$

where Eqs. (6.3.10), (6.3.11), and the initial condition $\phi_0 = -\delta\sin(\omega_m t + \beta y_0)$ have been used. Note that in the above integration $y_0(y, z, t)$ is a constant along the ray. Differentiating Eq. (6.3.9) about y gives

$$\frac{\partial y_0}{\partial y} = \left\{ 1 + \frac{\delta\beta^2 z}{k_0} \sin[\omega_m t + \beta y_0(y, z, t)] \right\}^{-1}. \quad (6.3.13)$$

Using this result, the laser intensity can be obtained directly from Eq. (6.3.7):

$$I(y, z, t) = \left\{ \frac{1 + \frac{\delta\beta^2 z_1}{k_0} \sin[\omega_m t + \beta y_0(y, z, t)]}{1 + \frac{\delta\beta^2 z}{k_0} \sin[\omega_m t + \beta y_0(y, z, t)]} \right\} I_0(y_1, z_1, t) \exp\left\{ \int_{z_1}^z [\alpha_r(\omega_i)]_{y_0} dz' \right\}, \quad (6.3.14)$$

where

$$y_1 = y_0(y, z, t) - \frac{\delta\beta z_1}{k_0} \cos[\omega_m t + \beta y_0(y, z, t)]. \quad (6.3.15)$$

The integration of the power gain coefficient is along the trajectory described by Eq. (6.3.9).

Equations (6.3.9), (6.3.12), and (6.3.14) are only valid in the range $|z| < z_r$,

where

$$z_r \equiv \frac{k_0}{\delta\beta^2} \quad (6.3.16)$$

is the radius of curvature of the initial phase front ϕ_0 near $\sin(\omega_m t + \beta y_0) = -1$, that is, the local focal length (in geometrical optics approximation) of the rays coming from the vicinity of $\sin(\omega_m t + \beta y_0) = -1$. When $z \geq z_r$ there exists a caustic line¹⁴

$$1 + \frac{\delta\beta^2 z}{k_0} \sin[\omega_m t + \beta y_0(y, z, t)] = 0 \quad (6.3.17)$$

that gives the laser intensity equal to infinity in this approximation. In practical, however, when $z \approx z_r$ diffraction becomes significant and the light rays will no longer be straight.

Equation (6.3.14) shows, in a nice form, that we can treat the intensity modulations due to propagation and power gain separately. We first neglect the power gain in Eq. (6.3.14) and focus on a simple free propagation case, $I = I_0 / \{1 + (\delta\beta^2 z / k_0) \sin[\omega_m t + \beta y_0(y, z, t)]\}$ for $z_1 = 0$. Figure 6-2 shows the intensity modulation of the initially phase-modulated light after free propagating a distance $z = 20$ m, with $\delta = 4$, $\omega_m / (2\pi) = 10$ GHz, (bandwidth $\approx 3\text{\AA}$), $\lambda_0 = 1053$ nm, ($k_0 = 5.967 \times 10^6 \text{ m}^{-1}$ in air), and $d\theta/d\lambda = 67 \mu\text{rad}/\text{\AA}$, ($\beta = 148 \text{ m}^{-1}$). This gives $z/z_r = 0.29$. The laser pulse has a Gaussian envelope with a pulse width 750 ps (FWHM) and a Gaussian beam profile with a beam diameter 10 cm (FWHM). A three dimensional plot of laser intensity is shown in Fig. 6-2(a). The peaks are at the positions where $\sin[\omega_m t + \beta y_0(y, z, t)] = -1$. The intensity profile of the central part of the beam, $y = 0$, is shown in Fig. 6-2(b). The intensity modulation across the beam at a certain time is not shown here, but is similar to Fig. 6-2(b) with a different number of peaks.

To explain the intensity modulation due to spectral gain-narrowing, we neglect the angular dispersion effects in Eq. (6.3.14), that is, calculate the intensity at the image-relay plane, $z=0$. Within small-signal-gain regime the amplified laser intensity becomes, $I = I_0 \exp[\alpha_r(\omega_i)L]$, where L is the amplifier length. The instantaneous frequency ω_i can be derived from Eq. (6.3.12):

$$\omega_i(y, z, t) = \omega_0 - \frac{\partial\phi}{\partial t} = \omega_0 + \delta\omega_m \cos[\omega_m t + \beta y_0(y, z, t)], \quad (6.3.18)$$

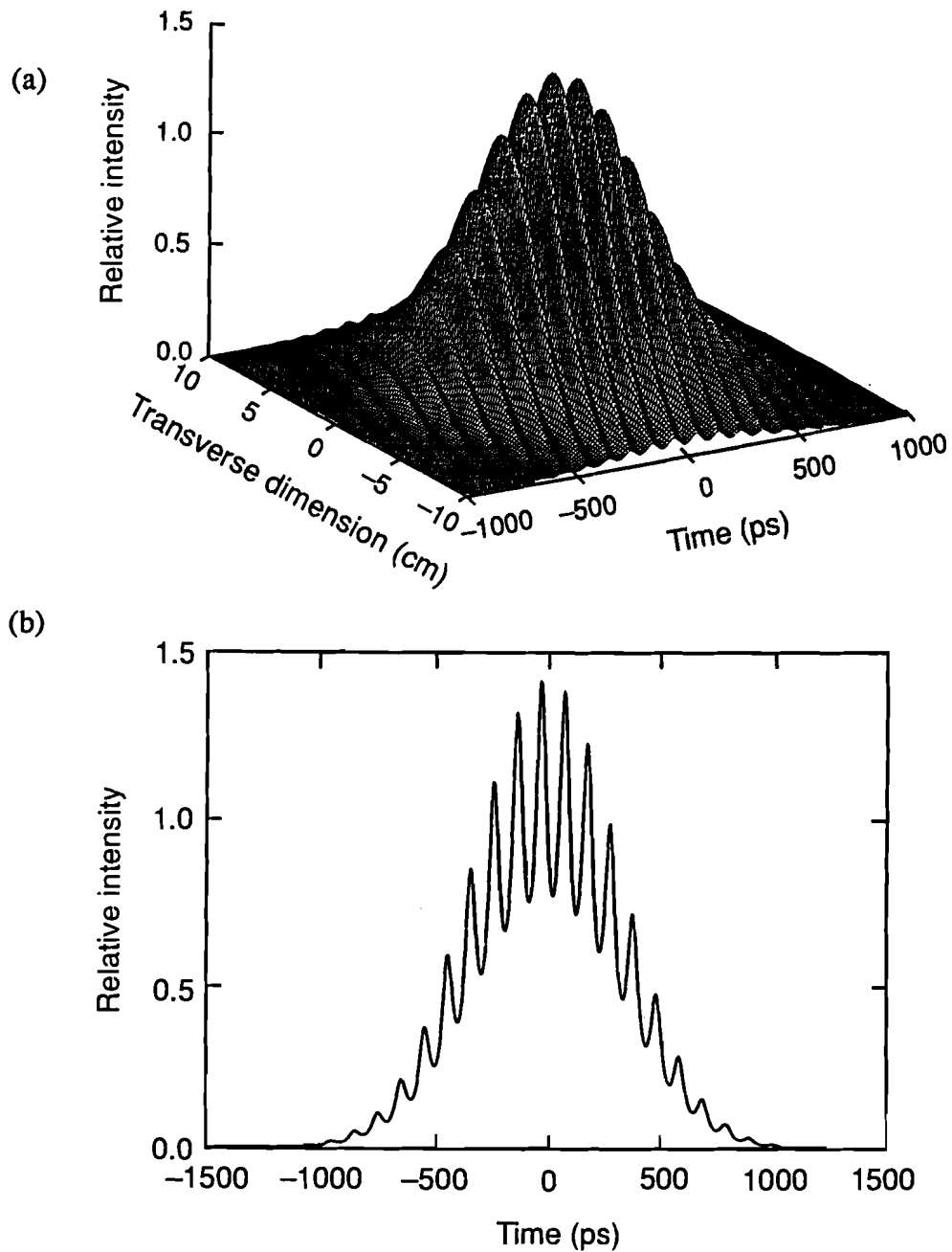


Fig. 6-2 Intensity modulation of initially phase-modulated light after free propagating a distance $z = 30$ m in air, with $\delta = 4$, $\beta = 148 \text{ m}^{-1}$, and $k_0 = 5.967 \times 10^6 \text{ m}^{-1}$. (a) Three dimensional plot of laser intensity. The peaks are at the positions where $\sin[\omega_m t - \beta y_0(y, z, t)] \approx -1$. (b) The intensity profile of a 750 ps pulse at center part of the beam, $y = 0$.

which is a constant within the integral in Eq. (6.3.14) because the function $y_0(y,z,t)$ is invariant along the ray. When the bandwidth of the applied signal, $\Delta\omega_L \approx 2\delta\omega_m$, is much smaller than the atomic linewidth of the gain medium $\Delta\omega_a$, the gain coefficient can be simplified with a quadratic form, $\alpha_r[\omega_i(t)] \approx \alpha_0 - (\alpha''/2)[\omega_i(t) - \omega_a]^2$, where $\alpha'' = -d^2\alpha_r(\omega)/d\omega^2$ evaluated at midband frequency ω_a . The power gain of the amplifier becomes

$$G(t) = G_0 \exp(- a \{d + \cos[\omega_m t + \beta y_0(y,z,t)]\}^2), \quad (6.3.19)$$

where $G_0 \equiv \exp(\alpha_0 L)$ is the power gain at midband, and parameters

$$a \equiv \alpha'' L \delta^2 \omega_m^2 / 2 \approx \alpha_0 L (2\delta\omega_m / \Delta\omega_a)^2 \quad (6.3.20)$$

and

$$d \equiv (\omega_0 - \omega_a) / (\delta\omega_m) \quad (6.3.21)$$

represent, respectively, the magnitude of spectral gain narrowing and the degree of frequency mismatch between the fundamental laser frequency ω_0 and the linecenter of the gain medium ω_a . In the last part of Eq. (6.3.20) we have assumed the curvature $\alpha'' \approx 8\alpha_0 / (\Delta\omega_a)^2$, which is exact for a Lorentzian lineshape.

Figure 6-3 shows the intensity modulation due to spectral gain narrowing. Since the laser intensity is calculated at the image-relay plane, the intensity modulation due to propagation is not shown in this figure, i.e., in the absence of gain narrowing, the curve will be smooth. The solid line represents the intensity profile of the amplified pulse at $y = 0$ with the frequency match, $d = 0$. The dotted line represents the frequency-mismatched case, $d = 1.08$. The numbers used in this example are: $\alpha_0 L = 25$ (for the entire amplifier system), $\delta = 4\pi$, $\omega_m / 2\pi = 10$ GHz, $\Delta\omega_a / 2\pi = 5.4 \times 10^{12}$ Hz (200 Å FWHM), $\omega_0 / 2\pi = 2.8470 \times 10^{14}$ Hz ($\lambda_0 =$

10530 Å), Gaussian pulse width 750 ps (FWHM), frequency offset 5 Å, and at $z = 0$, the image plane of the grating surface. Therefore, $a = 0.054$ and the initial spectral bandwidth is about 9.3 Å ($\Delta\omega_L \approx 2\delta\omega_m$). In the frequency-mismatched case, the intensity modulation is enhanced because of larger gain difference within the laser bandwidth.

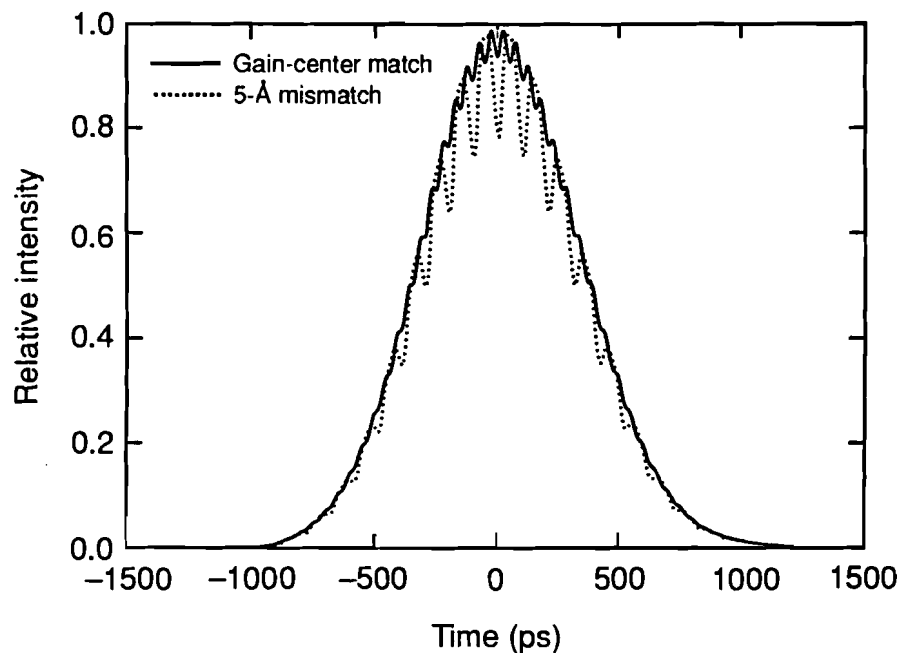


Fig. 6-3 Spectral gain narrowing of phase-modulated light can cause intensity modulation. The solid line represents the frequency matched case. The dotted line represents the case with 5 Å linecenter mis-match. The intensity modulation is enhanced because of larger gain difference within the laser bandwidth. Parameters: $\ln(G_0) = 25$, $\delta = 4\pi$, $\omega_m/2\pi = 10$ GHz, at $y = 0$.

For a homogeneous gain medium in the gain-saturation regime, the population inversion equation (6.2.4) becomes

$$\frac{\partial N}{\partial t} = -\frac{2^*}{\hbar\omega_0} \sigma(\omega_i) N I(y_1, z_1, t) \exp\left[\sigma(\omega_i) \int_{z_1}^z (N)_{y_0} dz'\right] \left(\frac{\partial y_0}{\partial y}\right) / \left(\frac{\partial y_0}{\partial y}\right)_{z_1}, \quad (6.3.22)$$

where Eq. (6.3.7) has been used. From Eq. (6.3.22) we know that gain saturation is coupled with gain narrowing and angular dispersion. The former comes from the fact that the gain cross section σ depends on the instantaneous frequency ω_i . If the angular dispersion is small and therefore $(\partial y_0/\partial y)/(\partial y_0/\partial y)_{z_1} \rightarrow 1$, Eq.(6.3.22) can be further simplified as

$$\frac{\partial N_{\text{tot}}}{\partial t} = -\frac{2^*}{\hbar\omega_0} I(z_1) \left\{ \exp[\sigma(\omega_i) N_{\text{tot}}] - 1 \right\}, \quad (6.3.23)$$

where $N_{\text{tot}} \equiv \int N dz$ is the total inverted population per unit amplifier area. Our calculation shows that for a small laser band width, $\Delta\omega_L/\Delta\omega_a < 0.1$, the dependence of gain saturation on instantaneous frequency is negligible in a single amplifier. Thus classical gain saturation theory⁸ can be used here. However, if the angular dispersion within the amplifier is large, a numerical solution for Eq. (6.3.22) is required.

C.2. Phase Modulation

The phase variation described in Eq. (6.3.12) is a result of propagating the initially phase-modulated light. Careful image relaying can bring this phase variation back to the originally designed phase modulation (at $z = 0$) for SSD. Other small phase variations can be obtained as perturbation solutions from Eq. (6.3.2). The reactive (or phase-shift) part of the atomic response in a homogeneous gain medium is

$$\phi_{\text{amp}}(t) \equiv -(1/2) \int \alpha_i(\omega_i) dz, \quad (6.3.24)$$

and the phase shift due to SPM is

$$\phi_{\text{SPM}} = k_0 n_2 \int I(z) dz, \quad (6.3.25)$$

where the instantaneous frequency ω_i and the laser intensity $I(z)$ are estimated from Eq. (6.3.18) and Eq. (6.3.14), respectively. Both phase variations can accumulate over the entire laser system. If the fundamental laser frequency ω_0 is matched to the linecenter of the gain medium ω_a , the value of ϕ_{amp} calculated from Eq. (6.2.3) and Eq. (6.3.24) is $\leq (1/2)(\Delta\omega_l/\Delta\omega_a) \ln(G)$ which is small and can be neglected. The peak value of ϕ_{SPM} is usually designed near 5 to optimize the energy extraction efficiency of the amplifier system.

Figure 6-4(a) shows the power spectrum of the amplified pulse at $y = 0$ and at an image-relay plane, $z = 0$. The bandwidth is about 9.3 Å, and the total B-integral is 5. Other parameters are the same as the gain narrowing case, except $a = 0$ and $d = 0$. The spectral distribution is almost the same as when the total B-integral is equal to zero, that is, the amplitude of each frequency mode is still described by the Bessel functions in Eq. (6.1.1). Fig. 6-4(b) shows the detailed view of the power spectrum. The finite width of each frequency mode is due to the finite laser pulse width. Each frequency mode separates into two bumps due to SPM. Whether this frequency split affects the frequency up-conversion or the beam uniformity should be further studied.

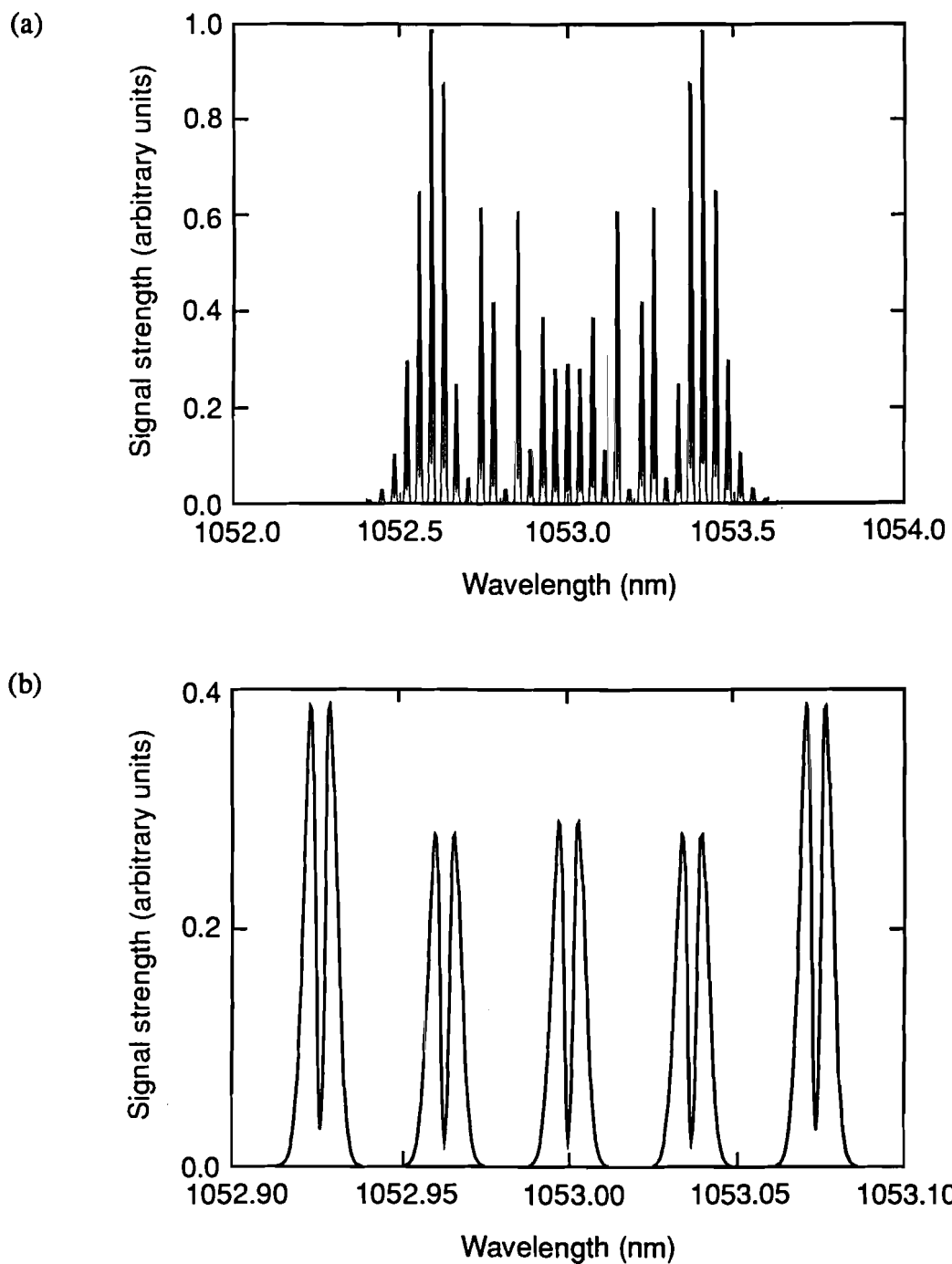


Fig. 6-4 (a) Power spectrum of the amplified pulse at $y = 0$, with B-integral = 5, $\delta = 4\pi$, and $\omega_m/2\pi = 10$ GHz. (b) Detailed view of (a) shows that each frequency mode separates into two bumps due to SPM.

C.3 Self-Focusing

In our analysis we will consider a constant intensity profile $I(z=0) = I_0$ in the y direction. In this approximation there would be no self-focusing in the absence of SSD phase modulation. For simplicity we let $z_1 = 0$, $\alpha_r = \text{constant}$, and $\alpha_i = 0$. Substituting Eq. (6.3.7) into Eq. (6.3.3) and then into Eq. (6.3.8) gives

$$\frac{d^2y}{dz^2} = \frac{1}{4k_0^2} \frac{\frac{\partial^4 y_0}{\partial y^4} \left(\frac{\partial y_0}{\partial y}\right)^2 - 2 \frac{\partial^3 y_0}{\partial y^3} \frac{\partial^2 y_0}{\partial y^2} \frac{\partial y_0}{\partial y} + \left(\frac{\partial^2 y_0}{\partial y^2}\right)^3}{\left(\frac{\partial y_0}{\partial y}\right)^3} + \frac{n_2 I_0}{n_0} \frac{\partial^2 y_0}{\partial y^2} \exp(\alpha_r z). \quad (6.3.26)$$

We try the ray in the form

$$y = y_0 - \frac{1}{\beta} M(z, y_0) \cos(\omega_m t + \beta y_0) \quad (6.3.27)$$

as a modification of the straight ray described in Eq. (6.3.9), and substitute it into Eq. (6.3.26). Then we choose the rays initially from the region $\sin(\omega_m t + \beta y_0) \approx -1$, where the light with initial angular dispersion tends to focus. With this choice, we find that the function M in this region is independent of y_0 , and obtain

$$z_r^2 \frac{d^2 M}{dz^2} = -\frac{1}{4\delta^2} \frac{M(7M+1)}{(1-M)^5} + \frac{UM}{(1-M)^3} \exp(\alpha_r z), \quad (6.3.28)$$

with initial conditions $M(0) = 0$ and $M'(0) = \delta\beta^2/k_0 = 1/z_r$, where

$$U = \left(\frac{n_2 I}{n_0}\right) \left(\frac{k_0^2}{\delta^2 \beta^2}\right) \quad (6.3.29)$$

is an index describing the ratio of the self-focusing force to the diffraction force. In this region the relative intensity modulation becomes $I/I_0 = \exp(\alpha_r z)(\partial y_0/\partial y) \approx \exp(\alpha_r z)/(1-M)$, and the relative beamlet width becomes $\Delta y/\Delta y_0 \approx (I/I_0)^{-1} \approx (1-M)/\exp(\alpha_r z)$.

In the right hand side of Eq. (6.3.28), the first term describes the diffraction force and the second term describes the self-focusing force. When $U > 1/4\delta^2$ the value of M increases as z increases. However as M approaches 1, the diffraction force grows with a factor $1/(1-M)^2$ stronger than the self-focusing force, and decreases the value of M .

If the power gain in Eq. (6.3.28) is neglected, this equation can be integrated to give

$$z_r^2 \left(\frac{dM}{dz} \right)^2 = \frac{(4\delta^2 + 4\delta^2 U + 1)(1-M)^4 - 8\delta^2 U(1-M)^3 + (4\delta^2 U - 7)(1-M)^2 + 10(1-M) - 4}{4\delta^2(1-M)^4}. \quad (6.3.30)$$

Further integration gives the local focal length z_f in a nonlinear medium,

$$\frac{z_f}{z_r} = \int_0^{M_{\max}} \frac{2\delta(1-M)^2 dM}{\sqrt{(4\delta^2 + 4\delta^2 U + 1)(1-M)^4 - 8\delta^2 U(1-M)^3 + (4\delta^2 U - 7)(1-M)^2 + 10(1-M) - 4}}, \quad (6.3.31)$$

where M_{\max} is the root of $dM/dz = 0$ between 0 and 1, obtained from Eq. (6.3.30).

For $U \gg 1$, or $\delta \gg 1$, we can approximately solve the integral in Eq. (6.3.31) leading to analytic form

$$\frac{z_f}{z_r} = \frac{1 - \sqrt{U}}{1 + U} + \frac{U}{(1 + U)^{3/2}} \log \left[(1 + \sqrt{1 + U}) (\sqrt{U^2 + U} + U) / U \right]. \quad (6.3.32)$$

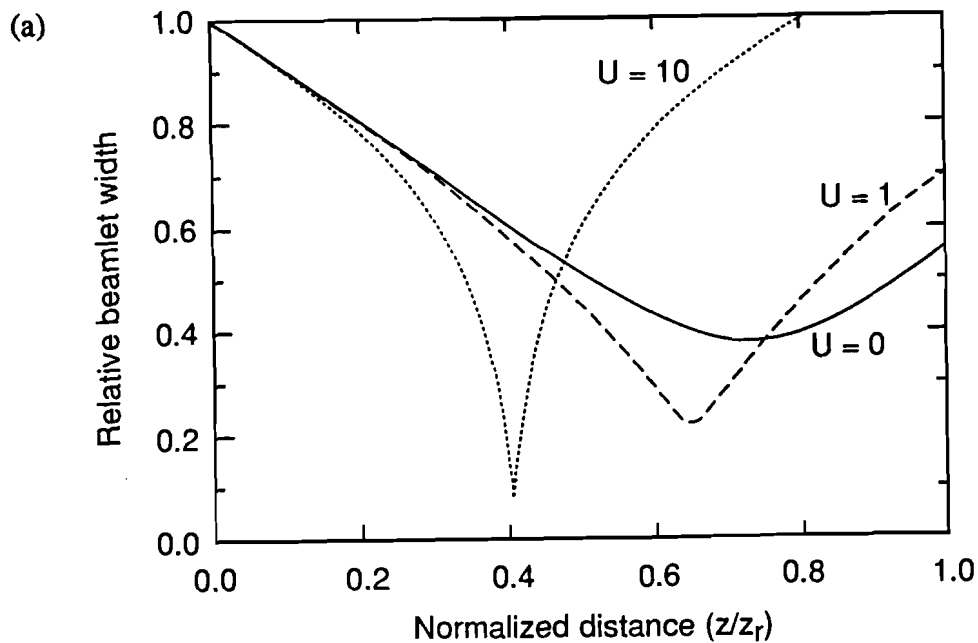
The maximum intensity modulation, $r = (I/I_0)_{\max}$, at the focus, can be obtained from solving

$$4r^4 - 10r^3 + 7r^2 - 1 - 4\delta^2 [U(r-1)^2 + 1] = 0 \quad (6.3.33)$$

with known δ and U . Equation (6.3.33) is derived from Eq. (6.3.30) by setting $dM/dz = 0$ and $r = 1/(1-M)$.

Figure 6-5(a) shows the ray trajectories under different self-focusing conditions $U = 0, 1, 10$. $U=0$ corresponds to the results from Subsection C.1 with

diffraction included. This figure is obtained from numerical integration of Eq. (6.3.28) with $\delta = 4$, and the power gain coefficient $\alpha_r = 0$. Figure 6-5(b) shows the local self-focusing length as a function of U with different values of δ . These curves are obtained from Eq. (6.3.31). For large U , they approach the same curve described by Eq. (6.3.32), which is shown in Fig. 6-5(c). Since the local self-focusing length is always smaller than the parameter $z_r = k_0/\delta\beta^2$, it is important to know the value of z_r when designing the initial phase modulation. For example, if we design the initial phase modulation with the following data, $\delta = 4$, $\omega_m/2\pi = 10$ GHz, (bandwidth = 3 Å), $\lambda_0 = 1053$ nm, $d\theta/d\lambda = 500$ $\mu\text{rad}/\text{Å}$, ($\beta = 1100$ m^{-1}), $n_2 = 3 \times 10^{-16}$ cm^2/W , $n_0 = 1.5$, and $I_0 = 5$ GW/cm^2 , then $z_r = 1.85$ m and $U = 4.14$. From Eq. (6.3.32) we obtain the local self-focusing length $z_f = 90$ cm. At the focus the local intensity will increase ~ 8 times as a result of Eq. (6.3.33).



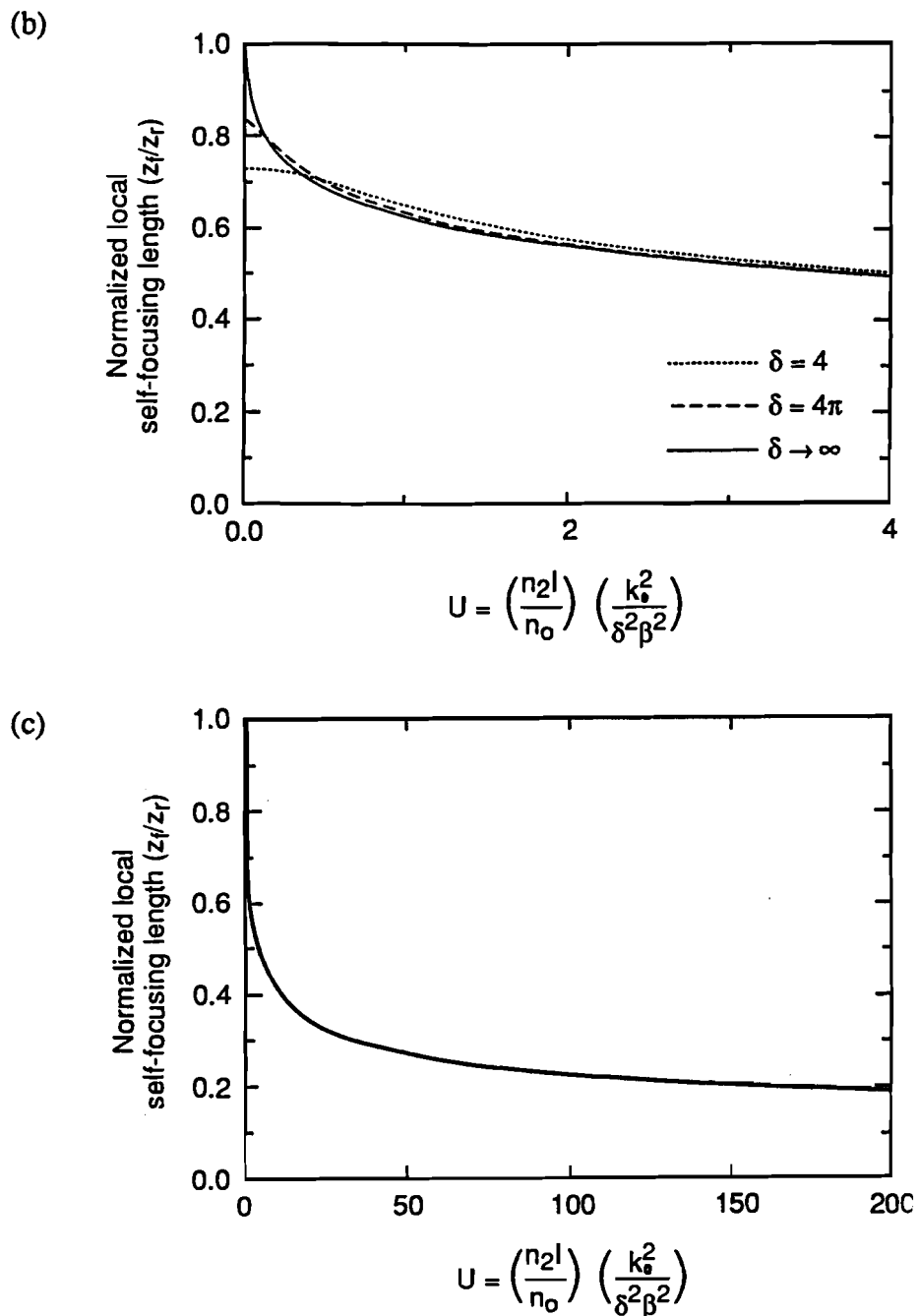


Fig. 6-5 Local self-focusing of light induced by the initial phase modulation. (a) The ray trajectories under different self-focusing conditions, $U = 0, 1,$ and $10,$ and $\delta = 4, \alpha_r = 0.$ (b) The normalized local self-focusing length z_f/z_r as a function of U in different values of $\delta.$ (c) Asymptotic solution of z_f/z_r for large $U.$

CONCLUSION

We can treat the power-gain coefficient as a function of instantaneous frequency and thus simplify the equations for the amplification of broad-band phase-modulated laser pulse. Through this treatment and following the light rays, we can solve for the intensity and phase modulation of this initially phase-modulated light during propagation and amplification.

Intensity modulations due to propagation (angular dispersion) and amplification (gain narrowing) can be treated separately within the geometrical optics approximation. This helps the design of the initial phase modulation in SSD to avoid the problems arising from propagation, image relay and amplification. For an amplification system with the total B-integral equal to 5, each frequency mode of the phase-modulated light split into two bumps. This may affect the final performance of the laser pulse in SSD.

Local self-focusing is an important issue in amplification of the initially phase-modulated light. The amplitude of the electro-optical modulation δ , and the parameter $U = (n_2 I / n_0) (k_0 / \delta \beta)^2$ determine the local self-focusing strength, where $\beta = 2\pi (d\theta / d\lambda) (\omega_m / \omega_0)$. The local self-focusing length is always shorter than the reference distance $z_r = k_0 / \delta \beta^2$. For a laser pulse with a large angular dispersion amplified to the GW/cm^2 range, the local self-focusing length can be shorter than one meter.

REFERENCES

1. R. H. Lehmberg and S. P. Obenschain, "Use of induced spatial incoherence for uniform illumination of laser fusion targets," *Opt. Comm.* **46**, 27 (1983).
2. S. P. Obenschain et al., "Laser-target interaction with induced spatial incoherence," *Phys. Rev. Lett.* **56**, 2807 (1986).
3. Y. Kato, K. Mima, N. Miyanaga, S. Arinaga, Y. Kitagawa, M. Nakatsuka, and C. Yamanaka, "Random phase of high-power lasers for uniform target acceleration and plasma-instability suppression," *Phys. Rev. Lett.* **53**, 1057 (1984).
4. T. Kessler et al., "OMEGA Phase Conversion with Distributed Phase Plate," *LLE Rev.* **33**, 1 (1987).
5. S. Skupsky, R. W. Short, T. Kessler, R. S. Craxton, S. Letzring, and J. M. Soures, "Improved Laser-Beam Uniformity Using the Angular Dispersion of Frequency-Modulated Light," *J. Appl. Phys.* **66**, 3456, (1989).
6. Y.-H. Chuang, L. Zheng, and D. D. Meyerhofer, "Propagation of light pulses in a chirped-pulse-amplification laser," submitted to *IEEE J. Quantum Electron.*
7. A. E. Siegman, in *Lasers*, (University Science, Mill Valley, CA, 1986), Chaps. 5 and 10.
8. L. M. Frantz and J.S. Nodvik, "Theory for pulse propagation in a laser amplifier," *J. Appl. Phys.* **34**, 2346 (1963).
9. D. W. Hall, R. A. Haas, W. F. Krupke, and M. J. Weber, "Spectral and Polarization Hole Burning in Neodymium Glass Lasers," *IEEE J. Quantum Electron.* **QE-19**, 1704, (1983); D. W. Hall, W. F. Hagen, and M. J. Weber,

- "Modeling Broad-Band and Multiple-Frequency Energy Extraction from Glass Laser Amplifiers," *IEEE J. Quantum Electron.* **QE-22**, 793, (1986).
10. J. W. Goodman, Introduction to Fourier Optics, (McGraw-Hill, NY, 1968), Chap. 5.
 11. W. G. Wagner, H. A. Haus, and J. H. Marburger, "Large-scale self-trapping of optical beams in the paraxial ray approximation," *Phys. Rev.* **175**, 256 (1968).
 12. Y. R. Shen, The Principles of Nonlinear Optics, (Wiley-Interscience, NY, 1984), Chap. 17.
 13. F. P. Mattar and J. Teichmann, "Fluid formulation of high intensity laser beam propagation using Lagrangian coordinates," *Comput. Phys. Commun.* **22**, 1 (1981).
 14. M. Born and E. Wolf, Principles of Optics, (Pergamon Press, NY, 1980), Chap. 3.

CHAPTER VII

SUMMARY

The amplification and propagation of broad-bandwidth, phase-modulated laser pulses was studied experimentally and theoretically. The near 1053 nm Chirped-Pulse-Amplification (CPA) laser system at the Laboratory for Laser Energetics (LLE) at the University of Rochester was used for these experiments. In theoretical analysis the power gain of the amplifier was treated as a function of the laser's instantaneous frequency. With this approximation non-ideal amplification processes, such as gain narrowing, gain saturation, and self-phase modulation (SPM), have been clearly expressed and understood.

Several techniques that are currently desired in laser applications are successfully accomplished. Theoretical analyses and experiments on CPA lasers led to the production of high-power ultrashort pulses with an intensity contrast exceeding $10^5:1$. Experiments on second harmonic generation of 1.6-ps pulses resulted in the energy conversion efficiency of up to $\sim 75\%$, the highest for ultrashort pulses ever being reported. The combination of the spectral shaping and CPA techniques creates a jitter-free wave-mixing condition for nonlinear-refractive-index measurement, which is currently strongly in need in nonlinear optics. The use of ray-trajectory function in SSD calculations gives an intuitive understanding of energy conservation for light propagation. This calculation technique is also important in nonlinear optics.

In Chapter II, we used the concept of instantaneous frequency to simplify the pulse propagation equations for CPA. As a result, the power gain and phase

variations generated from the nonlinear amplification process became functions of time. An optical diffraction analogy illustrated the amplitude and phase modulations of the chirped pulse during amplification, and intuitively showed the distortion of the compressed pulse and its power spectrum.

In the CPA process the bulk of the amplitude modulation is due to spectral gain narrowing, and most of the phase modulation is from SPM. Gain narrowing, which may cause broadening of the final compressed pulse can be, however, employed as a pulse shaping tool. SPM not only broadens the compressed pulse but also enhances the background pedestal and should be avoided. In the gain saturation regime, both gain saturation and gain narrowing distort the pulse envelope and must be considered together. A frequency mismatch between the applied signal and the amplifiers may also distort the amplified pulse and further degrade the compressed pulse.

SPM in phosphate Nd:glass CPA laser systems that use fiber and expansion gratings to process the initial chirped pulses has been identified experimentally and theoretically. If the peaked edges of the chirped pulse are not well suppressed by spectral gain narrowing and frequency matching, they may undergo a high-frequency phase shift when SPM occurs. This high-frequency phase shift with its own wide-spread group velocity in compression gratings contributes to the background pedestal of the final compressed pulse.

In Chapter III, we investigated four different contributions to the pedestal associated with a CPA laser system and the techniques to reduce them leading to the production of high-intensity contrast ($>10^5:1$), 0.9-ps Gaussian pulses. The pedestal consists of: (a) a background pedestal resulting from SPM during the operation of the regenerative amplifier near gain saturation; (b) etalon effects; (c)

pulse wings; and (d) satellite pulses. The last two result from the square top envelope and the nonlinear chirp generated in the optical fiber, respectively. The pulse was switched out before gain saturation to avoid further frequency modulation in the regenerative amplifier. The pulse wings were suppressed by gain-narrowing in the spectral line-center matched regenerative amplifier. A saturable absorber was used to suppress the satellite pulses and further reduce the pedestal.

With this pedestal reduction, high-intensity contrast picosecond pulses with intensities exceeding 10^{16} W/cm² were produced with the current system, with higher intensities available with larger gratings. The results of this work make possible the study of high-intensity ultra-short laser plasma interactions with a fiber-grating CPA system.

In Chapter IV experiments on frequency doubling of picosecond pulses using Wang and Dragila's scheme¹ were presented. A KD*P crystal was used to give the pre-delay in this experiment for its well known properties and low absorption losses at 1053 nm. A type II KDP crystal was used as a frequency doubler. When a pre-delay between o and e waves was introduced in front of the doubling crystal the conversion efficiency increased from ~40% (without pre-delay) to ~75% (with pre-delay). The agreement between the experiment and theory is excellent. Experiments on polarization matching for frequency doubling are also reported. Depolarization or polarization mismatching of the laser pulse decreases the conversion efficiency. This is consistent with theoretical predictions.

This simple and effective conversion scheme is well suited for picosecond high power lasers. Further experiments should include the second-harmonic pulse-shape measurement to investigate the pulse-shortening and pedestal

reduction predicted in Ref. 1. Frequency tripling using two type II crystals (Ref. 2 and 3) for picosecond pulses should be also considered since the group velocity delay is automatically compensated in this tripling scheme. The capability of operating high-power picosecond lasers at several different frequencies should be possible in the near future.

In Chapter V, a simple solution to synchronization jitter among CARS input sources was presented. Spectral shaping of a linearly chirped pulse in the expansion gratings of a CPA laser was used to produce two pulses with different frequencies. A regenerative amplifier of appropriate bandwidth was used to amplify these two pulses. After amplification these two pulses were temporally mixed through compression gratings. With this technique two pulses are jitter-free and spatially identical. The alignment and synchronization are thus greatly simplified. In general, any ultra-short pulse source used in conjunction with expansion and compression grating pairs can serve as driver for this kind of four-wave mixing experiment. To reach other wavelength, sources such as Ti:sapphire could be used in a similar manner.

The energy transfer between two beams in this experiment is treated as a noise source. This two beam coupling phenomena, however, provides the relaxation time measurement by using the beating between the two lines. As the beating period is equal to the relaxation time of the nonlinear medium, the energy transfer between two signals is maximized. From the line ratio change one can measure the resonant condition and, as a result, the relaxation time.

The laser technique for producing two pump waves used in this experiment can be extended to produce synchronized multiple waves by changing the spectral window. These synchronized waves can be mixed by compression gratings for

wave-mixing applications. They also can have different delays between each other by applying optical delay near the spectral window. This technique can be used for pump-probe experiments. The advantage is that each signal has its own distinguishable frequency but nearly the same group velocity so that collinear pump-probe experiments are possible. A single spectrometer is enough to measure the results. The identical beam profiles of pump and probe waves generated from the same regenerative amplifier also reduce the experimental uncertainty due to beam pattern fluctuation in usual two-beam pump-probe experiments.

In Chapter VI, we again treated the power-gain coefficient as a function of instantaneous frequency and thus simplify the equations for the amplification of broad-band phase-modulated laser pulse for SSD. Through this treatment and by following the light rays, we calculated the intensity and phase modulation of this initially phase-modulated light during propagation and amplification.

Intensity modulations due to propagation (angular dispersion) and amplification (gain narrowing) can be treated separately within the geometrical optics approximation. This helps the design of the initial phase modulation in SSD to avoid the problems arising from propagation, image relay and amplification. For an amplification system with the total B-integral equal to 5, each frequency mode of the phase-modulated light splits into two bumps. This may affect the final performance of the laser pulse in SSD.

Local self-focusing is an important issue in amplification of the initially phase-modulated light. The amplitude of the electro-optical modulation δ , and the parameter $U = (n_2 I / n_0) (k_0 / \delta \beta)^2$ determine the local self-focusing strength, where $\beta = 2\pi (d\theta / d\lambda) (\omega_m / \omega_0)$. The local self-focusing length is always shorter than the

reference distance $z_r = k_0/\delta\beta^2$. For a laser pulse with a large angular dispersion amplified to the GW/cm² range, the local self-focusing length can be shorter than one meter.

In the appendix detailed derivations of the instantaneous-frequency approximation for the amplification of phase-modulated light is presented. We first simplify the resonant-dipole equation and obtain the modified rate equation. We then compare the results to those from the conventional rate-equation approximation for narrow-band pulses.

REFERENCES

1. Yanjie Wang and R. Dragila, "Efficient conversion of picosecond laser pulses into second-harmonic frequency using group-velocity dispersion," *Phys. Rev. A* **41**, 5645 (1990).
2. R. S. Craxton, "High efficiency frequency tripling schemes for high power Nd:glass lasers," *IEEE J. Quantum Electron.* **QE-17**, 1771 (1981).
3. W. Seka, S. D. Jacobs, J. E. Rizzo, R. Boni, and R. S. Craxton, "Opt. Commun." **34**, 469 (1980).

APPENDIX

In this appendix we simplify the resonant-dipole equation¹ for broadband, phase-modulated lasers through the use of the instantaneous frequency approximation. We then compare the results from this approximation to those from the conventional rate-equation approximation for narrow-band pulses.¹

In the standard approach for a quasi-monochromatic beam propagating in an isotropic medium along z direction, the applied signal and the resulting electric polarization (electric dipole moment per unit volume) are first written in the form

$$E(\mathbf{r}, \hat{t}) = \text{Re}\left\{E_0(\mathbf{r}, \hat{t})\exp[i(\omega_0\hat{t} - k_0z)]\right\} \quad (\text{A1})$$

and

$$P(\mathbf{r}, \hat{t}) = \text{Re}\left\{P_0(\mathbf{r}, \hat{t})\exp[i(\omega_0\hat{t} - k_0z)]\right\}, \quad (\text{A2})$$

where Re means the real part, k_0 is the wavevector (in the medium) at the carrier frequency ω_0 , \mathbf{r} is the shorthand for spatial coordinates x, y, z , and \hat{t} is the ordinary laboratory time coordinate. We then follow the same procedure described in Chapter II to obtain the basic equations that govern the light propagation in a homogeneous amplifier. This includes the use of the slowly varying envelope approximation (SVEA) and the introduction of the moving pulse time frame

$$t = \hat{t} - z/c, \quad (\text{A3})$$

where c is the speed of light in the gain medium. We further consider the transverse variation of the laser field in this appendix, which is not shown in Chap.

II. The three basic equations are: the resonant-dipole equation

$$\frac{\partial P_0(\mathbf{r}, t)}{\partial t} + \frac{\Delta\omega_a}{2} \left[1 + i \frac{2(\omega_0 - \omega_a)}{\Delta\omega_a}\right] P_0(\mathbf{r}, t) = i \frac{K}{2\omega_0} N(\mathbf{r}, t) E_0(\mathbf{r}, t), \quad (\text{A4})$$

the population-inversion equation

$$\frac{\partial N(\mathbf{r}, t)}{\partial t} = i \frac{2^*}{4\hbar} \left[E_0^*(\mathbf{r}, t) P_0(\mathbf{r}, t) - E_0(\mathbf{r}, t) P_0^*(\mathbf{r}, t) \right], \quad (\text{A5})$$

and the paraxial wave equation

$$\frac{\partial E_0(\mathbf{r}, t)}{\partial z} = -i \frac{\omega_0}{2\epsilon c} P_0(\mathbf{r}, t) - i \frac{1}{2k} \nabla_{\perp}^2 E_0(\mathbf{r}, t) + i \frac{k''}{2} \frac{\partial^2 E_0(\mathbf{r}, t)}{\partial t^2} - i \frac{\beta_2}{2} |E_0|^2 E_0(\mathbf{r}, t), \quad (\text{A6})$$

where ω_a and $\Delta\omega_a$ are atomic transition frequency and atomic linewidth, $N(\mathbf{r}, t)$ is the number density of the inverted population, K is a constant, 2^* is a dimensionless population saturation factor with values between 1 and 2, depending on the gain medium¹, ϵ is the dielectric permeability of the gain medium, k'' is the second derivative of $k(\omega)$ with respect to ω and evaluated at ω_0 , $\beta_2 \equiv 2\pi n_{2E}/\lambda_0$ is a parameter related to the optical Kerr coefficient n_{2E} , and λ_0 is the laser wavelength in vacuum. In Eq. (A5) we have neglected both pumping effects and upper-level relaxation during the transit time of the amplified pulse. The right hand side of Eq. (A6) includes the common effects encountered in laser-pulse amplification: signal gain, diffraction, dispersion, and nonlinear effects.

The resonant-dipole equation (A4) is a first order ordinary differential equation. It can be solved and written in the following integral form:

$$P_0(\mathbf{r}, t) = i \frac{K}{2\omega_0} \int_0^{\infty} N(\mathbf{r}, t - \tau) A(\mathbf{r}, t - \tau) \exp\left[-\frac{\Delta\omega_a}{2}\tau + i(\omega_a - \omega_0)\tau - i\phi(\mathbf{r}, t - \tau)\right] d\tau. \quad (\text{A7})$$

In Eq. (A7) we have used the expression

$$E_0(\mathbf{r}, t) = A(\mathbf{r}, t) \exp[-i\phi(\mathbf{r}, t)] \quad (\text{A8})$$

to describe the phase-modulated light. Both $A(\mathbf{r}, t)$ and $\phi(\mathbf{r}, t)$ are real functions. The term $\exp(-\Delta\omega_a\tau/2)$ in Eq. (A7) describes the impulse response of the resonant dipoles. The response time is equal to the dephasing time $T_2 \equiv 2/\Delta\omega_a$.²

The integral in Eq. (A7) can be carried out as an asymptotic power series using integration by parts. The leading behavior of $P_0(\mathbf{r},t)$ is

$$P_0(\mathbf{r},t) = i \frac{K}{\omega_0 \Delta\omega_a} \left\{ \frac{N(\mathbf{r},t)A(\mathbf{r},t)}{1 + i \frac{2[\omega_i(\mathbf{r},t) - \omega_a]}{\Delta\omega_a}} - \left(\frac{2}{\Delta\omega_a} \right) \frac{\frac{\partial}{\partial t}[N(\mathbf{r},t)A(\mathbf{r},t)]}{\left\{ 1 + i \frac{2[\omega_i(\mathbf{r},t) - \omega_a]}{\Delta\omega_a} \right\}^2} - \left(\frac{2}{\Delta\omega_a} \right)^2 \frac{i\phi''(\mathbf{r},t)N(\mathbf{r},t)A(\mathbf{r},t)}{\left\{ 1 + i \frac{2[\omega_i(\mathbf{r},t) - \omega_a]}{\Delta\omega_a} \right\}^3} + \dots \right\} \exp[-i\phi(\mathbf{r},t)] \quad , \quad (\text{A9})$$

where

$$\omega_i(\mathbf{r},t) = \omega_0 - \frac{\partial\phi(\mathbf{r},t)}{\partial t} \quad (\text{A10})$$

is the instantaneous frequency and $\phi''(\mathbf{r},t)$ is the second derivative of the phase variation with respect to time t . Repeated integration by parts gives the full asymptotic expansion of $P_0(\mathbf{r},t)$.

Equation (A9) can be further simplified by the following assumptions. First, for an optical pulse with large frequency modulation the pulse duration τ_p is much larger than the dephasing time T_2 . This can be understood by the fact that the laser pulse is far from the Fourier transform limited and the bandwidth of the amplifier is chosen to be large enough to cover the entire bandwidth of the laser pulse, i.e.

$$\tau_p \gg \frac{2}{\Delta\omega_L} > \frac{2}{\Delta\omega_a} \equiv T_2. \quad (\text{A11})$$

Second, the laser field is not strong enough to create Rabi-frequency oscillations,¹ so the population inversion $N(\mathbf{r},t)$ varies slowly. With these two assumptions we can conclude

$$\frac{2}{\Delta\omega_a} \frac{\partial}{\partial t} [N(r,t)A(r,t)] \ll N(r,t) A(r,t), \quad (\text{A12})$$

and drop the second term of the series in Eq. (A9). The last assumption for the phase-modulated light is

$$\left| \left(\frac{2}{\Delta\omega_a} \right)^2 \phi''(t) \right| \ll 1. \quad (\text{A13})$$

This statement can be verified for both chirped-pulse amplification (CPA)³ and smoothing by spectral dispersion (SSD).⁴ In CPA the phase modulation can be expressed in a quadratic form $\phi(t) = -b(t/\tau_p)^2/2$, where $b \approx \tau_p \Delta\omega_L/2$ is a parameter describing the frequency chirp.⁵ Relationship (A13) is equivalent to

$$\left| \left(\frac{2}{\Delta\omega_a} \right)^2 \phi''(t) \right| \approx \frac{1}{b} \left(\frac{\Delta\omega_L}{\Delta\omega_a} \right)^2 \ll 1. \quad (\text{A14})$$

This is commonly true since the value of b is typically chosen from a few hundred to several thousands for a practical CPA laser. In SSD, the initial phase modulation of the laser pulse can be described as $\phi = \delta \sin(\omega_m t + \beta y)$, where δ is the amplitude of the electro-optical modulation, ω_m is the angular frequency of the modulation, and β is a parameter related to the angular dispersion.⁴ Statement (A13) becomes

$$\left| \left(\frac{2}{\Delta\omega_a} \right)^2 \phi''(t) \right| \approx \delta \left(\frac{2\omega_m}{\Delta\omega_a} \right)^2 \ll 1. \quad (\text{A15})$$

This is also true since $\omega_m \ll \Delta\omega_a$. Therefore the third term of the series in Eq. (A6) is negligible. As a result of the three assumptions stated above, Eq. (A6) becomes

$$P_0(\mathbf{r}, t) = i \left(\frac{K}{\omega_0 \Delta \omega_a} \right) \left\{ \frac{1}{1 + i \frac{2[\omega_i(\mathbf{r}, t) - \omega_a]}{\Delta \omega_a}} \right\} N(\mathbf{r}, t) E_0(\mathbf{r}, t), \quad (\text{A16})$$

where $A(\mathbf{r}, t) \exp(\mathbf{r}, t) = E_0(\mathbf{r}, t)$ has been used again.

Equation (A16) describes the relation between the electric field and the electric polarization. By using Eq. (A16) the term describing the signal gain in Eq. (A6) can be written in the familiar form

$$-i \frac{\omega_0}{2\epsilon c} P_0(\mathbf{r}, t) = \frac{1}{2} \alpha(\omega_i, \mathbf{r}, t) E_0(\mathbf{r}, t) \quad (\text{A17})$$

with

$$\alpha(\omega_i, \mathbf{r}, t) = \alpha_r + i\alpha_i = \left\{ \frac{1 - i \frac{2(\omega_i - \omega_a)}{\Delta \omega_a}}{1 + \left[\frac{2(\omega_i - \omega_a)}{\Delta \omega_a} \right]^2} \right\} \sigma_0 N(\mathbf{r}, t), \quad (\text{A18})$$

where $\sigma_0 \equiv K/\epsilon c \Delta \omega_a$ is the gain cross section at linecenter, and ω_i is the instantaneous frequency described by Eq. (A10). The imaginary part of the gain coefficient α describes the phase shift of the signal due to the gain. The effect of this phase modulation is usually negligible in pulse amplification. Therefore we can treat the power gain coefficient as a real number. For convenience we define the gain cross section as a function of the instantaneous frequency,

$$\sigma(\omega_i) = \frac{\sigma_0}{1 + \left[\frac{2(\omega_i - \omega_a)}{\Delta \omega_a} \right]^2} \quad (\text{A19})$$

such that the power gain coefficient can be described as the conventional form

$$\alpha(\omega_i, \mathbf{r}, t) = \sigma(\omega_i) N(\mathbf{r}, t). \quad (\text{A20})$$

Substituting Eq. (A16) into the population equation (A5), gives the rate equation in the form

$$\frac{\partial N(\mathbf{r}, t)}{\partial t} = -\frac{2^*}{\hbar\omega_0} \sigma[\omega_i(\mathbf{r}, t)]N(\mathbf{r}, t)I(\mathbf{r}, t), \quad (\text{A21})$$

where $I(\mathbf{z}, t) = \epsilon c |E_0(\mathbf{z}, t)|^2/2$, is the laser intensity. Equation (A21) can then be used to describe the gain saturation for broadband phase-modulated laser pulses.

The conventional rate-equation approximation for narrow-band (homogeneous) lasers assumes

$$\frac{\partial P_0}{\partial t} \ll \frac{\Delta\omega_a}{2} P_0. \quad (\text{A22})$$

The resonant-dipole equation (A4) can then simplified as a linear-susceptibility relation

$$P_0(\mathbf{r}, t) \approx \chi \epsilon E_0(\mathbf{r}, t) = i \left(\frac{K}{\omega_0 \Delta\omega_a} \right) \left\{ \frac{1}{1 + i \frac{2[\omega_0 - \omega_a]}{\Delta\omega_a}} \right\} N(\mathbf{r}, t) E_0(\mathbf{r}, t), \quad (\text{A23})$$

where χ is the electric dipole susceptibility and ω_0 is the carrier frequency of the laser pulse. Under the approximation (A23), the population equation (A5) becomes the usual rate equation

$$\frac{\partial N(\mathbf{r}, t)}{\partial t} = -\frac{2^*}{\hbar\omega_0} \sigma(\omega_0)N(\mathbf{r}, t)I(\mathbf{r}, t), \quad (\text{A24})$$

where

$$\sigma(\omega_0) = \frac{\sigma_0}{1 + \left[\frac{2(\omega_0 - \omega_a)}{\Delta\omega_a} \right]^2} \quad (\text{A25})$$

is the gain cross section at the laser carrier frequency ω_0 .

We now compare the results of the instantaneous-frequency approximation for broadband phase-modulated lasers to those of the conventional rate-equation approximation for narrow-band lasers, that is, compare Eqs. (A16), (A19), and (A21) to Eqs. (A23), (A25), and (A24), respectively. For phase-modulated pulse the only difference is that the instantaneous frequency ω_i is used instead of the carrier frequency ω_0 . For a laser pulse without phase modulation the instantaneous frequency defined by Eq. (A10) is equal to the carrier frequency. In this case the instantaneous frequency approximation reduced to the conventional rate-equation approximation as expected.

There is another method, presented by D. W. Hall et al.,⁶ to model the amplification of broadband phase-modulated pulses. The broadband laser pulse was separated into several monochromatic waves. The amplification of each frequency mode was assumed to be described by the rate-equation approximation. This approach, however, may not be convenient for a real case, since the nonlinear effects, such as self-phase modulation and self-focusing, become important. For example, the initial SSD pulse can be expressed as⁴

$$E(t) = A \exp[i\omega_0 t + i\delta \sin(\omega_m t + \beta y)] = A \sum_n J_n(\delta) \exp\{i[\omega_0 t + n(\omega_m t + \beta y)]\}, \quad (\text{A26})$$

where we have dropped the notation Re for simplicity. The initial amplitude of the frequency mode $\omega_0 + n\omega_m$ is $AJ_n(\delta)$. A spatial phase modulation $n\beta y$ is also presented in this frequency mode. To describe the nonlinear effects, one needs to deal with all couplings among all frequency modes, which will be difficult. Instead, the advantage of using the instantaneous frequency approximation is clear shown in Chapter VI. Several features of the pulse distortion due the propagation and the non-ideal amplification process are successfully described in that chapter.

REFERENCES

1. A. E. Siegman, in *Lasers*, Mill Valley, CA: University Science, 1986, Ch. 5.
2. The homogeneous linewidth is actually defined as $\Delta\omega_a \equiv 1/T_1 + 2/T_2$, where T_1 is the energy relaxation time and T_2 is the dephasing time. However for most laser systems the condition that $1/T_1 \ll 2/T_2$ is satisfied.
3. P. Maine, D. Strickland, P. Bado, M. Pessot, and G. Mourou, "Generation of ultrahigh peak power pulses by chirped pulse amplification," *IEEE J. Quantum Electron.* **QE-24**, 398 (1988).
4. S. Skupsky, R. W. Short, T. Kessler, R. S. Craxton, S. Letzring, and J. M. Soures, "Improved Laser-Beam Uniformity Using the Angular Dispersion of Frequency-Modulated Light," *J. Appl. Phys.* **66**, 3456, (1989).
5. Y.-H. Chuang, D. D. Meyerhofer, S. Augst, H. Chen, J. Peatross, and S. Uchida, "Suppression of the pedestal in a chirped-pulse-amplification laser," *J. Opt. Soc. Am. B* **8**, 1226 (1991).
6. D. W. Hall, W. F. Hagen, and M. J. Weber, "Modeling broad-band and multiple-frequency energy extraction from glass laser amplifiers," *IEEE J. Quantum Electron.* **QE-22**, 793 (1986).